# CONTROL LIMITATION ANALYSIS FOR DISSIPATIVE PASSIVE HAPTIC INTERFACES

A Dissertation
Presented to
The Academic Faculty

By

**Dalong Gao**

In Partial Fulfillment
of the Requirements for the Degree
Doctor of Philosophy in Mechanical Engineering

Georgia Institute of Technology
December, 2005

# CONTROL LIMITATION ANALYSIS FOR DISSIPATIVE PASSIVE HAPTIC INTERFACES

Approved by:

Dr. Wayne J. Book, Advisor
School of Mechanical Engineering
*Georgia Institute of Technology*

Dr. Stephen P. DeWeerth
School of Electrical and Computer Engineering
*Georgia Institute of Technology*

Dr. Imme Ebert-Uphoff
School of Mechanical Engineering
*Georgia Institute of Technology*

Dr. Ronald Arkin
College of Computing
*Georgia Institute of Technology*

Dr. Raymond P. Vito
School of Mechanical Engineering
*Georgia Institute of Technology*

Date Approved: October 6, 2005

*To my mother Zhang, Xirong and father Gao, Chun.*

# Acknowledgements

First I give my thanks to my thesis advisor, Dr. Book, not only for his generous support, but his broad-mindedness and his advice on my research and my life. He has shown me a professional standard which will always stay with me. I also want to thank Dr. Ebert-Uphoff for her strong encouragement since the beginning of the research. I would like to thank Dr. Vito, Dr. DeWeerth and Dr. Arkin too for their precious time.

The students and fellows in IMDL have provided me with valuable feedback on my research. They also created a nice working environment around me. I'd like to thank J.D. Huggins, L.J. Tognetti, Ryan Krauss, Matt Kontz, Joe Frankel, Haihong Zhu, Ho Ching, Amir Shenouda, Scott Driscoll and Ben Black.

Finally and most specially, I thank my wife, Bin, for her love and her strong belief in me during the past years. Her presence and support throughout the program was an enormous encouragement.

# TABLE OF CONTENTS

# LIST OF FIGURES

# SUMMARY

This research addresses the ability of dissipative passive actuators to generate control effects on a passive haptic interface. A haptic display is a human-machine interface that constructs a sensation of touch for the human operator. Applications can be found in various industries, space, medicine and construction etc. A dissipative passive haptic display contains passive actuators that can remove energy from the system by resisting motions in the system. The advantage of a dissipative passive haptic display is better safety compared to an active display. Its disadvantage is the limited control ability from the passive actuators.

This research starts with the identification of the control ability and limitations of dissipative passive haptic interfaces. The ability is identified as the steerability, the ability to redirect motions of a manipulator. The force generation analysis of each individual actuator is then selected as an approach to evaluate the steerability. Steerability metrics are defined to evaluate the steerability. Even though non-redundant manipulators don't have desired steerability, optimal steering configurations are found for the best operation. Steerability is improved by redundancy in serial or parallel structures. A theorem is developed to evaluate steerability for redundant manipulators. The influence of system dynamics on their steerabilities is discussed. Previously developed haptic interfaces are evaluated based on their steerabilities. Steerability analysis of three-dimensional haptic interfaces is also given to a limited extent as an extension of the two-dimensional cases. Brakes and clutches are the two types of dissipative passive actuators in this research.

# 1. INTRODUCTION

## 1.1 Haptics, Haptic Display and Its Applications

In the process of exploring the physical world, man uses all his basic sensing abilities including vision, hearing, touch, smell and taste to learn about the objects around. Even though it seems not as important as visual sensation the sense of touch provides important information which is not fully provided by other senses, for example the hardness of material, temperature etc. The word haptic (adj) came from Greek word *haptesthai*. It means to touch. Haptics is the science of touch sensation's influence on the interfaces between a human and the outside world.

A haptic display is a human-machine interface that constructs a sensation of touch for the human operator. The sense of touch is either a (scaled) real sense directly from the object being handled or a virtual one. The virtual sense of touch could simulate real objects, forces, torques etc. For example, a master arm for teleoperation can provide the operator with forces that the slave robot, which is driven by the master, is encountering in real time. It could be very useful in some applications such as construction equipment, like a backhoe. The operator may thereby tell the difference between soft sand and a hard stone remotely. The virtual sense of touch could also be just virtual constraints. For example, there are restricted areas in many industry operations. Most of them are clearly labeled. However it is always difficult to work around them because it is hard to tell the boundary. A haptic interface could make it much easier by placing a virtual wall around the restricted areas. The operator could feel the wall once the machine reaches it.

The idea of haptic display could be used in many areas. Haptic master/slave robots for teleoperation as mentioned above provide to the operator extra information in addition to sight and hearing to provide a better feel of the remote circumstances. They could be used in environments not suitable for human operators, such as space, hostile environments etc. The idea of virtual constraints could bring in many applications. The automobile industry uses them to guide heavy parts into a vehicle body on an assembly line. Doctors could use them to train or refine operations in surgery where hand-eye coordination is strongly emphasized. Athletes could use them to adjust fine motions. Therapists could use them to treat patients in rehabilitation. Soldiers could even use them to simulate combat conditions.

## 1.2 Energetically Active and Passive Haptic Displays

An energetically active haptic display is a haptic interface containing active actuators that can add energy into the overall system, such as electric motors, hydraulic cylinders, pneumatic actuators etc. An energetically passive haptic display, on the contrary, is a haptic interface containing only passive actuators that can not add energy into the system. Passive actuators, such as the transmission, clutch and brakes etc., can store, redirect or dissipate energy of the system.

A large amount of research work has focuses on haptic displays. The majority of the research was focused on energetically active interfaces. The inherent advantage of active actuators is that they make it easy to develop various control schemes for active haptic displays.

One disadvantage of an active haptic display is safety. An active device will perform any command sent from its controller. If by any chance a wrong command were made by

the controller because of a component malfunction or a program error, the haptic device could result in unexpected motions and bring serious injuries to the operator.

Safety of a haptic display is improved by the introduction of passive actuators. A passive device is not capable of moving without an operators' input. Any motion would only be initiated by the human operator. In the case of any failure during operations, no part of the device can be speeded up by the device. However, the improved safety is obtained at a price, which is difficulty to achieve control efforts. As a result, existing control methods for active haptic displays are not directly applicable to passive interfaces. And certain applications such as power assisting equipment are not possible with passive devices alone.

## 1.3 Dissipative and Steerable Passive Haptic Interfaces

Current passive haptic displays fall into two groups, dissipative and steerable passive haptic displays.

A dissipative passive haptic display contains passive actuators that can remove energy from the system by resisting motions in the system. Typical actuators used are brakes in various forms, such as electromagnetic friction brakes [1], electrorheological [2] and magnetorheological brakes [3, 4].

A steerable passive haptic display does not intend to use actuators to remove kinetic energy from the system. Cobot, developed by Colgate et al. [5-8], is the typical steerable passive haptic device. Cobot has only one mechanical degree of freedom. The direction of this degree of freedom is steered by actuators. The motion of the steered degree-of freedom is fully controlled by a human operator. Because of the careful design of the system, cobot will not dissipate system kinetic energy theoretically speaking.

## 1.4 Measures of Haptic Interfaces

Measures have been developed to evaluate the performance of a haptic interface. Several common ones are listed here.

### *1.4.1 Transparency and Stability*

A haptic display is a human-machine interface that constructs a sensation of touch for the human operator. The sensation of touch is constructed through the elements of the interface. The human operator could also have the feeling from the dynamics of these elements other than the desired touch sensation. The transparency of a haptic interface compares the interface dynamics to the sensation to be constructed.

Ideally, the human operator should not "feel" the inherent dynamics in a transparent haptic interface. In a real case, it is desired that the dynamics of a haptic interface should be dominated by the virtual environment (touching sensation to be displayed) rather than any inherent dynamics. It is desirable to have structures with less mass for transparency consideration. However, stronger and stiffer structures would improve system stability. A discussion on the trade-off of stability and transparency was made in Flemmer's research [9] for a surgical teleoperator system.

Another stability issue came up in teleoperator systems. The signal transformation over media has an unexpected delay and sometimes the link could be lost for a small amount of time. The energy stored during the delay could be large which makes the system unstable or even harmful. Some research has been done for this stability problem. Hannaford and Ryu [10] used a passivity observer and a passivity controller to measure the energy flowing in/out. Yoshikawa used an energy balance monitor [11] and a passivity monitor [12] with a software limiter which can turn a system stable.

### *1.4.2 Singularity*

In a serial robot, there are configurations in which motion in a special direction is not possible. These are called the leg singularities, kinematic singularities or twist singularities of the robot. Some joints can move through an infinitesimal motion even though the end-effector is fixed in a leg singularity condition. There also exist end-effector wrenches [13] which require zero-actuator loads to maintain robot static equilibrium. However, singularities are not desirable in robot design. A robot could end up with very unstable behavior near a singularity.

Leg singularities exist in parallel robot systems as well. In addition, there also are configurations for which force generation in a certain direction is not possible. They are called platform singularities or wrench singularities. Under platform singularities, the end-effector could still move even with all the actuators locked. Singularity configurations are not desirable in parallel robot systems either. Singularities for a Gough-Stewart platform structure were researched by many researchers, see Merlet [14]. Singularity-free load distribution algorithms were proposed by Kim et al. [15]. Voglewede [16] used redundant actuation to reduce singularities in parallel structures.

### *1.4.3 Manipulability*

Manipulability concepts have been used as indices for evaluating manipulator performance [17]. A velocity manipulability ellipsoid is used to represent the ability of a manipulator to change the end-point's position. Figure 1 (a) shows the velocity manipulability ellipsoid for a two-link robot at different configurations. When the two links are close to each other, the robot end-point could be moved at a higher velocity in the horizontal direction than the vertical direction for joint space speed with constant

norm. When the two links open up, the robot end-point could be moved at a higher velocity in the vertical direction than the horizontal direction.

A force manipulability ellipsoid is used to represent the ability of a manipulator to generate end-point forces. Figure 1 (b) shows the force manipulability ellipsoid for the same two-link robot at different configurations as (a). Similarly, when the two links are close to each other, the robot could generate greater force at the end-point in the vertical direction than in the horizontal direction. Compared to Figure 1 (a), the direction of greater velocity manipulability is the direction of smaller force manipulability.

(Velocity and force ellipsoids are not well-defined for manipulators that provides translation and orientation capacities. However all manipulators considered in this thesis are position only, thus these concepts are well-defined.)

Velocity and force manipulability ellipsoids do not consider system dynamics. If a system dynamic model is available, a dynamic manipulability ellipsoid could be obtained as an evaluation of the system's dynamic performance. Rosenstein and Grupen [18] obtained the dynamic manipulability ellipsoid for a 3R robot for a certain motion which is shown in Figure 2. The dynamic manipulability ellipsoid (shown ellipsoid) could be considered as the translation of the static ellipsoid (shown as cutout of hexagon). The distance of a point on the dynamic ellipsoid to the end-point gives a measure of the ability of the system to accelerate the end-point along the direction.

## 1.5 Underactuated Robots

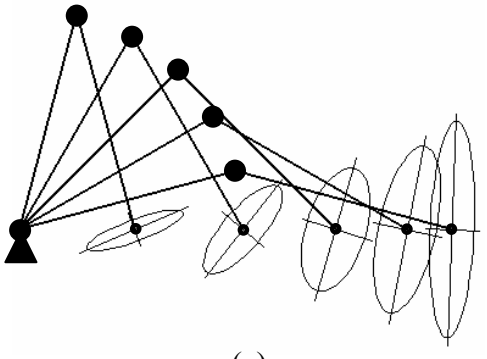

(a)

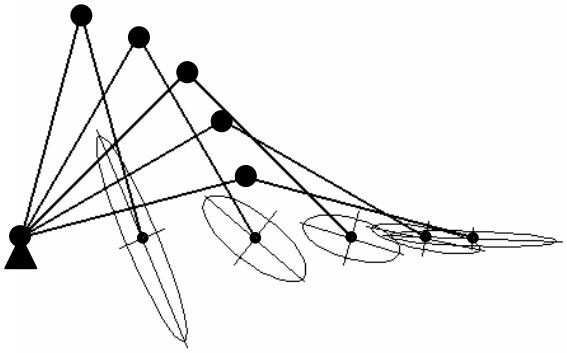

(b)

**Figure 1. Velocity (a) and Force (b) manipulability ellipsoid**

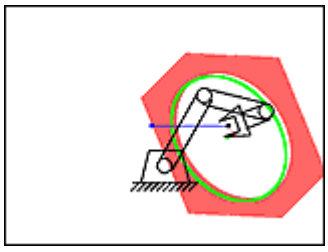

**Figure 2. Dynamic manipulability ellipsoid of a 3R robot, by Rosenstein, Grupen**

An underactuated mechanical system has fewer control inputs than degrees of freedom. An underactuated robot is similar to a passive interface in the sense of lack of control ability in some joints. The joints could be intentionally designed not to be actuated or could not be actuated when the actuators are broken.

A robot system tends to need more joints for completing complex tasks. While actuating a joint, an additional actuator increases the system's cost and overall weight. As the number of joints increases, it becomes unrealistic or even impossible to actuate all the joints. Leaving some of the joints unactuated is a choice for a robot system if it can still be controlled to finish the desired tasks. Also, as a backup strategy, underactuated robotics research is very useful considering the cases of controlling a fully actuated robot system when some active actuators are broken. However, because of the complex dynamics and lack of controllability, underactuated systems are known for their complexities in trajectory planning and control.

A lot of research has been done on underactuated robot systems and control. Acrobot is a two-link serial robot with two rotational joints (2R) and only one actuator in the second joint. Control strategies were developed by Spong [19] to control Acrobot in the "swing-up" problem. A 3R (3 rotational joints) planar serial robot with the last joint un-actuated was build by Lynch et al. [20]. Also, De Luca and Oriolo [21] proposed a general method of trajectory planning and control for an *n*-joint serial planar robot with the last joint un-actuated.

It is not always a last choice to use an underactuated system. Good systems could also be developed through careful design with fewer actuators. The one joint manipulator built by Lynch et al. [22] was capable of manipulating objects. It could roll over a square

object, throw and catch an object. The complexity of the robot system was transferred from hardware to planning and control. The snake-like locomotors and manipulators by Hirose could finish uncommon tasks like a live animal [23]. Underactuated robot systems could use more joints for smoother/easier and dexterous handling. An underactuated hand system designed and built by Birglen and Gosselin [24] is capable of gripping objects of different size, shape and compliance. Sometimes the complex dynamics effect of the robot could help the robot to achieve motions in an un-actuated direction. Ito et al. [25] proposed and built an underactuated crawling robot. The dynamic effect of the swing tail made the robot crawl forward even though no actuator is used for motions in this direction.

## 1.6 Muscle Controlled Human Body System

Biomimetics is a growing field in robotics research. Biological systems have refined themselves through evolution. The effectiveness and dexterity of biological systems are still way beyond most robotic systems today. Researchers have been trying to use biological systems as references for the design of the mechanical counterparts. Here robot actuators are treated as the counterparts of muscles in a human body.

A robot uses actuators to control its elements for various motions. Actuators can be divided into two groups based on the relationships with the system kinetic energy. An active actuator can add kinetic energy into the robot system while a passive actuator can not. An active actuator behaves like a passive actuator when not adding kinetic energy. A typical example is the “engine brake” of a manual shift vehicle. The engine is slowing down the vehicle speed by dissipating vehicle kinetic energy just as the brakes do. When not adding system kinetic energy, an actuator can be called “Passive-Like” actuator at the

time instant. An “Active-Like” actuator can be defined accordingly. An active actuator could be either “passive-like” or “active-like”, while a passive actuator can only be “passive-like”.

Compared to a robot, a human uses muscles (tendons etc.) to control body motions. Individual muscles could have different situations in motion. A muscle could be actively shortening which is called concentric contraction [26] (normal sense of contraction). A muscle could be actively lengthening which is called eccentric contraction. An example is slowly lowering a heavy object. A muscle could be actively held at a fixed length which is called isometric contraction. A muscle could also be passively lengthening which is called passive stretch. Also, muscles and tendons have potential for elastic energy storage and utilization.

Muscles are the “actuators” for humans. All muscles could have contraction. So they all fall into the “active actuator” category borrowing the concepts of active/passive actuators. As active actuators, muscles are capable of adding kinetic energy to the human body. However, muscles are not working to increase kinetic energy most of the time. They could dissipate kinetic energy by slowing down body motion. They could store some amount of energy because of their elasticity. When not adding system kinetic energy, muscles are “passive-like” actuators at the time instant.

The human body is a highly over-actuated system with muscles as actuators. Dozens of muscles are involved in even a simple motion. Only a few muscles are actually contributing to increase the body kinetic energy at a time instant while others are all passive-like. For example, in the extension of the forearm, the triceps contracts and works

while the biceps is extended along the arm. The biceps and triceps are called antagonistic muscles [27]. Operated by this over-actuated system with only active actuators the resulting motion control is safe, smooth and accurate. It is the passivity of the actuators to achieve the approved safety.

# 2. PREVIOUSLY DEVELOPED DISSIPATIVE PASSIVE HAPTIC INERFACES

There has been some research in dissipative passive haptic interfaces but only a few devices have been developed up until today.

P-TER, by Book et al. [28], is a four-link four-electromagnetic brake/clutch manipulator which provides direct and inverse coupling of links; it is shown in Figure 3. The inverse coupling of the clutch brings more control abilities into P-TER. Different control methodologies were developed. Impedance control was used by Charles in P-TER with proper choice of brakes/clutches. Velocity field control was studied by Gomes first with straight line experiments [29]. A velocity ratio controller and optimal controller were developed by Swanson [30] as the lower level controller of velocity field control. Single degree-of-freedom (SDOF) control was also used by completely locking all actuators except one for SDOF motions [31]. Human tests were used to evaluate some of the controllers.

The only 3D passive interface was developed by Matsuoka et al. [32] (Figure 4). It uses two revolute joints to form a universal joint. The third joint is a prismatic joint. Magnetic particle brakes are used for the joints. The device was used to create a virtual object and guide movements.

Figure 5 shows another four-link passive force display structurally similar to P-TER. It was built by Sakaguchi et al. [33]. Two links of the device are connected to the joints on the ground individually. And two ER (electro-rheological) brakes are installed at these two joints. The device was used to simulate a virtual wall and a virtual object collision.

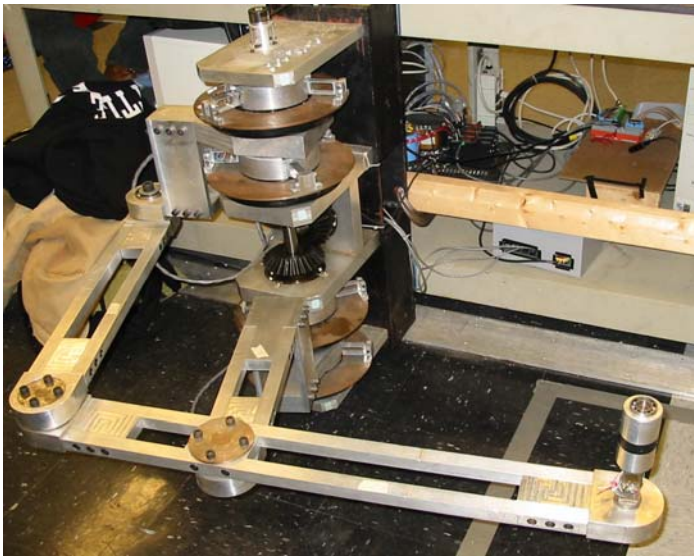

**Figure 3. P-TER**


**Figure 4. Matsuoka's 3D device**

MR (Magneto-rheological) P-TER is a four-link manipulator with different configurations from P-TER with four MR fluid brakes [3, 4]. Two configurations were studied. The diamond shaped configuration (Figure 6) uses three brakes, two on the grounded joints and one on a moving joint. A 5-bar linkage configuration (Figure 7) was also studied by changing the structure of the diamond-shaped robot. The two grounded joints were separated and the links connecting to the grounded joints were shortened. All of the 4 joints are actuated with MR brakes. Single degree-of-freedom (SDOF) control and proportional velocity control were tested.

The limited number of existing devices shows the limitation in the control of dissipative passive haptic interfaces. Without the ability to add system energy, dissipative passive actuators have limited ability to generate control effects in a haptic device compared to active ones. The existing control theories for active devices can not be easily transferred.

There has been no research directly on the control ability (distinct from controllability of control theory) and limitations of dissipative passive manipulators. One attempt was made by Cho, Kim and Song using the Force Manipulability Ellipsoid (FME) [34].

As another attempt, this thesis focuses on three major objectives. The control ability and limitations of a dissipative passive haptic interface must be clearly identified. Then it is possible to evaluate and improve the control ability. A planar dissipative passive haptic interface could be then be possibly designed with improved control ability similar to an active haptic interface.

**Figure 5. Sakaguchi's device**

**Figure 6. MR P-TER (diamond shaped configuration)**

**Figure 7. MR P-TER (5-bar linkage configuration)**

After the introductory chapters, the thesis is organized into six chapters: It starts with the identification of the control ability and limitations in chapter 3; steerability analysis for planar dissipative passive haptic interfaces using brakes and clutches are discussed in chapter 4 and 5 separately; the influence of system dynamics on steerability is studied in chapter 6 and there follows a chapter on the design of planar dissipative passive manipulators; the last chapter shows initial studies of steerability of three-dimensional dissipative passive haptic interfaces.

# 3. CONTROL ABILITY AND LIMITATION FOR DISSIPATIVE PASSIVE HAPTIC INTERFACES

A analysis of the control ability of a dissipative passive haptic interface should start with the clarification of the control effects of the dissipative passive actuators on haptic interfaces.

## 3.1 The Control Ability of a Dissipative Passive Actuator in a Haptic Interface

The actuation of a dissipative passive actuator, for example a brake, will slow down the existing relative motion of the two elements connected to it and therefore remove system kinetic energy. If no motion exists, the actuation will not bring in any change into the system. In a haptic interface, the slowing down of the existing relative motion of the two link elements will affect the motion of the end-point which is the location that is directly interacting with the human operator. The magnitude of the end-point velocity could be changed as well as the direction. The change of the end-point velocity results in a redirection of the original motion. Therefore the control effects of the actuators can redirect existing motion (operator induced for example) in a desired manner.

Because the control ability of dissipative passive actuators is redirection of existing motion, the main applications for the dissipative passive haptic interfaces are guiding systems, which include systems for obstacle avoidance and for path following. Virtual reality applications are to a lesser extent of interest here.

## 3.2 Desired Ability in Motion Redirection

Since the control effect is motion redirection, the control limitation of the dissipative passive actuators should be represented as the lack of the ability to redirect motions in the desired way. In order to find the shortage in this ability, the concept of desired ability of motion redirection should be addressed first.

Motion redirection problems are very common in our daily life. Driving a car to work is a typical two-dimensional motion redirection problem where a desired path or a corridor (any motion within is allowed) could be defined when a target is given. Based on the current situation (position, velocity etc.) relative to the desired path, people use the steering wheel to redirect motion of the vehicle. By turning the steering wheel, the vehicle's velocity direction is changed to either its left or right. With the capability of redirecting motion to the left or right the vehicle can be steered to follow a desired path and take the driver to the destination successfully.

From the driving example above, it is clear that the desired control ability for a two-dimensional motion redirection problem is to have the ability to steer the velocity to both left and right. If an operator is trying to use the diamond shaped MR P-TER to follow a pre-defined path (Figure 8), the manipulator has desired ability to redirect the current motion.

Having the ability to redirect a motion to either side of the existing velocity is only a minimum requirement for motion redirection. It doesn't consider the effectiveness of motion redirection. Similar to the driving example, the desired ability considers the ability to turn. It doesn't consider how small a circle a car can turn. After all, there's always a limitation on that.

Three-dimensional motion redirection problems are much more complex but are similar to two-dimensional cases. For example, steering an aircraft or a missile is not limited to only two sides of the current velocity. It involves all possible direction choices around the current velocity. The number of possibilities is infinite. The desired control ability for a three-dimensional motion redirection problem is therefore to have the ability to steer the velocity to any possible direction away.

## 3.3 The Control Limitation of Dissipative Passive Actuators in a Haptic Interface

Because of the passivity constraint of the dissipative passive actuators a dissipative passive haptic interface does not have the desired steerability at all times. For example, MR P-TER is guiding the operator to follow a predefined path shown in Figure 9. At the configuration shown the robot is moving away from the path. However the robot is not able to display the desired haptic feedback, which is the force that brings the motion back on track to the left. The actuations of the brakes could only drag the robot away from the path even more.

From the example, the limitation of dissipative passive actuators to generate control effects to redirect motion of a haptic interface is that sometimes the actuations fail to redirect toward the desired motion, in a planar case to one side of the velocity, in three-dimensional cases to certain directions away from the velocity. The limitation happens only at certain configuration of the manipulator and for certain directions of the velocities.

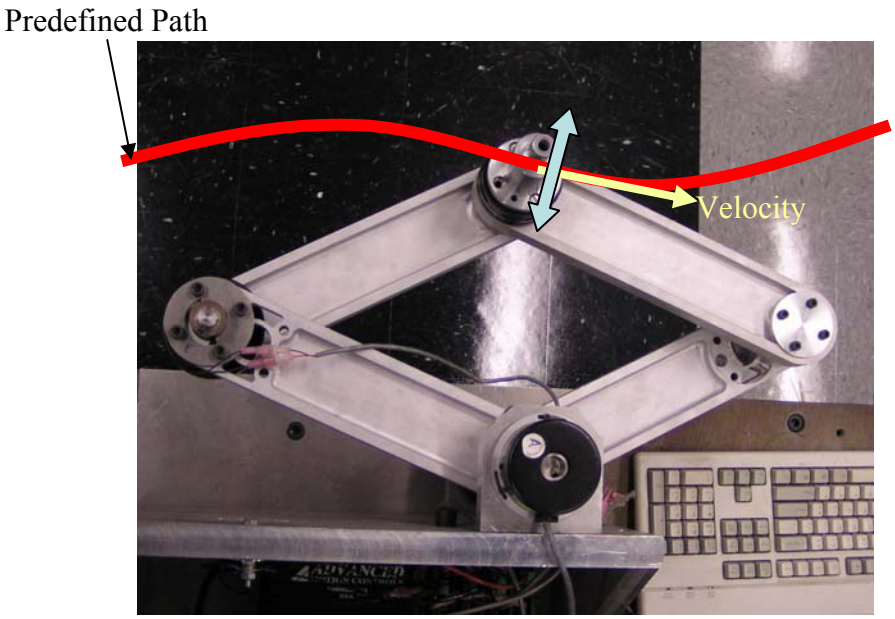


**Figure 8. Desired control ability in motion redirection, MR P-TER (diamond shaped configuration)**

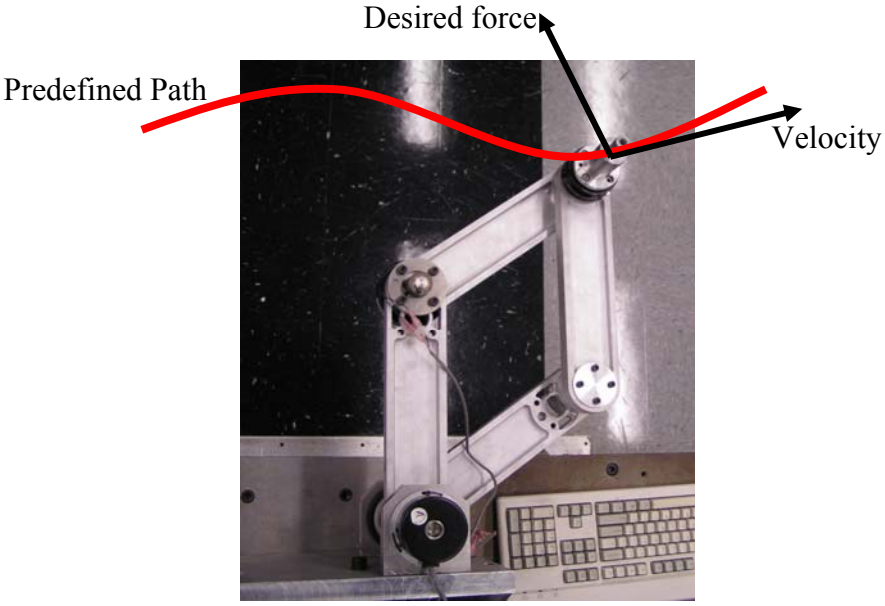


**Figure 9. Control limitation of MR P-TER (diamond shaped configuration)**

# 4. STEERABILITY ANAYSIS FOR PLANAR MANIPULATORS WITH BRAKES

The study of the control ability and limitation of dissipative passive haptic interfaces starts with planar cases first.

## 4.1 Where to Start: Generated Force

As a haptic interface, the haptic feelings are constructed through displaying a force to the operator. (For the extent of this research, no torque is involved in the haptic feeling constructed). The motion of the end-point of a haptic interface is redirected by exerting a desired force. The limitation happens when the actuators can't redirect a certain motion because it can not display an appropriate force. Therefore studying the capability of dissipative passive actuators to generate forces at the end-point of a haptic interface could be a logical approach to study their control ability and limitation.

## 4.2 Force Generation Analysis for a 2D Non-Redundant Dissipative Passive Haptic Interface with Brakes

The force generation analysis starts with a simple serial two-link planar manipulator. It consists of two links and two revolute joints as shown in Figure 10. The lengths of the two links are $l_1$, $l_2$. The parameters of the two-link manipulator are defined following the Denavit-Hartenberg (distal variant) notation. It is a non-redundant robot because it has two degrees of freedom and also full two degrees of mobility.

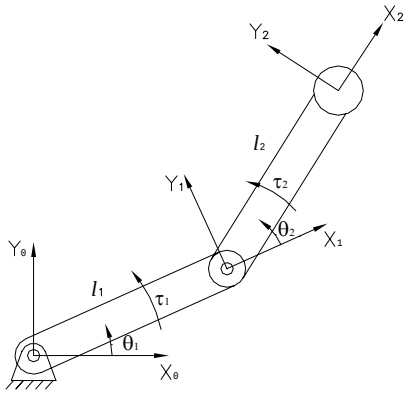


**Figure 10. Two-link plannar manipulator**

A brake, one type of passive revolute actuator, is installed at each joint. The output of a brake is torque which is a function of relative rotational velocity of the two links. A corresponding force could be generated at the end point of the manipulator when the brakes are excited. From the principle of virtual work:

$$\tau = J^T F \tag{4.1}$$

If the dynamics is not important, the generated force can be related with applied torques by

$$\vec{F} = \frac{1}{l_1 s_2}\tau_1 \hat{f}_2 + \frac{-1}{l_1 l_2 s_2}\begin{Vmatrix} l_1 c_1 + l_2 c_{12} \\ l_1 s_1 + l_2 s_{12} \\ 0 \end{Vmatrix}\tau_2 \hat{f}_1 \tag{4.2}$$

where

$$\hat{f}_1 = \begin{pmatrix} l_1 c_1 + l_2 c_{12} \\ l_1 s_1 + l_2 s_{12} \\ 0 \end{pmatrix} \Bigg/ \begin{Vmatrix} l_1 c_1 + l_2 c_{12} \\ l_1 s_1 + l_2 s_{12} \\ 0 \end{Vmatrix} \tag{4.3}$$

$$\hat{f}_2 = \begin{pmatrix} c_{12} \\ s_{12} \\ 0 \end{pmatrix} \tag{4.4}$$

$c_1 = \cos(\theta_1)$, $s_1 = \sin(\theta_1)$

$c_{12} = \cos(\theta_1 + \theta_2)$, $s_{12} = \sin(\theta_1 + \theta_2)$

$\|\vec{f}\|$ represents the magnitude of vector $\vec{f}$.

$\hat{f}_i$ is defined as the unit radial vector for joint *i*. Its direction is from joint *i* to the end-point as shown in Figure 11. It represents the generated force direction for the torque from one brake. If a torque is applied to the first joint and the second joint is free to move, an equivalent force will be generated along $\hat{f}_2$, the direction along the second link at the manipulator's end-point; if a torque is applied to the second joint and the first joint is free to move, an equivalent force will be generated along $\hat{f}_1$, the direction from the first joint to the end-point.

The generated force could be related with the velocity direction at the end-point because torques from passive actuators are related to link rotational speeds. The manipulator end-point velocity is:

$$\vec{v} = \left\| \begin{matrix} -l_1 s_1 - l_2 s_{12} \\ l_1 c_1 + l_2 c_{12} \\ 0 \end{matrix} \right\| \dot{\theta}_1 \hat{v}_1 + l_2 \dot{\theta}_2 \hat{v}_2 \tag{4.5}$$

where

$$\hat{v}_1 = \begin{pmatrix} -l_1 s_1 - l_2 s_{12} \\ l_1 c_1 + l_2 c_{12} \\ 0 \end{pmatrix} \Bigg/ \left\| \begin{matrix} -l_1 s_1 - l_2 s_{12} \\ l_1 c_1 + l_2 c_{12} \\ 0 \end{matrix} \right\| \tag{4.6}$$

$$\hat{v}_2 = \begin{pmatrix} -s_{12} \\ c_{12} \\ 0 \end{pmatrix} \tag{4.7}$$

$\hat{v}_i$ is defined as the unit tangential vector for joint *i* as shown in Figure 11. It is perpendicular to $\hat{f}_i$, and $\hat{f}_i \times \hat{v}_i = \hat{k} = [0 \quad 0 \quad 1]^T$. $\hat{v}_i$ represents the manipulator end-point velocity direction given positive rotation speed at joint *i* and zero velocity at the other joint.

As a dissipative passive actuator, a brake can only generate torque in the direction opposite to the relative rotational velocity direction. The brake torque can be written as:

$$\tau_i = -\text{sgn}(\dot{\theta}_i)|\tau_i| \tag{4.8}$$

The positive directions for $\tau_1$ and $\tau_2$ are shown in Figure 11.

When the angular velocity of any joint changes its sign, the generated force component changes its sign. Four cases were used to better illustrate the possible generated force when the angular velocities of the joints change as shown in Figure 12. For example, when the angular velocities for both joints are positive (Figure 12 a), the end-point velocity could be along any direction within the shown $\vec{v}$ range and a force along any direction within the shown $\vec{F}$ range (magnitude is not considered) could be generated by the manipulator. The sum of a velocity range angle and the corresponding generated force range angle is π.

Passivity is guaranteed by

$$\vec{F} \cdot \vec{v} = -\dot{\theta}_1^2|\tau_1| - \dot{\theta}_2^2|\tau_2| \le 0 \tag{4.9}$$

The equal sign is chosen only if either $\vec{F} = 0$ or $\vec{v} = 0$. The angle between the velocity and the generated force from brakes at the end-point of manipulators is always larger than π/2.

(Other than the two basic velocity components definitions, the Lock-Joint Velocity of a dissipative passive actuator of a joint can be defined as the manipulator end-point velocity when no motion exists at the joint. For the two-link manipulator shown in Figure 10, the lock-joint velocity of the brake at joint 1 is $\hat{v}_2$ and the lock-joint velocity of the brake at joint 2 is $\hat{v}_1$ (Figure 11). The generated force component from the actuator at a joint is perpendicular to the lock-joint velocity of the joint. More will be seen in the analyses of clutches and three-dimensional manipulators.)

## 4.3 Steerability Concepts for a Serial Two-Link Dissipative Passive Manipulator

The analysis of the force generation of dissipative passive actuators gives a way to evaluate their ability and limitation in the control of passive manipulators. First steerability and related concepts can be defined as follows.

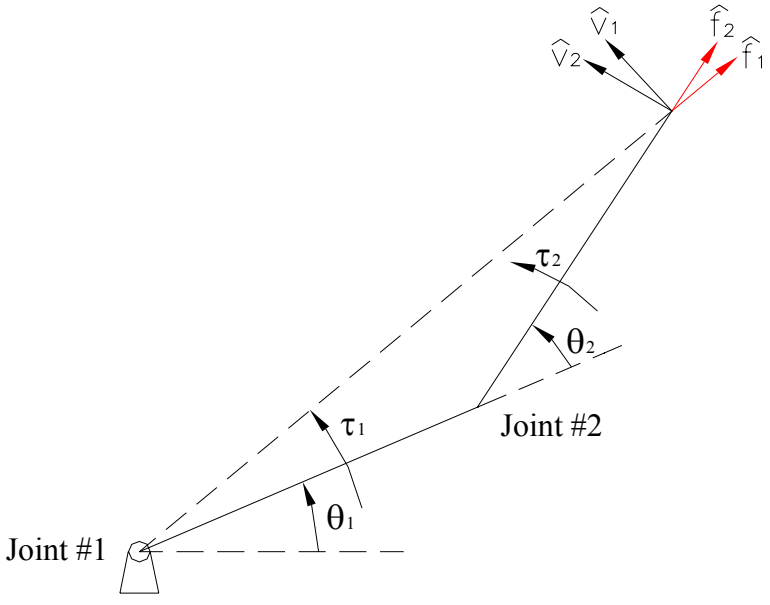


**Figure 11. Unit radial/tangential vectors for two-link manipulator**

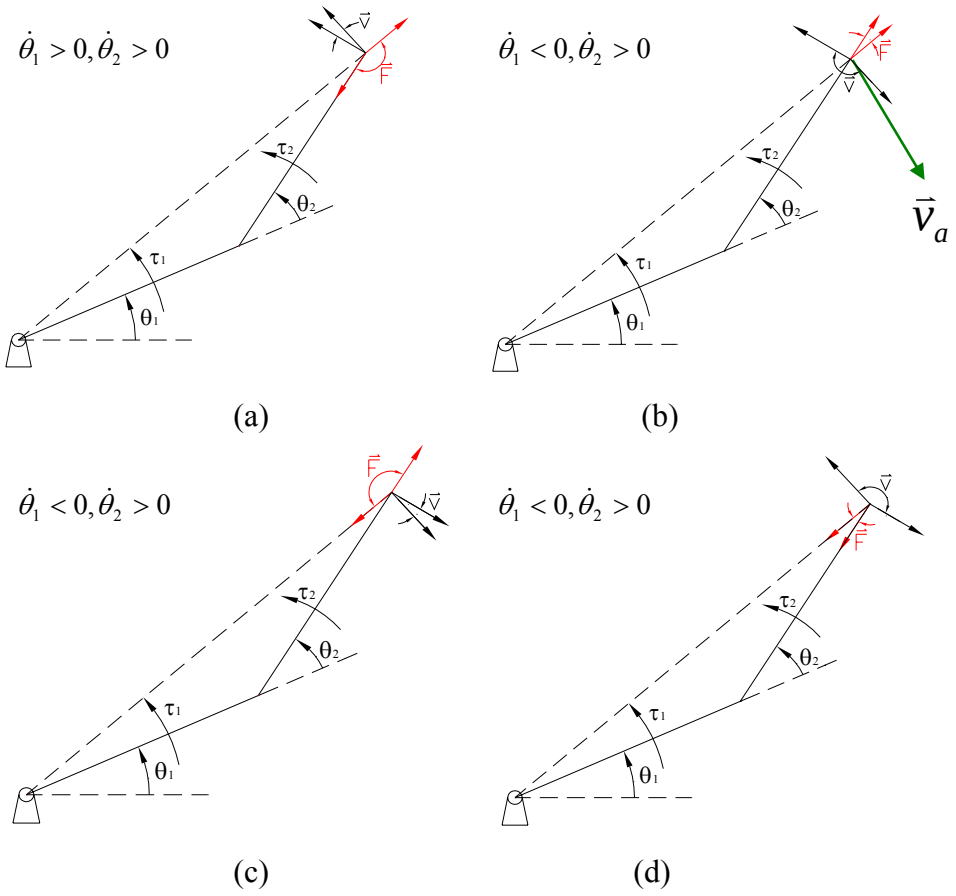


**Figure 12. Velocity and generated force at end-point of two-link manipulator with brakes**

**Steerability** is defined as the ability to redirect manipulator's motions for a given velocity at the end-point. The steerability represents the control ability of a dissipative passive haptic interface.

To evaluate the steerability, the **passive steerability angle** is defined as the angle range of actuator generated forces corresponding to a given velocity direction for a planar passive manipulator. The larger the passive steerability angle, the more ability the robot tends to have to redirect motion for a velocity. In any of the four cases shown in Figure 12, if the end point velocity direction is located in the velocity range the corresponding passive steerability angle is the force range angle shown for that case.

The passive steerability angle normally has one of two possible values $\alpha$ and $\pi$-$\alpha$ depending on velocity at a given configuration as shown in Figure 13. For example, the passive steerability angle is $\alpha$ for velocity $\vec{v}$ and $\pi$-$\alpha$ for velocity $\vec{v}'$. The two steerability angles change for different robot configurations. But when the end-point velocity direction is along one of the lock-joint velocity directions, only one of the two joints has relative rotation and only the corresponding actuator could generate torque. Therefore only one force component exists. The passive steerability angle is zero.

An **optimal steering configuration** for the 2R robot can be obtained conservatively by considering the worst case, the smaller value of the two possible passive steerability angles. The optimal steering configuration could be defined as the one with maximized minimum passive steerability angle $\alpha_{max}$, where $\alpha_{max} \leq \pi/2$. Analyses show that when $l_1 > l_2$, $\alpha_{max}=\pi/2$ when $\cos\theta_2 = -l_2/l_1$, and link 1 is the hypotenuse of the right triangle formed by the links. If $l_1 = l_2$, $\alpha_{max}=\pi/2$ when $\cos\theta_2 = -1$. However, the two links fold back on each other. This is a singularity of the manipulator which should be avoided.

When $l_1 < l_2$, $\alpha_{max}=\sin^{-1}(l_1/l_2)<\pi/2$ when $\cos\theta_2 = -l_1/l_2$, link 2 is the hypotenuse of the right triangle with link 1 as one side. Figure 14 shows the 3 cases.

In addition to the quantitative evaluation of the steerability, a binary criterion can also be found for the desired steerability.

**Two-sided steerability** is defined as the ability of a planar robot to steer the end-point away to both left and right of the current velocity direction. Two-sided steerability is also called full steerability of a velocity for a planar robot.

**Universal full steerability** is defined when full steerabilities exist for all velocities of a robot configuration.

Consider again the four cases in Figure 12. In (a) and (c) it is always possible for the generated force to steer the end-point to both sides of the velocity direction, two-sided steerability exists for the velocities in these ranges while in (b) and (d) it is possible for the generated force to steer the end-point to only one side of the velocity for velocities near the boundaries of the velocity range. For example, the generated force can only redirect motion to its upper right while not lower left if the end-point velocity is $\vec{v}_a$ in case (b). Hence two-sided steerability doesn't always exist for all the velocities in these cases.

From the four cases, the passive steerability angle must be larger than $\pi/2$ to ensure two-sided steerability for a given velocity. For the 2R manipulator with brakes, two-sided steerability for all velocities (except for the velocity along any of the tangential unit vector directions) only exists at the optimal steering configuration, and link lengths must satisfy $l_1 > l_2$.

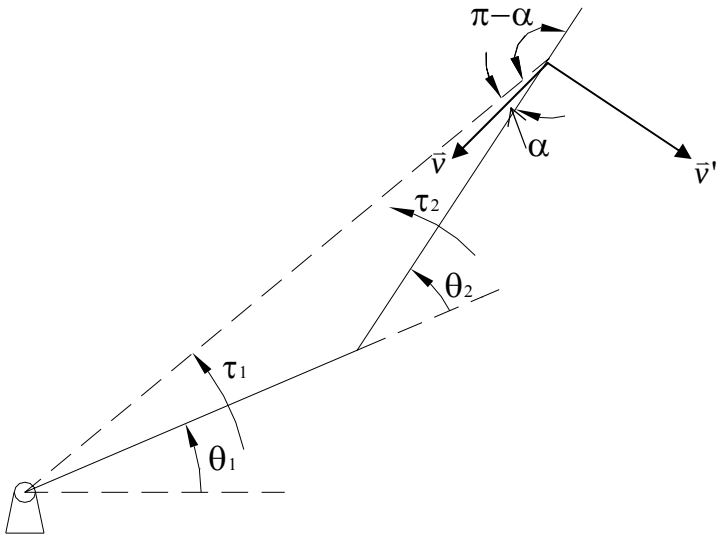


**Figure 13. Two possible passive steerability angle values**

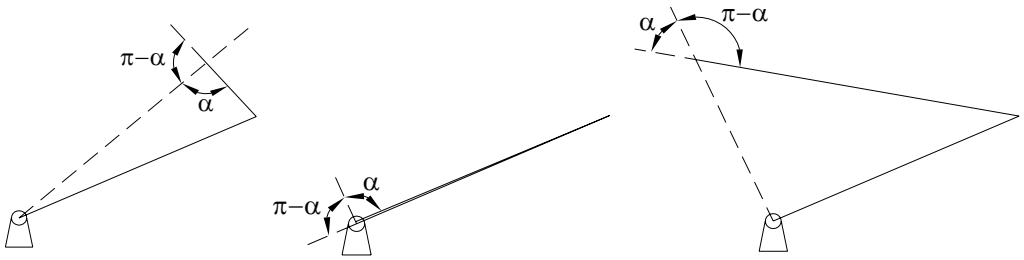


**Figure 14. Optimal steering configurations**

## 4.4 Steerability Improvement for Planar Dissipative Passive Haptic Interfaces

### *4.4.1 Improvement: Redundancy*

The passive steerability angle, which is the generated force range angle, should be larger than $\pi/2$ in order to have full steerability as analyzed in the previous section. A planar passive manipulator with two actuators has two generated force components. The force components can only divide the 2D plane into four angular zones 1-4 as shown in Figure 15 (a). They can not be all larger than $\pi/2$. Therefore universal full steerability doesn't exist for a planar passive manipulator with two brakes.

One approach to improve the steerability is from the idea of subdividing. Since some force zones are not big enough and some are, the ones that aren't big enough could make themselves larger by subdividing. For example, the small force zone 1 might be able to get bigger than $\pi/2$ if it could share a piece from its neighbor 2 or 4. It could possibly be done by introducing a third force component vector $\vec{f}_3$ as shown in Figure 15 (b). Then force zone 1 could borrow either force zone 2a or 4a to make itself large enough. Force zones 2 or 4 can still be used as one unit even though it's been divided. By this way universal full steerability is possible to obtain for the manipulator.

The proposed solution involves new generated force components. The new force components come from new actuators at new joints. That brings redundancy into the picture. The redundancy could be introduced by either parallel or serial structures.

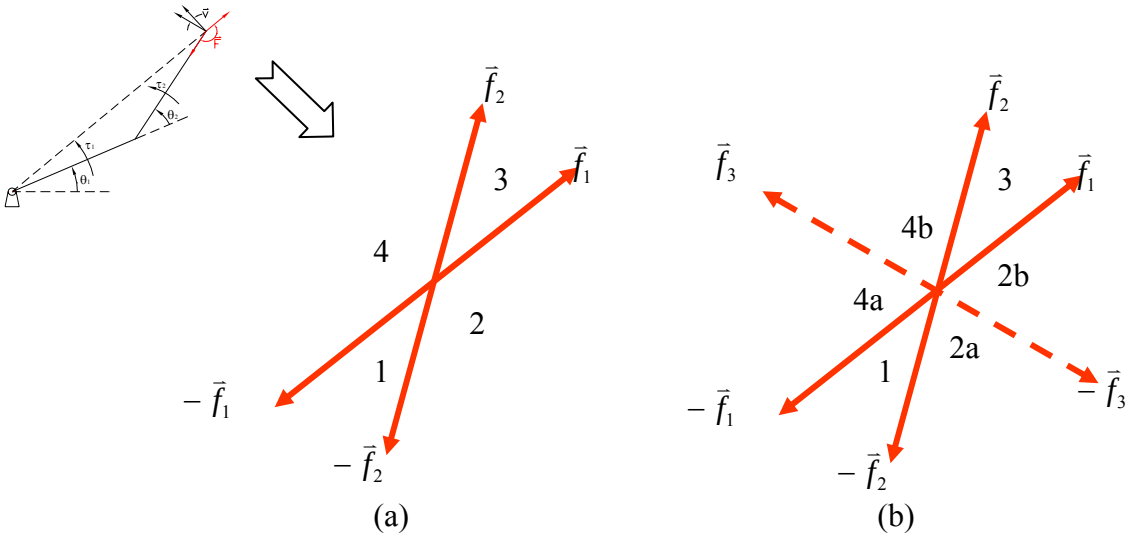


**Figure 15. Steerability improvement for 2R manipulator**

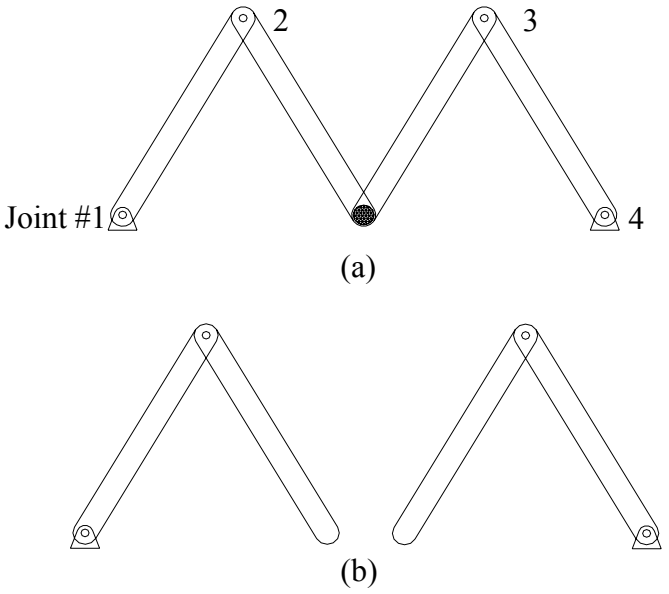


**Figure 16. Four-link four-actuator parallel manipulator (a) and its two branches (b)**

### *4.4.2 Steerability in a Four-Link Four-Actuator Parallel Manipulator*

A four-link four-actuator parallel manipulator is the sum of two two-link manipulators as shown in Figure 16. The end-points for both two-link manipulators connect with each other and form the end-point for the four-link device. The generated force of the parallel robot is the superposition of the forces from each two-link robot. The ability to steer the parallel robot is due to the combined effort of both two-link robots. The steerability of the manipulator is therefore improved.

### *4.4.3 Steerability in a Four-Link Four-Actuator Serial Manipulator*

Serial structure is another way to bring redundancy into the manipulator. A four-link four-actuator serial manipulator with the same joint and end-point positions is shown in Figure 17. The joints are numbered from 1 to 4 as labeled.

In the analysis for 2R planar robots, an assumption for the Virtual Work Principle is the static equilibrium of the manipulator. For a non-redundant manipulator, like the 2R manipulator discussed before, the links can be balanced by an external force applied at the end-point for any actuator inputs. Static equilibrium can always be satisfied. Mathematically, equation 4.1 will have a unique solution which is the end-point force if the manipulator is not at a singularity configuration. For a redundant serial manipulator, equation 1 will contain more linear equations than the unknown variables. Generally there is no solution for this system of linear equations. A solution exists only if the values of the actuations are a linear combination of the columns of the transpose Jacobian matrix of the manipulator. If a random set of actuator torques is applied, no end-point force

could balance all of the links, and static equilibrium is not satisfied any more. So the Virtual Work Principle could not be applied. The force generation analysis for 2R planar robots could not be applied directly.

One way to bypass this issue comes from practical experiences. It is known that a finite amount of torque is needed to move a joint. Consider a real planar serial manipulator with friction at the joint. A joint will start to move when the torque reaches a threshold. When two joints move, the manipulator has full 2 DOF and the torque on the other two joints will not increase. Therefore only two joints are actually moving in a real planar serial manipulator just like a non-redundant system. Borrowing this idea, two joints are intentionally locked in the serial structure to achieve a 2R robot and therefore the previous force analysis could be applied here.

The serial four-link robot is equivalent to a serial two-link manipulator when two joints are locked. Figure 18 shows the six possibilities of equivalent two-link manipulators. Figure 18 (a) can be obtained by locking joints 3, 4; (b) by locking 1, 2; (c) by locking 2, 4; (d) by locking 1, 3; (e) by locking 1, 4; and (f) by locking 2, 3.

When the motion at the end-point needs to be redirected, the manipulator will have six choices of equivalent manipulators to be used. The ability to redirect motion of the manipulator is the combination of the ability from all of the six equivalent two-link manipulators. The steerability of the serial manipulator is therefore also improved.

### *4.4.4 Steerability Comparison between Serial and Parallel manipulators*

For a non-redundant serial planar manipulator, two force components can be generated along the directions from the end-point to the two joints. For the redundant parallel manipulator (Figure 16) the two branches are both non-redundant manipulators.

The serial manipulator (Figure 17) also turns into a non-redundant robot when extra joints are locked. Consequently, if all the joints and the end-point are at the same coordinates, the same force components can be generated for both manipulators.

In a parallel system, the four achievable force components could be obtained simultaneously because each branch is capable of generating two components individually. In a serial system, the equivalent 2R manipulator can only generate two of the four components at one time. In order to achieve other components, different joints must be locked. However, both structures have the same capability to generate any two designated force components which could display a desirable output force. So the capability of generating a given force is the same for both structures. And from the definition, the passive steerability angle is the largest angle between any two force components, therefore the passive steerability angle is the same for both structures. If instant switching of lock schemes is assumed, the steerability could be considered the same for the two structures.

Even though the steerability could be considered equivalent there are differences between serial and parallel manipulators. For example, if two desired force components are coming from different branches of a parallel robot, the movable joints could be entirely different from a serial robot. In the four-link four-actuator parallel (Figure 16) and serial manipulators (Figure 17), if radial vectors $\hat{f}_2$, $\hat{f}_3$ are the force component directions, all the joints in the parallel robot are unlocked with actuator excitations at joint 1, 4, while in the serial robot only joints 2 and 3 are unlocked and the corresponding actuators are excited. And the torques in the two cases are not necessarily equal.

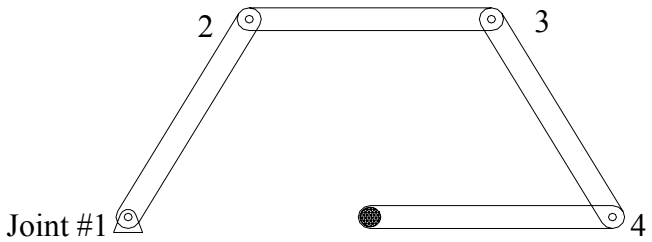


**Figure 17. Four-link four-actuator serial manipulator**

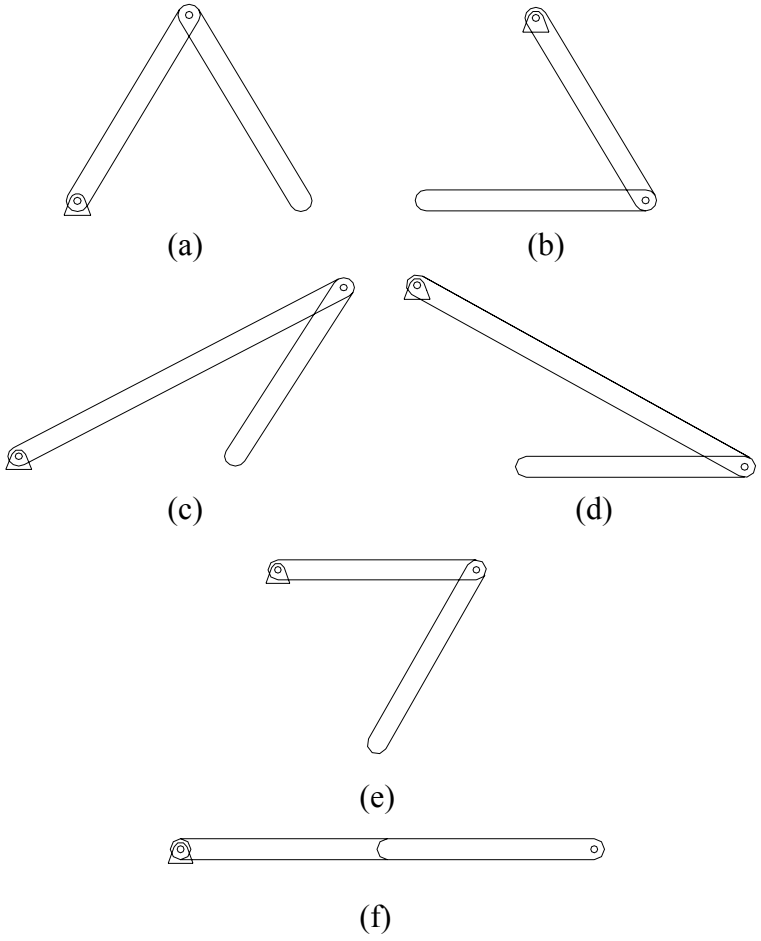

**Figure 18. Equivalent two-link manipulators by locking two joints of the serial manipulator**

Generally, a parallel robot gives redundancy in force generation and a serial robot provides redundancy in configuration. By locking different combinations of actuators, the serial robot behaves like the sum of multiple sub-robots. For the four-link four-joint case, the serial robot has the same redundancy in force generations as the parallel robot. However the redundancy in structure brings another question for the serial robot. The steerability of the robot depends on the configuration of the links. For an end-point position, the manipulator does not have a unique configuration and therefore does not have one steerability situation. Even starting from the same configuration, a serial manipulator will end up with different configurations after a short time period by choosing different sub-robots. So it will be hard to define a workspace with universal full steerability for passive serial manipulators.

## 4.5 Steerability Theorem

The analyses above show that redundancy could bring in improvement in the steerability for a manipulator. However the direct way to find steerability is to analyze the force generation capability for each sub-robot and then combine together. As the number of joints increases, the complexity of the analysis could increase dramatically. The steerability theorem developed in this section provides a simple and unified way to determine the universal full steerability.

The development of the steerability theorem starts with the definitions of several concepts that are used in the theorem.

The end-point of a manipulator is a point on the manipulator that is directly interacting with the outside world. The manipulator can apply force and/or torque to objects through the end-point.

Definitions:

The **end-point of a haptic interface** is a point on manipulator that is directly interacting with a human operator. The force generation ability for the manipulator is analyzed on this point.

A multiple joint manipulator is called "**end-effector constrained**" if the links and joints are not movable for a given end-point location and joint locking status.

For a serial planar robot, 2 DOF are removed from the structure if the end-effector position is held fixed. Therefore up to two 1-DOF joints can be left for free motion with fixed end-effector position and the manipulator is still fully constrained unless the robot is in a kinematic singularity. For a planar parallel robot, each leg of the robot now acts as a serial robot therefore should follow the previously mentioned requirements.

**Lemma**: A multiple joint planar manipulator is end-effector constrained if: for a serial robot, at most two 1-DOF joints are unlocked at any time instant unless for singularity configurations; for a parallel robot, each branch of the robot which connects the base to the end-point needs to be end-effector constrained, which means at most two 1-DOF joints are unlocked.

For a serial manipulator, the end-point velocities in task space and in joint space can be correlated by the Jacobian matrix $J$ as

$$\dot{x} = J\dot{\theta} \tag{4.10}$$

The Jacobian matrix $J$ is an $n$-by-$m$ matrix, $J = \begin{bmatrix} J_1 & J_2 & \dots & J_m \end{bmatrix}$. $n$ is the degree of freedom of the task space and $m$ is the degree of freedom of the manipulator, where $n \le m$. An end-effector constrained serial manipulator could be obtained from the serial manipulator by locking all joints except for joint $i$ and $j$. The Jacobian matrix of the end-effector constrained serial manipulator is

$$J_c = \begin{bmatrix} J_i & J_j \end{bmatrix} \tag{4.11}$$

If the manipulator is not at a singularity, the generated force can be found as

$$F = J_c^{-T}\tau \tag{4.12}$$

The generated force direction from a brake could be found by substituting

$$\tau = \begin{bmatrix} 1 & 0 \end{bmatrix}^T \tag{4.13}$$

or

$$\tau = \begin{bmatrix} 0 & 1 \end{bmatrix}^T \tag{4.14}$$

into equation 4.12. 4.13 is chosen for a brake at joint $i$ and 4.14 is chosen for a brake at joint $j$.

There are $k$ generated force lines for the serial manipulator with $l$ brakes, $l \le k \le m$. However if $l < m$, the manipulator could only generate one force component when an un-actuated joint is selected to be unlocked. And this force component can not be used with any other force component simultaneously for the serial manipulator. Full steerability does not exist for the serial manipulator if this force component exists. For simplicity, all joints in a redundant serial manipulator are actuated. Only the joints in a non-redundant serial robot could be un-actuated. That is $l = k = m$ if $m > 2$ and $l = k \le m$ if $m = 2$.

For an end-effector constrained parallel manipulator, the end-point velocities in task space and in joint space can be correlated by the inverse Jacobian matrix *G* as

$$\dot{\theta} = G\,\dot{x} \tag{4.10}$$

The inverse Jacobian matrix *G* is an *m*-by-*n* matrix. *n* is the degree of freedom of the task space and *m* is the degree of freedom of the end-effector constrained manipulator, where $n \le m$.

From the principle of virtual work:

$$F = G^T \tau \tag{4.1}$$

Similarly, by substituting unit actuation of brake $i$ $\tau_i = \begin{bmatrix} 0 & \ldots & \overset{ith}{\overset{\wedge}{1}} & \ldots & 0 \end{bmatrix}$ into equation 4.1 the generated force line from this brake could be found.

If the legs of the parallel manipulator are redundant serial manipulators (the actuation of the joints follows previous discussion), other generated force lines could be found by changing locking schemes. There are *k* generated force lines for the parallel manipulator with *l* brakes, $l = k \le m$.

There are *k* generated force lines for an *m*-joint manipulator with *l* brakes. The force lines intersect at the end-point of the manipulator. For example the four-link four-joint parallel manipulator shown in Figure 16 has four force lines intersecting at the end-point is shown in Figure 19. For this manipulator the force lines are along the radial vectors. The lines divide the 2D plane into 2*k* angular sections. The angular values for these sections are $\alpha_1$, $\alpha_1$, $\alpha_2$, $\alpha_2$, … $\alpha_m$, $\alpha_m$ (Figure 20) with the maximum value $\alpha_{max}$.

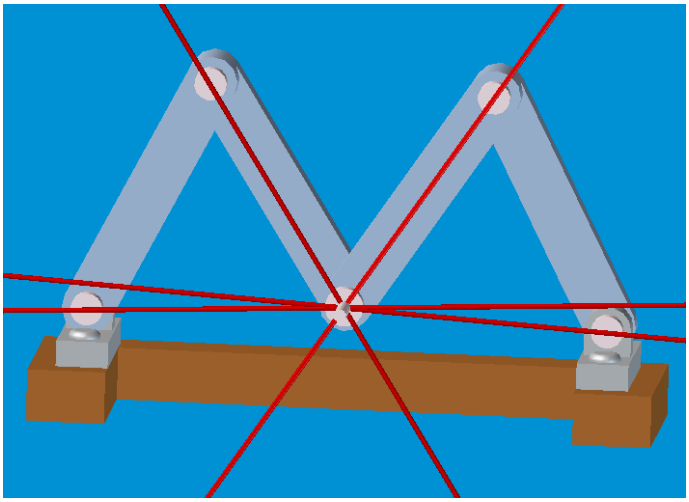

**Figure 19. Four force lines for a parallel manipulator**

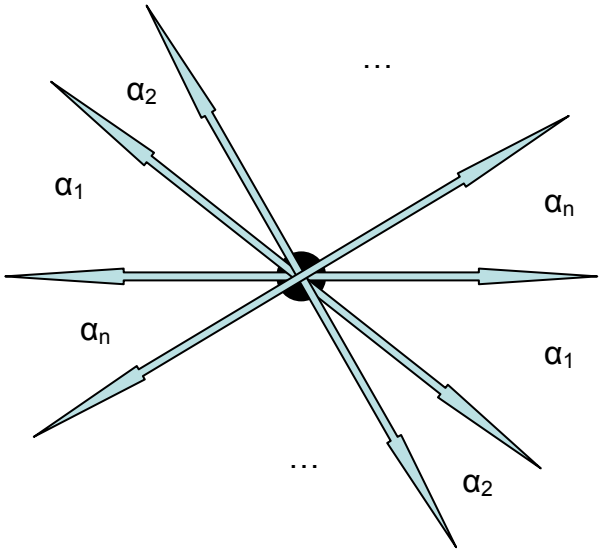


**Figure 20. Angular sections divided by the force lines**

**Steerability theorem:**

Let $m>2$, $l = k \leq m$ be natural numbers. Consider a planar (two degrees of mobility) position only serial or parallel manipulator with $m$ joints and $l$ brakes that is end-effector constrained. All the joints of a robot leg should be actuated if the leg is a serial redundant manipulator. Suppose that $\alpha_{max}$ is the largest angular value among the angles formed at the end-point by the $k$ generated force lines for the manipulator. If and only if $\alpha_{max} < \pi/2$, then the manipulator has universal full steerability for the considered configuration.

Proof of sufficiency:

$\alpha_{max} < \pi/2$ ➔ two-sided steerability exists for all end-point velocities

If the velocity vector $\vec{v}$ is not along the same line with any force lines, there exists an achievable force component $\vec{f}_a$ located on one side of the extension line of the velocity. Because $\alpha_{max} < \pi/2$, there must exist another force component $\vec{f}_b$ on the other side of the velocity (Figure 21). Two-sided steerability exists because the force components could steer current velocity to either side of $\vec{v}$.

If the velocity vector is along a force line and it is along the opposite direction of an achievable force component $\vec{v} = -\vec{f}_c$ (Figure 22), there exists one achievable force component on each side of the velocity, $\vec{f}_a$ and $\vec{f}_b$. Two-sided steerability exists because the force components could steer current velocity to either side of $\vec{v}$.

Sufficiency is proved.

Proof of Necessity:

$\alpha_{max} < \pi/2$ ← two-sided steerability exists for all end-point velocities

It is equivalent to prove the following problem:

$\alpha_{max} \geq \pi/2$ ➔ two-sided steerability doesn't exist for some end-point velocity

Suppose force lines labeled by $\vec{f}_a$, $\vec{f}_b$ are on the boundary lines of the largest angular section $\alpha_{max}$. A velocity vector is at the opposite direction of achievable force component $\vec{f}_a$ (Figure 23). If $\alpha_{max} > \pi/2$, no achievable force component exists on the lower side of the velocity. If $\alpha_{max} = \pi/2$, $\vec{f}_b$ will be perpendicular to the velocity. No force is achievable in the direction perpendicular to the velocity. The generated force could not steer the current velocity to its lower side. Two-sided steerability does not exist.

Necessity is proved.

Steerability theorem is proved.

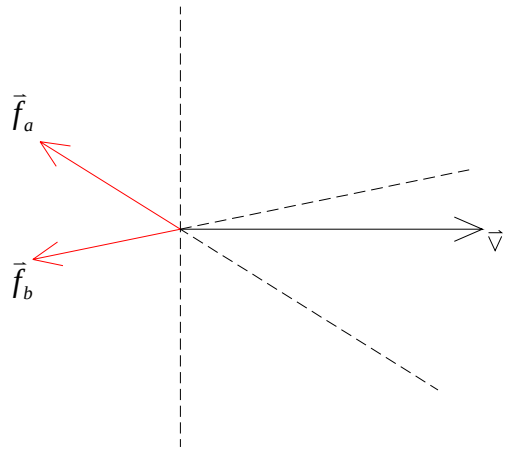


**Figure 21. Velocity not along the same line with any radial vectors**

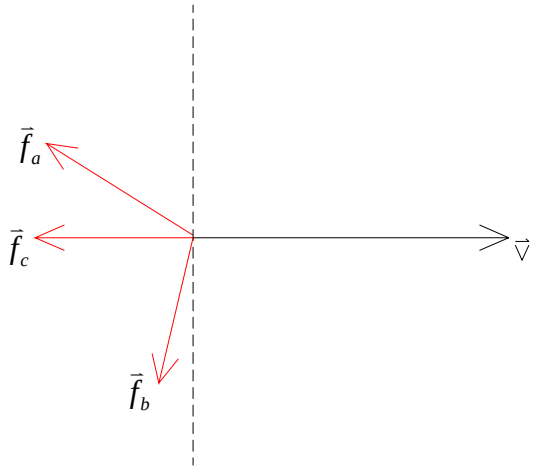


**Figure 22. Velocity along the same line with one radial vector**

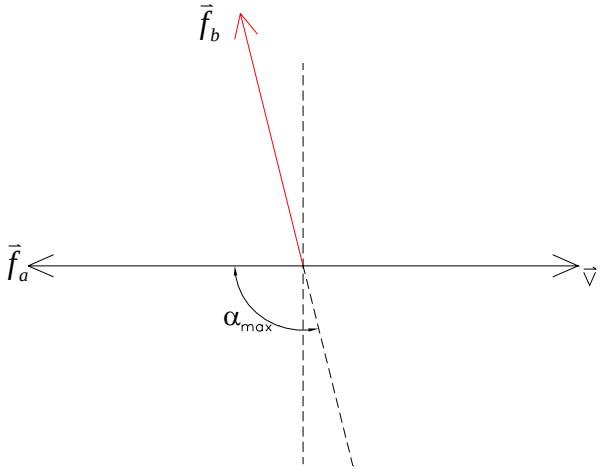


**Figure 23. Velocity along the same line with one radial vector and $\alpha_{max}$ not less than $\pi/2$**

The steerability theorem can be applied to the four-link four-joint parallel manipulator shown in Figure 16. If all the angles formed by the lines where the radial vectors lie are less than $\pi/2$, for example Figure 24 (a), universal full steerability exists at this configuration. If any angle formed by the lines where the radial vectors lie in are equal or larger than $\pi/2$, as for example Figure 24 (b) where the top and bottom angle are larger than $\pi/2$, full steerability is not guaranteed for all the possible velocities at this configuration and universal full steerability does not exist. Similar analyses were performed for all the possible robot configurations inside the reachable workspace. The values of $\alpha_{max}$ are shown in Figure 25 (a). The value of $\alpha_{max}$ is less than $\pi/2$ for any location within a certain region of the reachable workspace. The manipulator has universal full steerability if the end-point is inside this region. This region is defined as a **Universal Fully Steerable Workspace** or simply **Fully Steerable Workspace** for the manipulator. The parallel manipulator has two independent fully steerable workspaces A, B which is shown in Figure 25 (b). There is no singularity in any of the fully steerable workspaces. However the robot can not move from one fully steerable workspace to another without reaching a singularity.

The fully steerable workspace A in Figure 25 (b) is in a narrow strip shape and much smaller than B. It seems not as good as B for use in most of the applications. However the consideration of the possible interference of components, such as links, actuators etc. in fully steerable workspace B still makes A a reasonable choice. In order to utilize it, fully steerable workspace A has to be made relatively larger in the robot's reachable workspace. This could be done by changing the link lengths and the base joint spacing. The link and joint arrangement of MR P-TER (5-bar linkage) gives an example. MR P-

TER uses longer links connected to the end-point and smaller base joint spacing (Figure 7). The values of $\alpha_{max}$ is shown in Figure 26 (a) for all the location in its reachable workspace. The fully steerable workspace A in Figure 25 (b) corresponding to fully steerable workspace A in Figure 25 (b) is successfully enlarged within the manipulator's reachable workspace even though the size of the fully steerable workspace B (corresponding to fully steerable workspace B in Figure 25 b) is decreased. Different from the previously discussed parallel manipulator, singularities exist in fully steerable workspace A of MR P-TER. They separate fully steerable workspace A into two parts. The larger one occupies most of the fully steerable workspace A and therefore could serve as the outer boundary of possible operational workspace.

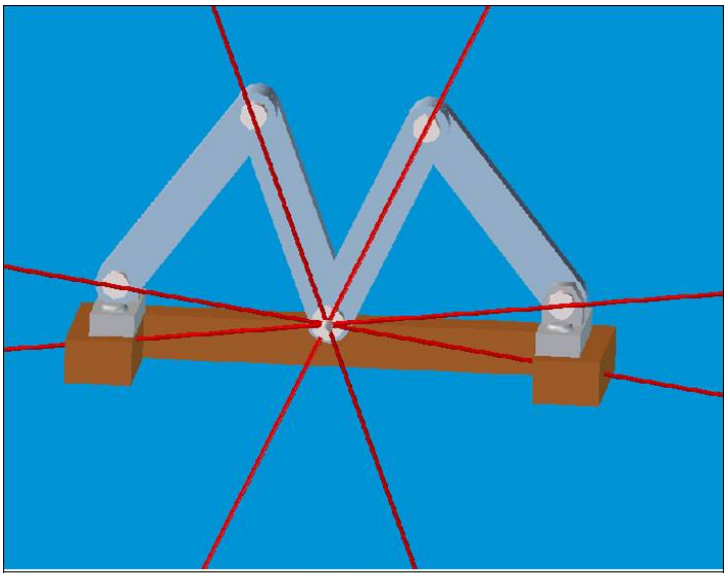

(a)

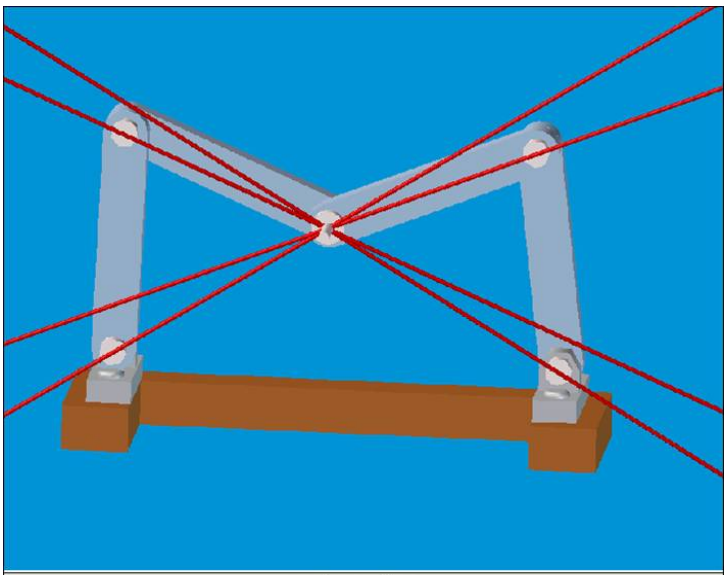

(b)

**Figure 24. Configuration with full steerability (a) and without (b)**

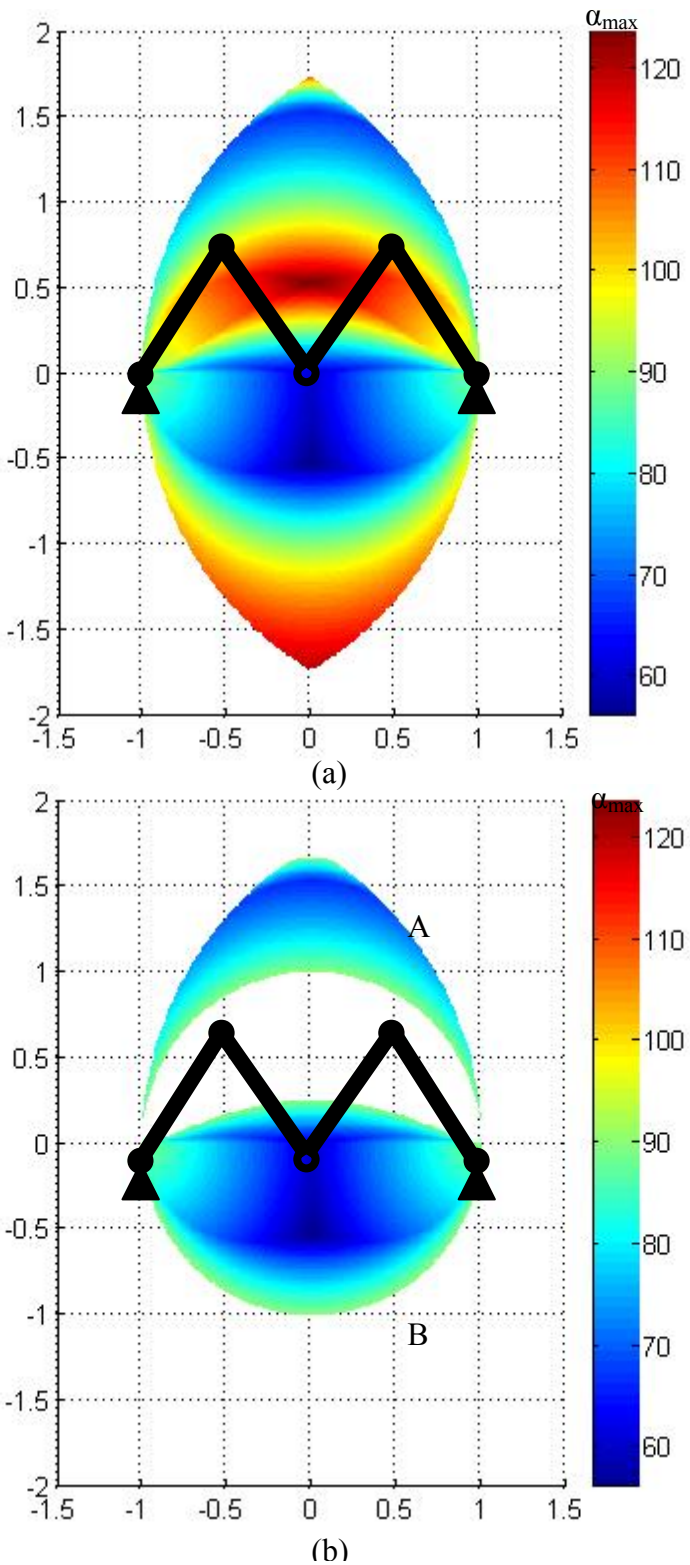


**Figure 25. (a) $\alpha_{max}$ and (b) fully steerable workspaces for a 4R parallel manipulator**

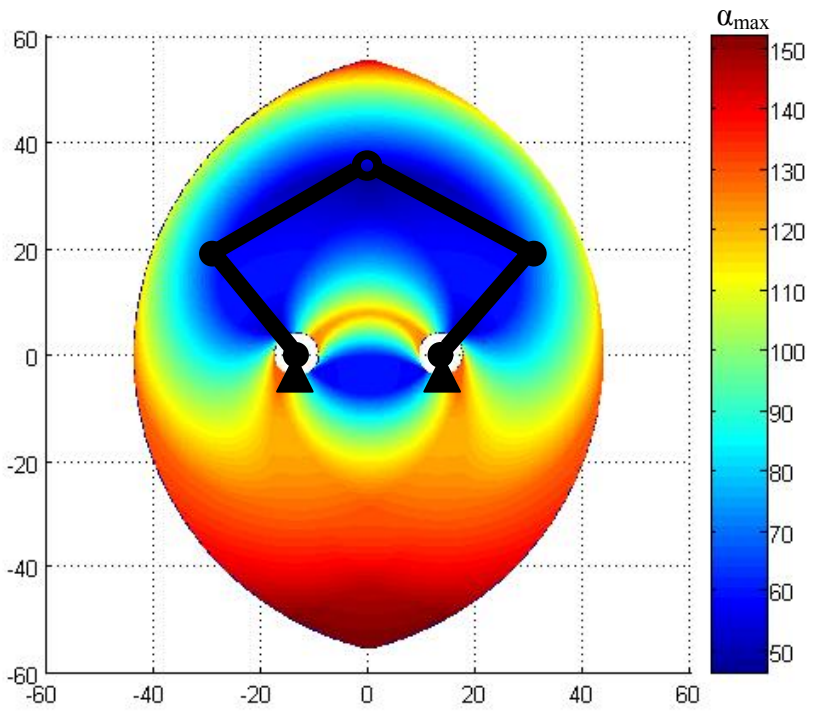


(a)

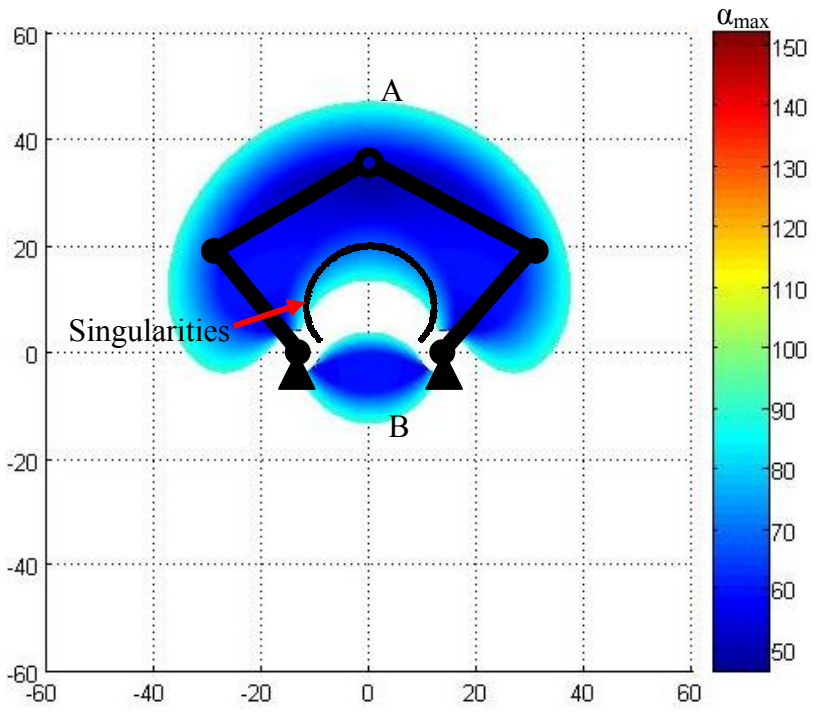


(b)

**Figure 26. (a) $\alpha_{max}$ and (b) fully steerable workspaces for MR P-TER (5-bar linkage configuration)**

## 4.6 Steerability Analyses for Previously Developed Devices

People want to use naturally safe haptic systems and therefore they started looking at dissipative passive haptic interfaces. Even without detailed knowledge of the control limitations of dissipative passive systems, researchers were still able to develop several devices to try to minimize the limitation. The design of the devices embodies their intelligence and experience. Study of these devices not only provides a chance to implement the steerability research but it benefits the device design by bringing in possible ideas in structure selection, linkage arrangements etc.

There are four developed dissipative passive haptic interfaces up until now as discussed in chapter 2. They are P-TER, Sakaguchi's four-link device, Matsuoka's 3D device and MR P-TER.

P-TER uses two electromagnetic friction brakes and two clutches to actuate a four link parallel mechanism. The clutches work similar to brakes by resisting relative motions. However a clutch needs an extra support while a brake does not. The actuation of a clutch has different effects in motion redirection in a dissipative passive haptic interface. All of these will be addressed in chapter 5.

The three-dimensional device by Matsuoka will be discussed in chapter 8 of three-dimensional interfaces and steerability.

Sakaguchi's four-link device has a structure similar to P-TER. The "9" shaped manipulator shown in Figure 27 has two actuators. The actuators are electro-rheological ER brakes. One is installed between the base and link 1. The other is installed between the base and link 3. All the other joints are not actuated.

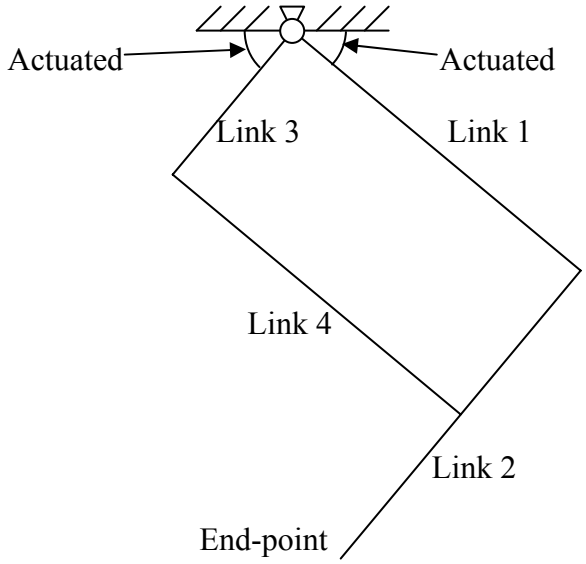


**Figure 27. Sakaguchi's four-link device**

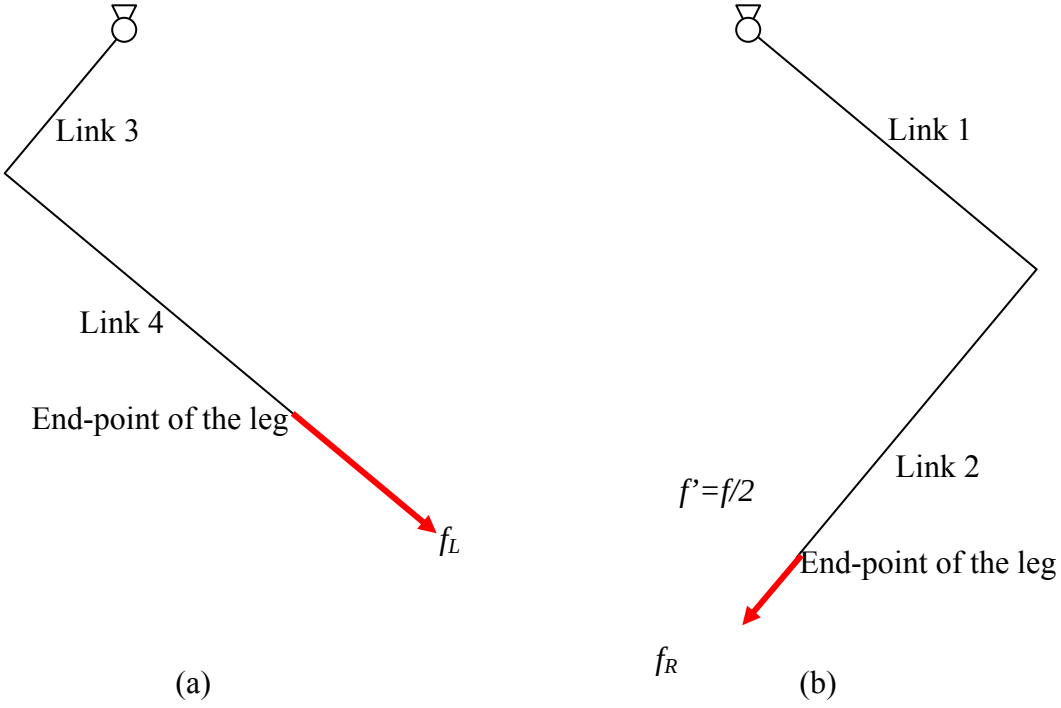


**Figure 28. Generated force from the legs of Sakaguchi's device**

Sakaguchi's device is a parallel mechanism with two legs. One leg consists of links 3 and 4; the other consists of links 1 and 2. Based on the previous analyses, it is not hard to point out that the generated force directions for both legs $f_L$ and $f_R$ at their end-points (Figure 28). The end-point of the left leg (Figure 28 a) is not the end-point of the manipulator. An equivalent force $f_L$' will be generated at the end-point of the manipulator from the actuation in the left leg.

Figure 29 (a) shows the free-body diagrams of the links in the right leg. At static equilibrium, link 1 can only sustain axial forces as shown. Because link 1 is parallel to link 4 and therefore $f_L$, there must be a force $f_L/2$ applied at the end-point in order to keep link 2 in equilibrium. Therefore the generated force at the end-point of the manipulator from the actuation of the brake between ground and link 3 is parallel to link 1 and 3. The magnitude is half of the generated force at the end-point of the left leg $f_L$ (Figure 29 b).

When considering the ability to generate end-point force, the Sakaguchi's device is similar to a diamond shaped parallel manipulator as shown in Figure 30 (b). And by using equation 4.4, the generated forces are the same for both manipulators under the same amount of actuations. The steerability, the ability to redirect motion, is the same for both structures.

Only two force components could be generated in Sakaguchi's device. It is a non-redundant manipulator. Based on earlier discussion, universal full steerability does not exist. However there are still advantages of using this parallel structure compared with the 2R serial structure as shown in Figure 10. This parallel structure could save potential trouble of installing a brake at a moving joint and therefore could reduce the internal dynamics of the interface. Also, when the two force components are perpendicular to

each other (when link 1 is perpendicular to link 3) the manipulator reaches its optimal steering configuration. Sakaguchi's device operates around this optimal steering configuration. The third, at the optimal configuration, the force manipulability ellipsoid is a circle [35]. The manipulator has equal ability to generate force in all directions when possible. At the same time the end-point can move isotropically along all directions in the 2D working space.

MR (Magneto-rheological) P-TER is the second generation dissipative passive haptic interface developed in IMDL. Magneto-rheological brakes replace the dry friction brakes/clutches. The link arrangement is also changed to simpler parallel structures.

MR P-TER has two structural arrangements. The diamond shaped structure was built earlier with three MR brakes installed at the following joints: #1 at joint 1 between link 1 and ground, #2 at joint 2 between link 1 and 2, #3 at joint 3 between link 3 and ground (Figure 31). The actuations of the brakes at joint 1, 2 and 3 generate force components $f_1$, $f_2$, and $f_3$, accordingly as shown.

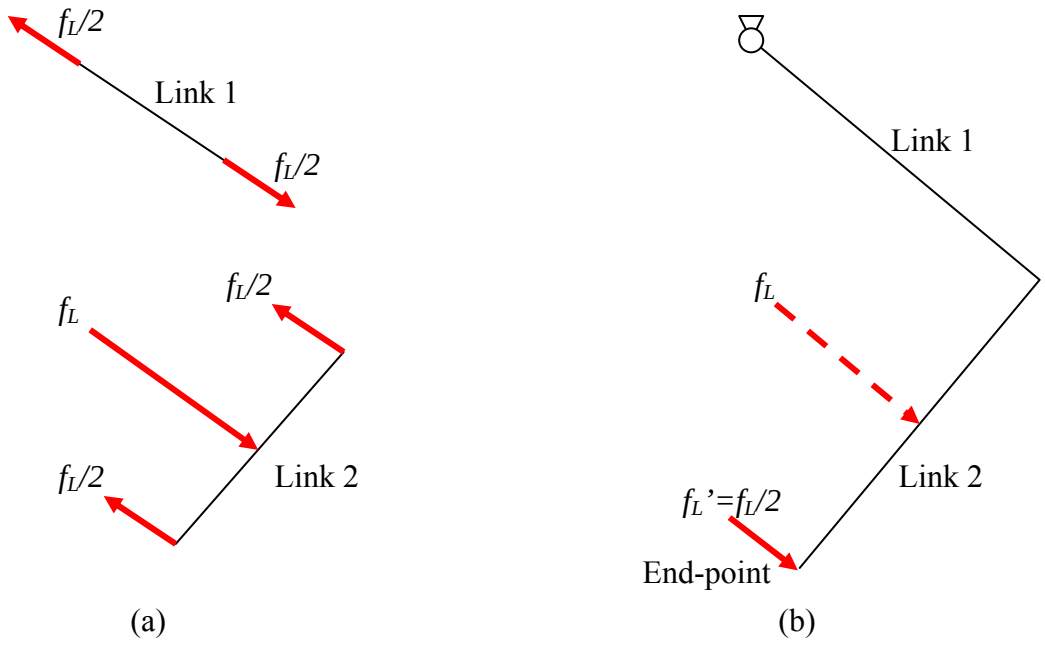


**Figure 29. Generated force from left leg at the end-point of the manipulator**

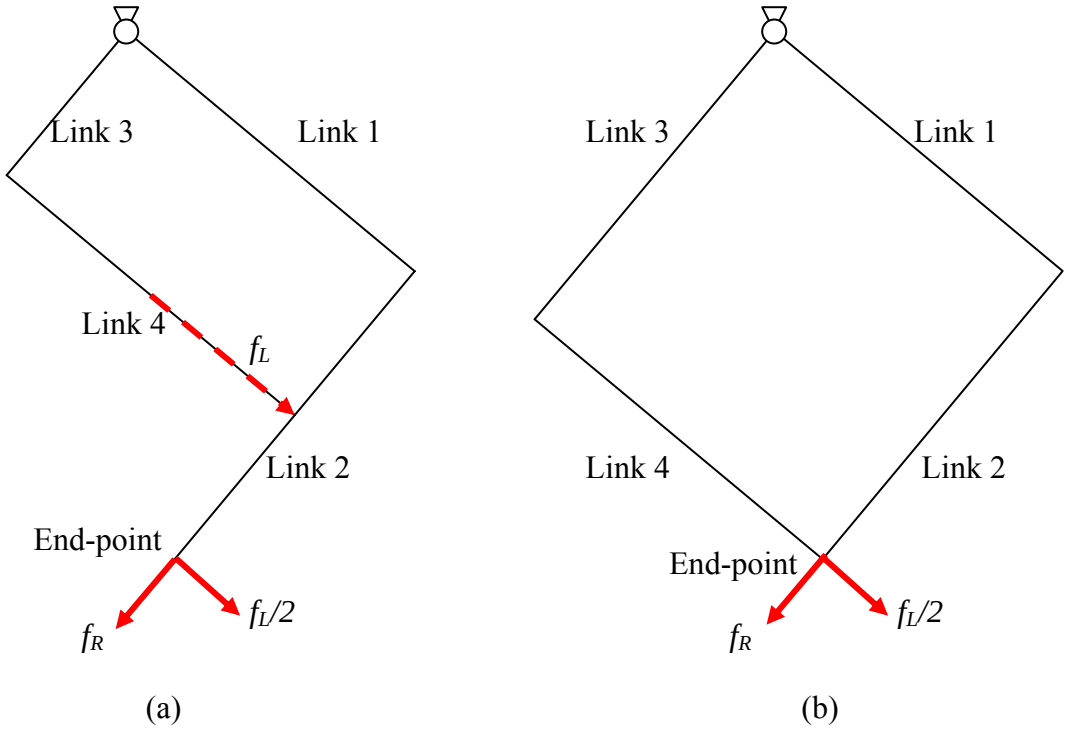


**Figure 30. (a) Sakaguchi's four-link device and (b) its steerability equivalent**

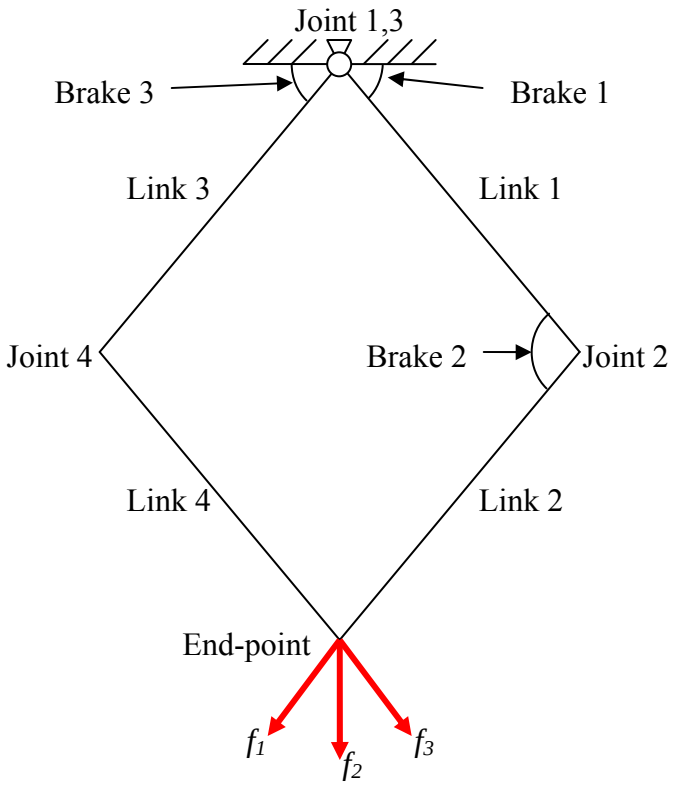


**Figure 31. Diamond shaped MR P-TER**

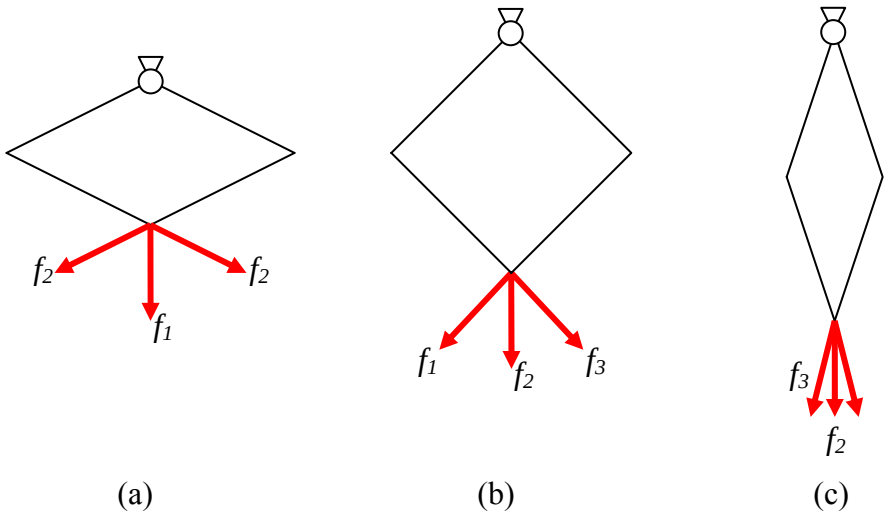


**Figure 32. Steerabilities of diamond shaped MR P-TER**

Because of the symmetry of the structure, the steerability of diamond shaped MR P-TER is only a function of the distance between the base and the end-point. If the distance is small, three generated force components $f_1$, $f_2$, and $f_3$ spread out on the two-dimensional plane (Figure 32 a). Based on the steerability theorem, the manipulator has universal full steerability. If the distance is too great, the three generated force components line up. The angles divided by the lines that the forces are on are either very small or very large (Figure 32 c). Full steerability does not exist for some velocities at this configuration. Between the two extremes, the distance reaches a critical value when the largest angle divided by the lines that the forces are on is $\pi/2$. The manipulator looses its full steerability if the distance increases. This is when the four links of the manipulator form a square (Figure 32 b).

Further steerability analysis shows the values of $\alpha_{max}$ for all the locations in its reachable workspace in Figure 33 (a). The results are symmetric about the base joint of the manipulator. The value of $\alpha_{max}$ decreases as the distance between the joint and the end-point increases at the beginning. It reaches its minimum of $\pi/3$ when the distance is equal to the link length and then starts to increase. When the distance reaches $\sqrt{2}$ times the link length (the links form a square), the value of $\alpha_{max}$ is equal to $\pi/2$. Universal full steerability does not exist for any point further away from the base joint. The fully steerable workspace is shown in Figure 33 (b). The analysis result agrees with our previous discussion.

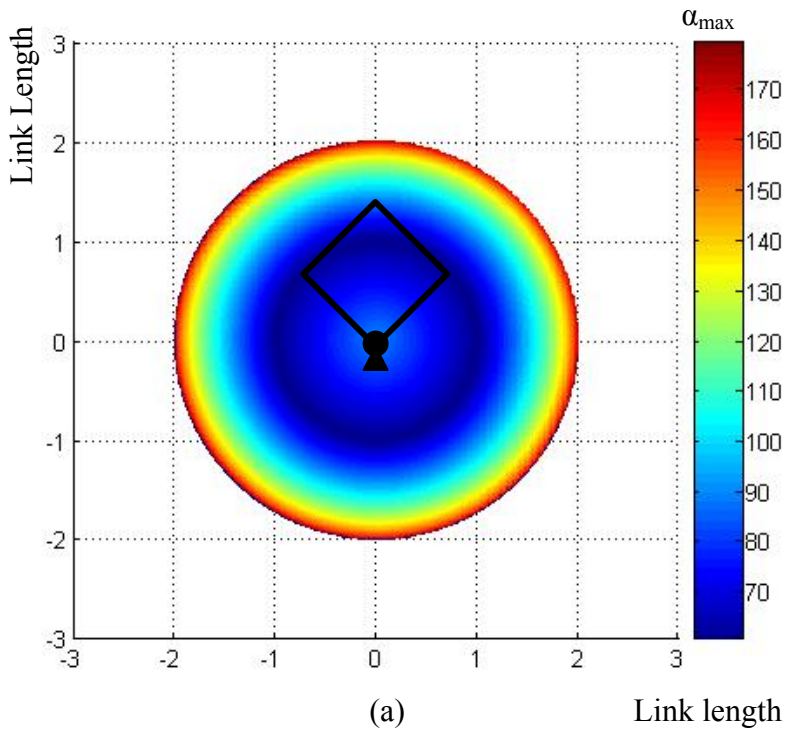


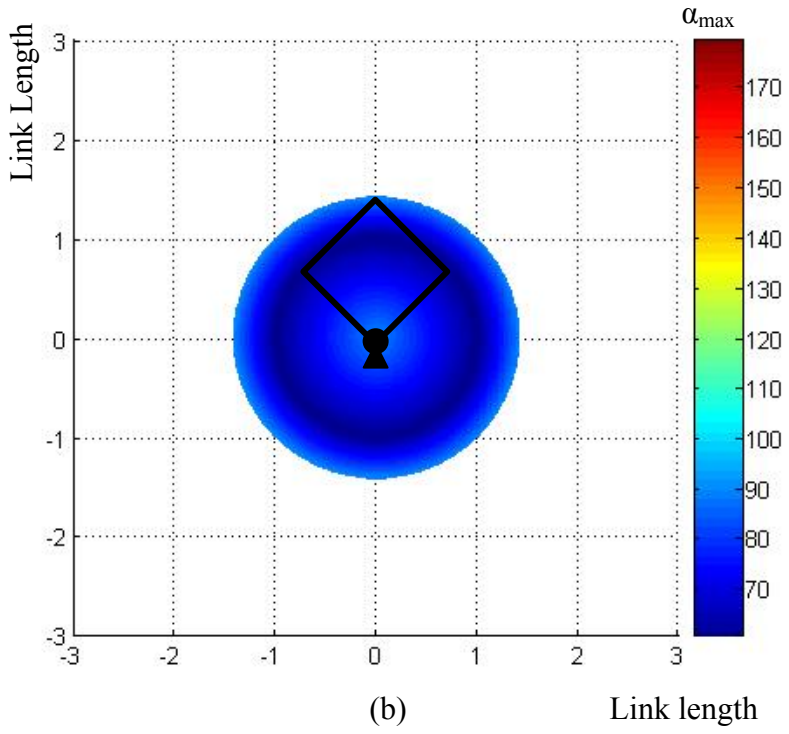


**Figure 33. (a) $\alpha_{max}$ and (b) fully steerable workspaces for diamond shaped MR P-TER**

The other structural arrangement of MR P-TER, the 5-bar linkage was discussed in section 4.5. Compared to the diamond-shaped structure, this new arrangement separates the two base joints. There is one moving joint (#4 in Figure 31) left un-actuated in the diamond-shaped MR P-TER. This is because the actuation of the brake at this joint would generate the same force as the brake installed at the other moving joint (#2 in Figure 31). By separating the two base joints, the forces generated by the actuators at the two moving joints can be distinguished from one other. Therefore one more brake was added to the fourth joint in the new arrangement. From our previous studies, adding more generated force components is a way to improve the manipulator's steerability. However there are also disadvantages of separating the base joints, such as smaller reachable workspace, complex singularities analysis etc.

After the change in the base joint spacing, the steerability for the manipulator changes dramatically from the diamond shaped structure. The unique fully steerable workspace splits into two and they are packed towards one side of the base joints. And within the fully steerable workspaces, the values of $\alpha_{max}$ are not quite evenly distributed. Figure 34 (a) shows the values of $\alpha_{max}$ and (b) shows the fully steerable workspaces.

The 5-bar linkage MR P-TER also shortened the links connecting the ground. Shortening links decrease the size of the manipulator's reachable workspace which could potentially reduce the size of the fully steerable workspaces. In this case, the sizes of the fully steerable workspaces for MR P-TER are smaller than those obtained with equal-size links (see Figure 34 b and Figure 26 b). However the values of $\alpha_{max}$ are much more evenly distributed over the fully steerable workspace for the manipulator design with

shorter links. The ability to redirect motion of this manipulator will not change as much as the one with equal size links.

The design of MR P-TER was optimized based on getting near equal angles between single-degree-of-freedom (SDOF) lines. Each SDOF line is perpendicular to a generated force component. The optimization is then equivalent to get near equal angles between the lines where the force components lie. In sense of steerability analysis, it is to minimize $\alpha_{max}$. The analysis using SDOF lines and the steerability analysis start from different concepts but end up with similar results.

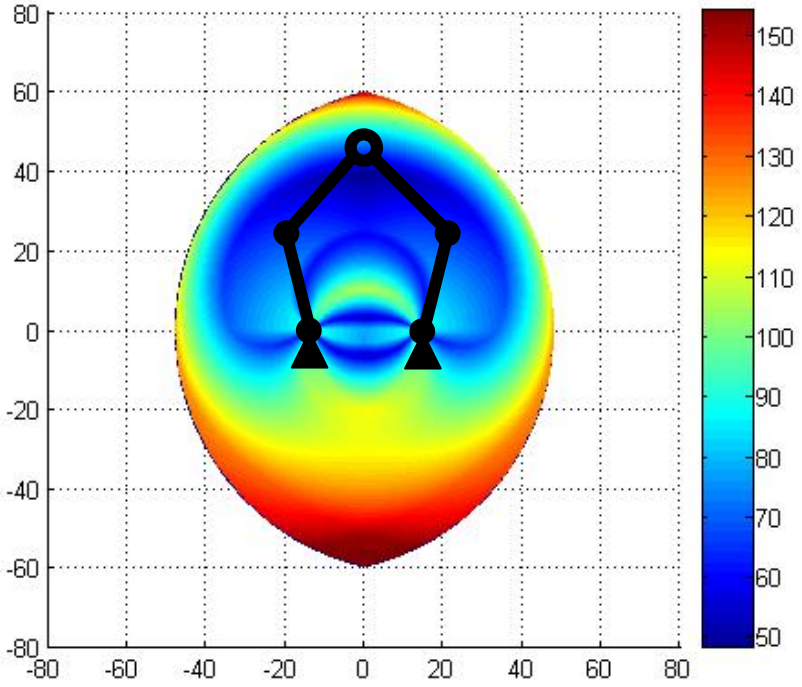


(a)

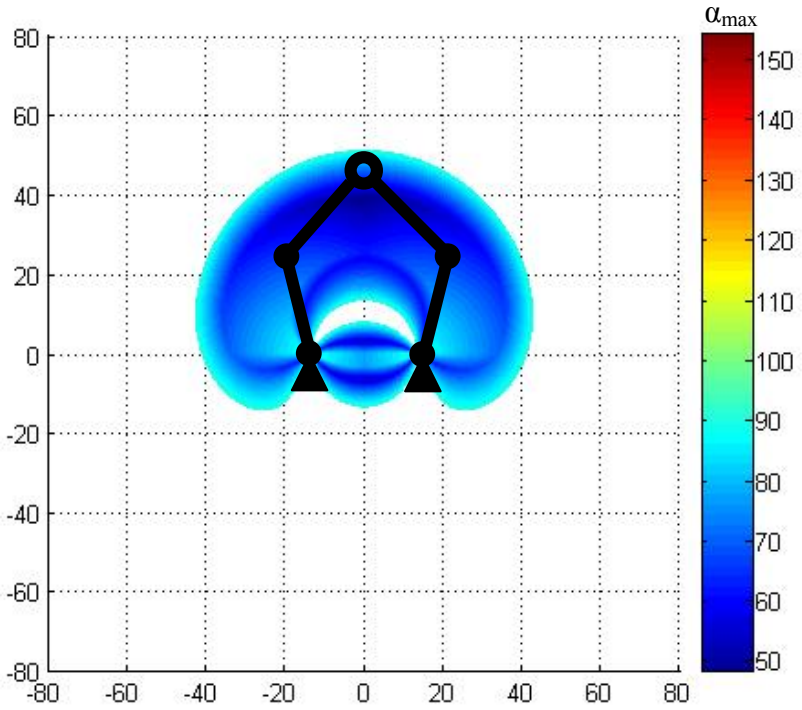


(b)

**Figure 34. (a) $\alpha_{max}$ and (b) fully steerable workspaces, MR P-TER with un-shortened links**

# 5. STEERABILITY ANAYSIS FOR PLANAR MANIPULATORS WITH CLUTCHES

As dissipative passive actuators, the names of brakes and clutches are sometime interchangeable for the actuators that could slow down the relative motion of two elements of a manipulator. Roughly speaking, a brake could be used for an actuator that can slow down or stop the motion of one link relative to another; while a clutch could be used when referring to an actuator that can connect and disconnect one link to another. In this research a clutch is considered as a brake plus a gearbox.

The passive actuators used in P-TER are two brakes and two clutches (Figure 35). Each one of the two brakes in P-TER couples one moving link to the ground link. The actuation of one of the brakes will slow down or stop the rotation of one link relative to the ground. The two links are also coupled to each other through two clutches. Each clutch has two disks. In the direct coupling configuration, the two links are connected directly to the two disks of one clutch. The actuation of the clutch is slowing down the relative rotation of the two clutch disks. Therefore the relative rotation which is the speed difference of the two links is reduced. In the inverse coupling configuration, a bevel gear differential is used to change the rotation direction of one shaft. The rotation speed of the corresponding clutch disk is the opposite of the link speed. The actuation of the clutch reduces the summation of speeds of the two links.

The introduction of the inverse coupling of the two links brings extra control abilities into the manipulator. The effect of the inverse coupling will be analyzed as an advantage of clutches.

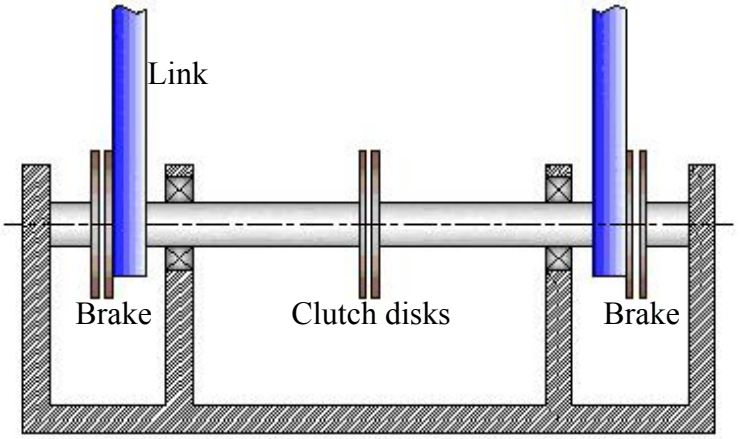


(a) Direct coupling

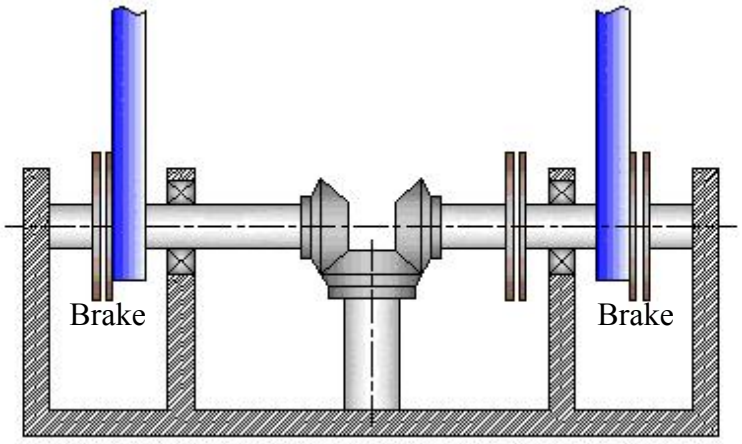


(b) Inverse coupling

**Figure 35. Brakes and clutches in P-TER, (a) direct coupling configuration and (b) inverse coupling configuration**

## 5.1 Force Generation Analysis for a Clutched Structure

Similar to a brake, the actuation of a clutch could also generate a force at the end-point of the manipulator. The generated force could be used to redirect existing motion at the end-point of the manipulator. The generated force can be found through the following analyses.

The use of a clutch generates a parallel structure in a robot system. The parallel structure needs also to be end-effector constrained in order to analyze the generated force as discussed in chapter 4. Following the definition of an end-effector constrained structure, the simplest possible configuration for a planar robot with a clutch would be a robot with the link supporting the clutch grounded while the other two links, which are connecting with the clutch disks, are in motion. The two movable links are the starting links for the two branches of the parallel robot. Each branch is required to be fully constrained too. Therefore each of the two links is a two-link manipulator such as the one shown in Figure 10 in the simplest configuration.

The simplest robot system with a clutch is shown in Figure 36. Links and joints are named as labeled. Links 1 and 4 are connected with two sets of disks (directly and through a gear chain) of a clutch which is supported by the ground. No other joint is actuated. Link 2 connects with link 1. Link 3 connects with link 4. Links 2 and 3 connect with each other and form the end-point. The lengths of the links are $l_1$, $l_2$, $l_3$ and $l_4$. The parameters of the manipulator are defined following the Denavit-Hartenberg (distal variant) notation. Define $\theta_{1e}$ as the angle of vector from joint 1 to the end-point and $l_{1e}$ as

the length of the vector; $\theta_{4e}$ as the angle of vector from joint 4 to end-point and $l_{4e}$ as the length of the vector. Joints 1 and joint 4 overlap, therefore

$$l_{1e} = l_{4e} \tag{5.1}$$

$$\theta_{1e} = \theta_{4e} \tag{5.2}$$

The parameters can be seen in Figure 37.

### *5.1.1 The Lock-Joint Velocity of a Clutch*

Each clutch disk is connected with one manipulator link directly or through a gear chain. The relationship between the rotational speed of a clutch disk $\dot{\theta}_i'$ with respect to the support link and the speed of the corresponding link $\dot{\theta}_i$ with respect to the support link can be expressed as:

$$\dot{\theta}_i' = a_i \dot{\theta}_i \tag{5.3}$$

where $a_i \neq 0$ is the gear ratio ($i$ = 1, 4).

The clutch is working in direct coupling configuration if $a_1 a_4 > 0$; it is working in inverse coupling configuration if $a_1 a_4 < 0$. For example, the gear ratios in P-TER for the two links connecting with the clutch are $a_1 = 1$, $a_4 = 1$ in the direct coupling case and $a_1 = -1$, $a_4 = 1$ in the inverse coupling case.

The angular velocities of the links are $\dot{\theta}_1$, $\dot{\theta}_2$, $\dot{\theta}_3$ and $\dot{\theta}_4$ where $\dot{\theta}_1 = \dot{\theta}_1' / a_1$, $\dot{\theta}_4 = \dot{\theta}_4' / a_4$. $\dot{\theta}_2$ and $\dot{\theta}_3$ are not independent variables and can be also determined from $\dot{\theta}_1$ and $\dot{\theta}_4$.

Assume links 2 and 3 are located at one side of the wrench singularity (Figure 38) which is further away from the base joint. The velocity of the manipulator's end-point is

$$\vec{v}_e = \dot{\theta}_1 l_{1e} \hat{v}_1 + \dot{\theta}_2 l_2 \hat{v}_2 = \dot{\theta}_4 l_{4e} \hat{v}_4 + \dot{\theta}_3 l_3 \hat{v}_3 \tag{5.4}$$

where $\hat{v}_i$ is the unit tangential vectors for joint *i*, *i*=1, 2, 3 and 4 which is shown in Figure 37.

Because joint 1 overlaps with joint 4

$$\hat{v}_1 = \hat{v}_4 \tag{5.5}$$

If $\dot{\theta}_1 = \dot{\theta}_4$, $\dot{\theta}_2$ and $\dot{\theta}_3$ vanish.

If $\dot{\theta}_1 > \dot{\theta}_4$, the relationship of the velocity vectors can be shown in Figure 39, where

$$\alpha = -\theta_1 - \theta_2 + \theta_{1e} \tag{5.6}$$

$$\beta = \theta_3 + \theta_4 - \theta_{4e} \tag{5.7}$$

The following expression can be written based on the Law of Sines:

$$\frac{\dot{\theta}_1 l_{1e} - \dot{\theta}_4 l_{4e}}{\sin(\alpha + \beta)} = \frac{-\dot{\theta}_2 l_2}{\sin \beta} = \frac{\dot{\theta}_3 l_3}{\sin \alpha} \tag{5.8}$$

Therefore,

$$\dot{\theta}_3 l_3 = \frac{\sin \alpha}{\sin(\alpha + \beta)} \left( \dot{\theta}_1 l_{1e} - \dot{\theta}_4 l_{4e} \right) \tag{5.9}$$

Substitute equation 5.9 into equation 5.4

$$\vec{v}_e = \dot{\theta}_4 l_{4e} \hat{v}_4 + \frac{\sin \alpha}{\sin(\alpha + \beta)} \left( \dot{\theta}_1 l_{1e} - \dot{\theta}_4 l_{4e} \right) \hat{v}_3 \tag{5.10}$$

Equation 5.10 is also valid when $\dot{\theta}_1 < \dot{\theta}_4$.

If we assume links 2 and 3 are located at the other side of the wrench singularity (opposite to the singularity shown in Figure 38), which is closer to the base joint, equation 5.10 still holds if equations 5.6 and 5.7 are replaced by equations 5.11 and 5.12 as follows.

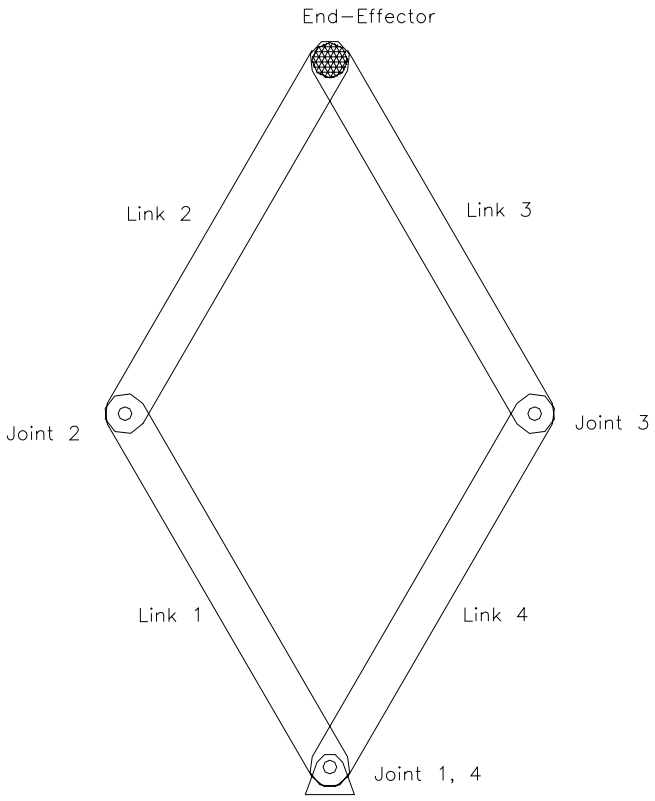


**Figure 36. The simplest robot system with clutch**

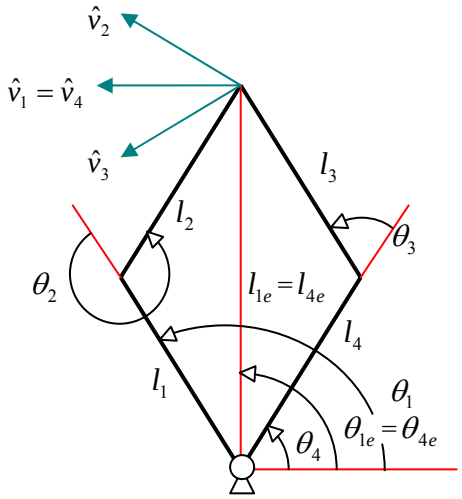


**Figure 37. Parameters for the clutched structure**

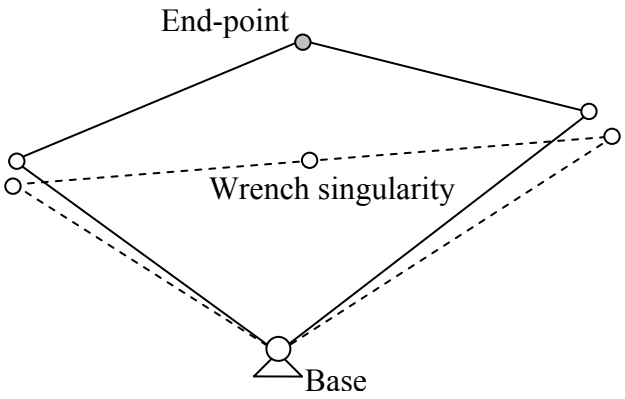


**Figure 38. Wrench singularity for clutched structure**

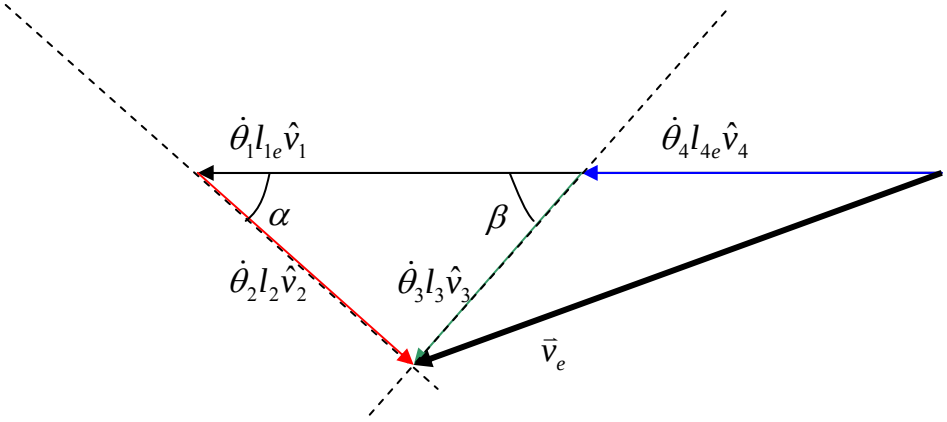


**Figure 39. Relationship of the velocity vectors**

$$\alpha = \theta_1 + \theta_2 + \theta_{1e} \tag{5.11}$$

$$\beta = -\theta_3 - \theta_4 - \theta_{4e} \tag{5.12}$$

If the two clutch disks rotate at the same speed

$$\dot{\theta}_1' = \dot{\theta}_4' \tag{5.13}$$

The parallel structure with two degrees of freedom turns into a one-degree-of-freedom structure. The direction of this reduced degree of freedom at the manipulator end-point is defined as the clutch's **lock-joint velocity direction**.

From equation 5.10 the end-point velocity when the clutch is locked is:

$$\vec{v}_{LJ} = \dot{\theta}_4 l_{4e}\left(\hat{v}_4 + \frac{a_4 - a_1}{a_1}\frac{\sin\alpha}{\sin(\alpha+\beta)}\hat{v}_3\right) \tag{5.14}$$

Define

$$\hat{v}_{LJ} = \frac{\vec{v}_{LJ}}{\|\vec{v}_{LJ}\|} \tag{5.15}$$

as the lock-joint velocity direction of the manipulator with clutch.

### *5.1.2 Generated Force Direction of a Clutch*

When the two clutch disks rotating at different speeds approach to each other under a certain amount of axial compression load, equal amounts of torque are applied to the disks. The torques are in opposite directions of the relative disk speeds. The torques work to slow down the rotation of one disk relative to another. The torques can be expressed as:

$$\tau_1' = -\text{sgn}\left(\dot{\theta}_1' - \dot{\theta}_4'\right)|\tau| \tag{5.16}$$

$$\tau_4' = -\text{sgn}\left(\dot{\theta}_4' - \dot{\theta}_1'\right)|\tau| = -\tau_1' \tag{5.17}$$

The torques applied onto the links will then be expressed as:

$$\tau_1 = a_1\tau_1' = -a_1\,\mathrm{sgn}\left(\dot{\theta}_1' - \dot{\theta}_4'\right)|\tau| = -a_1\,\mathrm{sgn}\left(a_1\dot{\theta}_1 - a_4\dot{\theta}_4\right)|\tau| \tag{5.18}$$

$$\tau_4 = a_4\tau_4' = -a_4\,\mathrm{sgn}\left(\dot{\theta}_4' - \dot{\theta}_1'\right)|\tau| == -a_4\,\mathrm{sgn}\left(a_4\dot{\theta}_4 - a_1\dot{\theta}_1\right)|\tau| \tag{5.19}$$

The parallel system could be considered as the combination of two sub robot systems (Figure 40). When the clutch is activated, torques $\tau_1$ and $\tau_4$ will be applied to the 1st joints of both robots. Force will be generated at the end-point for each sub robot as discussed in chapter 4. The overall force generated for the parallel system is the superposition of the two force components from each sub robot.

From equation 4.2, the force component generated by the left branch can be written as

$$\vec{F}_L = \frac{1}{l_1 s_2}\tau_1 \hat{f}_2 \tag{5.20}$$

And the force component generated by the right branch is

$$\vec{F}_R = \frac{1}{l_4 s_3}\tau_4 \hat{f}_3 \tag{5.21}$$

$\hat{f}_2$ and $\hat{f}_3$ are shown in Figure 40.

The generated force of the manipulator can be expressed as

$$\vec{F}_c = \vec{F}_L + \vec{F}_R = -\frac{a_1}{l_1 s_2}\tau_4' \hat{f}_2 + \frac{a_4}{l_4 s_3}\tau_4' \hat{f}_3 \tag{5.22}$$

Define $\hat{f}_c = \vec{F}_c / \left\|\vec{F}_c\right\|$ as the generated force direction vector.

The generated force and lock-joint velocity directions are perpendicular to each other because their inner product

$$\hat{f}_c \cdot \hat{v}_{LJ} = \frac{\vec{F}_c \cdot \vec{v}_{LJ}}{\left\|\vec{F}_c\right\|\left\|\vec{v}_{LJ}\right\|} = \frac{\dot{\theta}_4 l_{4e}\tau_4}{\left\|\vec{F}_c\right\|\left\|\vec{v}_{LJ}\right\|}\left(\frac{\sin\alpha}{l_1 s_2} + \frac{\sin\beta}{l_4 s_3}\right) = 0 \tag{5.23}$$

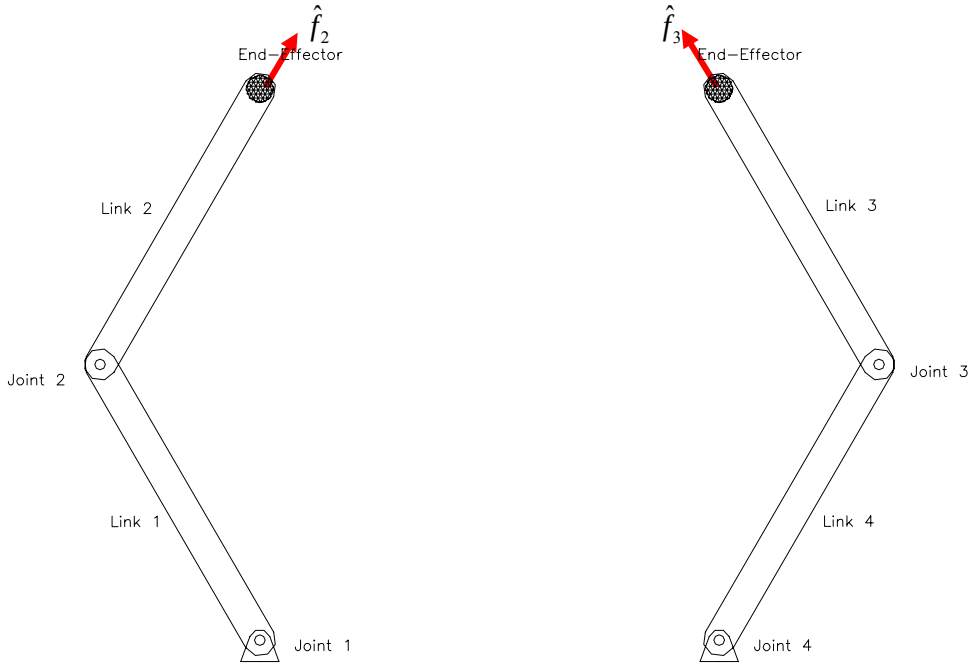


**Figure 40. Two sub robots for the clutched manipulator**

where

$$\frac{\sin\alpha}{l_1 s_2} + \frac{\sin\beta}{l_4 s_3} = 0 \tag{5.24}$$

Proof of equation 5.24 could be found in appendix. The definitions of α and β are the same as in equation 5.6 and 5.7.

### *5.1.3 Examples of the Generated Force of a Clutched Structure*

A clutch and the resulting parallel structure in a dissipative passive haptic interface bring in extra ability in force generation. The steerability of the haptic interface could be improved with the extra ability. The generated force of a simplest diamond-shaped planar manipulator is presented as follows.

A four-link manipulator with a shape similar to that shown in Figure 36 was studied. The link lengths are equal and joints 1 and 4 are coaxial. The wrench singularity

coincides with a twist singularity, which is when the end point overlaps with the base joint. From the geometries this occurs when,

$$\theta_2 = -\theta_3 \tag{5.25}$$

$$\alpha = \beta = \theta_3 / 2 \tag{5.26}$$

Then, the lock-joint velocity is

$$\vec{v}_{LJ} = \dot{\theta}_4 l\left( (1+\cos\theta_3)\hat{v}_4 + \frac{a_4 - a_1}{a_1}\hat{v}_3 \right) \tag{5.27}$$

And the generated force is

$$\vec{F}_c = \frac{\tau_4'}{ls_3}\left(a_1 \hat{f}_2 + a_4 \hat{f}_3\right) \tag{5.28}$$

Even though perpendicular to each other, the generated force and primary velocity directions change when the gear ratios change. In order to better visualize the vectors, the special cases similar to those in P-TER are discussed first.

A simple case in the direct coupling configuration is when $a_1 = a_4$ (in P-TER $a_1 = a_4 = 1$). When the clutch is locked, the diamond shape formed by the four links is fixed. The manipulator moves like a 1R structure. The velocity direction is perpendicular to the vector from base to endpoint. It is the lock-joint velocity direction, which is $\hat{v}_{LJ} = \hat{v}_4$. The generated force is $\vec{F}_c = \frac{a_4\tau_4'}{ls_3}\left(\hat{f}_2 + \hat{f}_3\right)$ which is along the vector from base to endpoint. So $\hat{f}_c = \hat{f}_4$ as shown in Figure 41. The force generation capability of the clutch is equivalent to a virtual brake installed at joint 2 (or joint 3, see Figure 36).

Changing the ratio of gear ratios $a_4 / a_1$ will change the lock-joint velocity direction and generated force direction. The force generation capability of the clutch is still

equivalent to a virtual brake installed at joint 2 (or joint 3). However the base joint of the equivalent manipulator, joint 1 (or joint 4) has to shift away from its original position. If $a_4 / a_1 \Rightarrow 0$, $\hat{f}_c \Rightarrow \hat{f}_4$, and the base shifts towards the extension line of link 2. If $a_4 / a_1 \Rightarrow \infty$, $\hat{f}_c \Rightarrow \hat{f}_2$, and the base shifts towards the extension line of link 3. Figure 41 shows the changes of the base joints in the equivalent manipulator structure.

A simple case of inverse coupling configuration is when $-a_1 = a_4$ (in P-TER $-a_1 = a_4 = 1$). When the clutch is locked, link 1 and link 4 can only move with the same speed but in opposite directions. The manipulator moves like a one-degree-of-freedom structure with a prismatic joint. The velocity direction is along the vector from the base to the endpoint. It is the lock-joint velocity direction, which is $\hat{v}_{LJ} = \hat{f}_4$. The generated force is $\vec{F}_c = \frac{a_4 \tau_4'}{l s_3}\left(-\hat{f}_2 + \hat{f}_3\right)$ which is perpendicular to the vector from base to endpoint. That is $\hat{f}_c = \hat{v}_4$ (Figure 42). Considering the force generation capability, the clutch is equivalent to a brake at base joint 1 (or joint 4) with a position shift of joint 2 (or joint 3). Joint 2 (or joint 3) is shifting to the extension line of $\hat{f}_c$.

Changing the ratio of gear ratios $a_4 / a_1$ will also change the lock-joint velocity direction and the generated force direction in the inverse coupling situation. The force generation capability of the clutch is still equivalent to a brake at base joint 1 (or joint 4) with a position shift of joint 2 (or joint 3). Joint 2 (or joint 3) is still shifted to the extension line of $\hat{f}_c$ from its original position. If $a_4 / a_1 \Rightarrow 0$, $\hat{f}_c \Rightarrow -\hat{f}_2$. Joint 2 does not shift and joint 3 shifts to the extension line of $\hat{f}_2$. if $a_4 / a_1 \Rightarrow \infty$, $\hat{f}_c \Rightarrow \hat{f}_3$. Joint 3 does not shift and joint 2 shifts to the extension line of $\hat{f}_3$. These are shown in Figure 42.

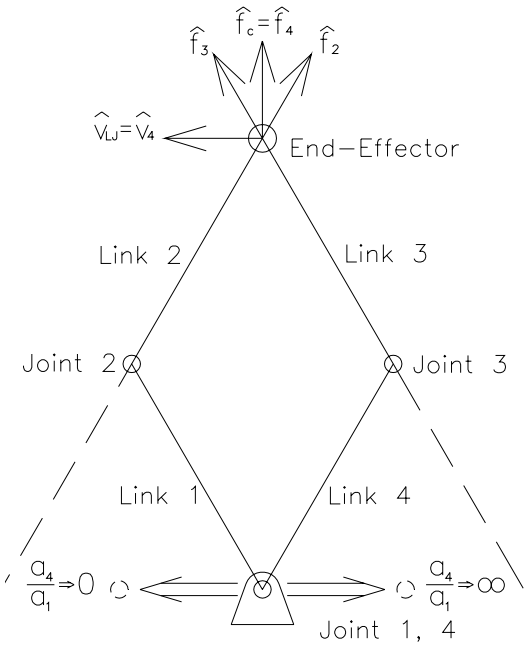


**Figure 41. Direct coupling for diamond shaped manipulator**

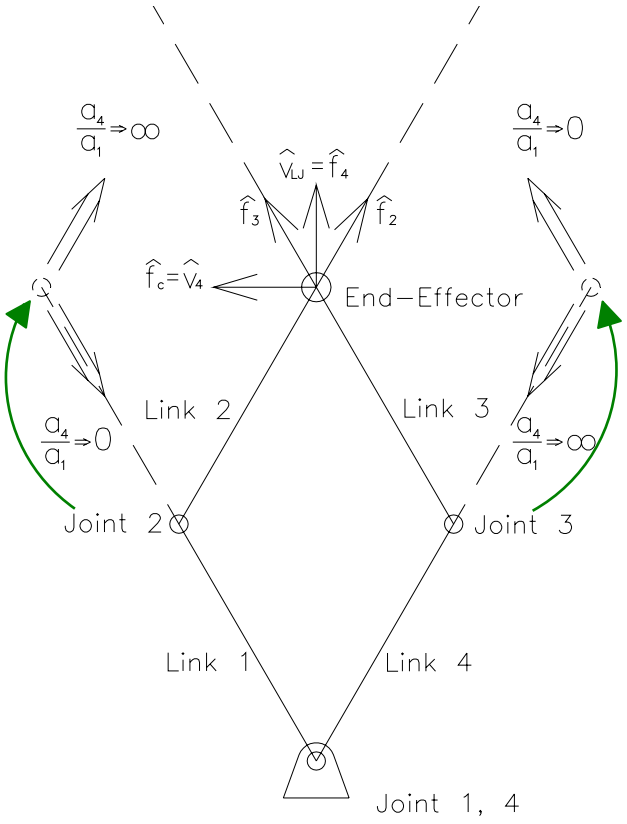


**Figure 42. Inverse coupling for diamond shaped manipulator**

In either direct or inverse coupling configuration of the clutched structure, the clutch function is equivalent to a virtual joint actuated with a brake in case of the force generation capability. The virtual joint could be placed on some location of the manipulator or even outside the manipulator. And the position of the virtual joint could be changed by adjusting the gear ratios.

## 5.2 Steerability of a Manipulator with Clutch

By using the virtual joints with brakes, the clutched manipulator is transferred into a virtual manipulator using only brakes as actuators. The two manipulators are equivalent to each other in case of the force generation capabilities, and therefore the steerabilities. The steerability of the clutched structure could then be analyzed based on the steerability theorem developed in chapter 4.

The diamond shaped manipulator discussed in 5.1.3 is used here again as an example for the steerability discussion. Other than the clutch, two brakes are also used in the manipulator. One is installed between the base and link 1. The other is installed between the base and link 4 (Figure 36).

### *5.2.1 Steerability for a Manipulator with Directly Coupled Clutch*

If the gear ratios of the clutch are the same, $a_1 = a_4$, the generated force from the clutch $\hat{f}_c$ will be along the vector from base joint to the end-point. And the generated force from the two brakes $\hat{f}_2$, $\hat{f}_3$ will be along the links connecting the end-point. The force vectors could be seen in Figure 43.

Having three force component vectors, the diamond shaped manipulator could have configurations with universal full steerabilities. For example as shown in Figure 43 (a), if

the end-point of the manipulator is close to the base joint, the three force components divide the 2D plane evenly into six angles. Universal full steerability exists for this configuration. However if the end-point is far away from the base joint as shown in Figure 43 (b), the value of $\alpha_{max}$ is larger than $\pi/2$. Universal full steerability does not exist.

Looking back at the analysis for diamond shaped MR P-TER (Figure 31, Figure 32), the generated force components for both structures are exactly the same. Therefore the steerabilities of both manipulators are the same. So Figure 33 also illustrates the steerability of the manipulator with two brakes and one directly coupled clutch.

### *5.2.2 Steerability for a Manipulator with Inversely Coupled Clutch*

If the gear ratios of the clutch are opposite to each other, $-a_1 = a_4$, the generated force from the clutch $\hat{f}_c$ will be perpendicular to the vector from the base joint to the end-point. The generated force from the two brakes $\hat{f}_2$, $\hat{f}_3$ will still be along the links connecting the end-point. The force vectors could be seen in Figure 44.

Similar to the direct coupling case, the diamond shaped manipulator could also have configurations with universal full steerabilities because of the extra force component. For example as shown in Figure 44 (b), if the end-point of the manipulator is far away from the base joint, the three force components divide the 2D plane evenly into six angles. Universal full steerability exists for this configuration. However if the end-point is close to the base joint as shown in Figure 44 (a), the value of $\alpha_{max}$ is larger than $\pi/2$. In such a case universal full steerability does not exist.

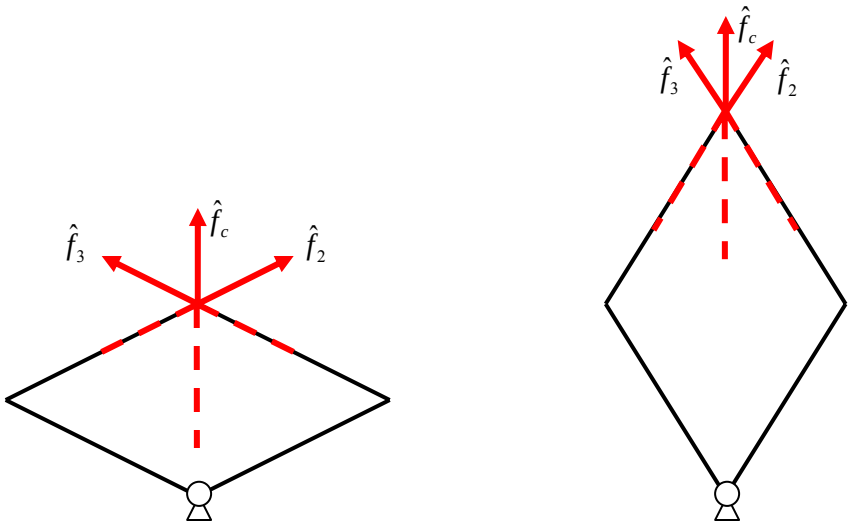


**Figure 43. Generated force components of diamond shaped manipulator with one directly coupled clutch and two brakes, (a) end-point is close to the base and (b) end-point is far away from the base**

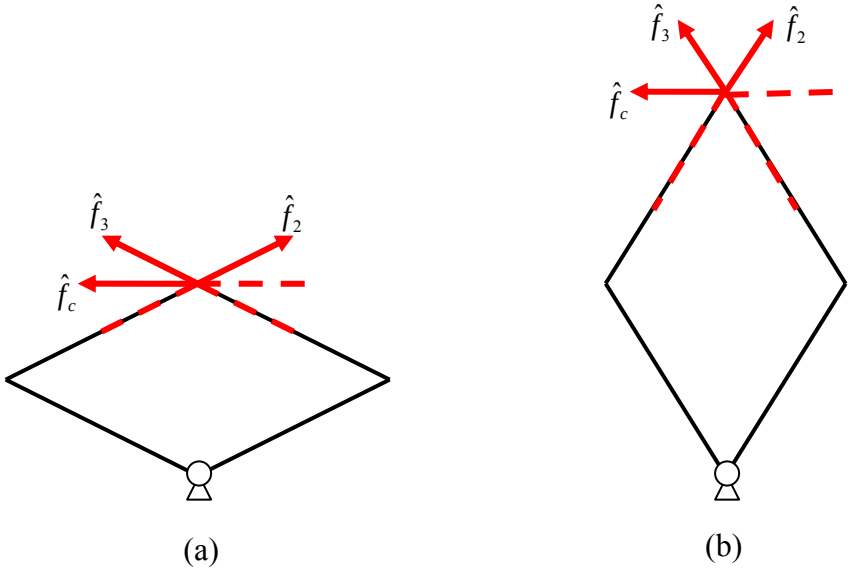


**Figure 44. Generated force components of diamond shaped manipulator with one inversely coupled clutch and two brakes, (a) end-point is close to the base and (b) end-point is far away from the base**

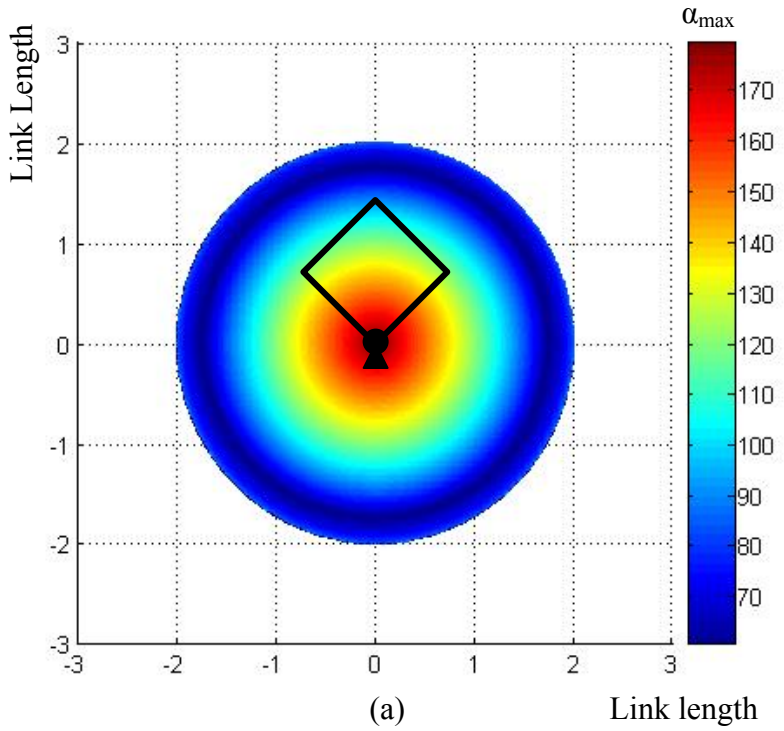


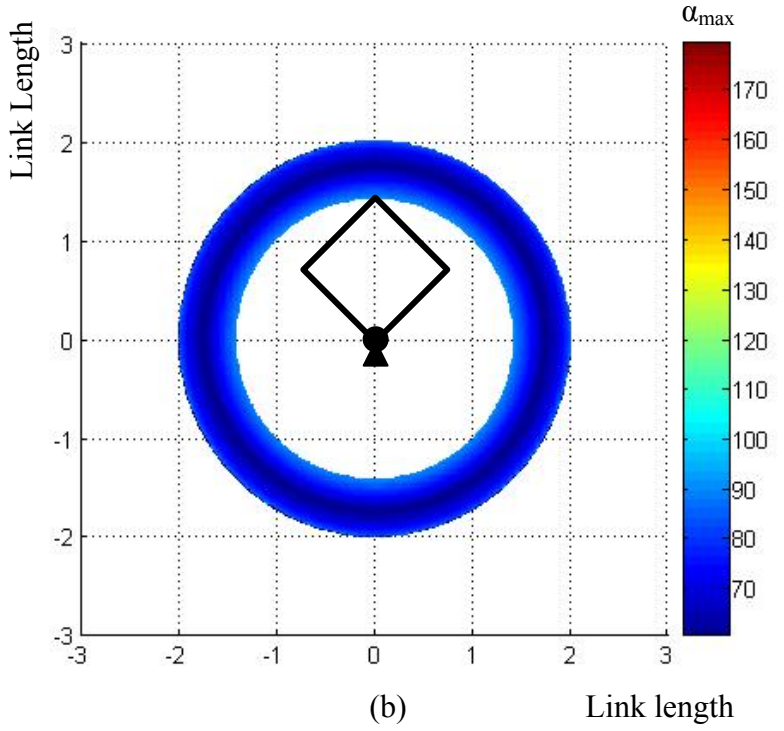


**Figure 45. (a) $\alpha_{max}$ and (b) fully steerable workspaces for a manipulator with 2 brakes and one inversely coupled clutch**

The values of $\alpha_{max}$ for all the locations in its reachable workspace are shown in Figure 45 (a). Different from the directly coupled structure, the values of $\alpha_{max}$ decrease from the maximum value, $\pi$, when the end-point starts to move away from the base joint. It reaches the critical value $\pi/2$ when the links form a square. The value of $\alpha_{max}$ has the minimum when the distance between the end-point and the base joint is $\sqrt{3}$ times the link length. After that, the value starts to increase until it reaches the boundary of the reachable workspace of the manipulator. The fully steerable workspace of the manipulator is shown in Figure 45 (b).

The fully steerable workspace of the manipulator with an inversely coupled clutch is in a ring shape. The inner diameter of the ring is the outside diameter of the circle-shaped fully steerable workspace of the manipulator with a directly coupled clutch.

The use of a clutch could improve the manipulator's steerability because of the extra force generation capability and the freedom in placing the actuator. What's more, the manipulator will also have the advantages of a parallel robot such as high load capacity and stiffness etc. On the other hand the disadvantages of a parallel robot also exist in the clutched robot. And a complex gear chain could increase the cost and control effort as well.

## 5.3 Previously Developed Devices

The only dissipative passive haptic interface that has been developed using clutches is P-TER by Book et al. [28]. Two clutches were used in addition to two brakes as shown in Figure 35.

The link arrangement in P-TER is similar to Sakabuchi's device (Figure 27) with a different base joint choice. Figure 46 shows the arrangement in P-TER. Link 1 and link 3 are connected with the base. Link 3 connects to the middle of link 4. Link 2 connects link 1 and 4. The free end of link 4 is the end point.

The actuation of the brake installed between link 3 and the base will generate a force component along link 4 as shown in Figure 47 at the end-point. The actuation of the brake between link 1 and the base will generate a force component along link 2 at the joint between link 2 and link 4. Similar to the analysis for Sakabuchi's device, it will generate a force component at the end-point. The force component is parallel to link 2. The direction of the component is opposite to the direction obtained with the component at the joint between link 2 and 4. The magnitude is half of that obtained by at the joint between link 2 and 4. Therefore the actuation effect of the two brakes on the end-point is equivalent to a diamond shaped manipulator which is shown in Figure 49, where link 1 of P-TER shown in (a) is replaced by link 1' shown in (b) and link 2 shown in (a) is replaced by link 2' in (b) as well. The generated force will be the same under the same amount of actuations on the brakes.

The actuation of a clutch will also generate a force at the end-point of P-TER. It might not be easy to tell if P-TER is equivalent in the case of force generation to the diamond shaped structure when using clutches. The analysis of clutches also involves velocity analysis in additional to the combination of force generation from each actuator. The end-point velocity is compared first for both structures.

The end-point velocities for both manipulators could be expressed as functions of the link angular velocities.

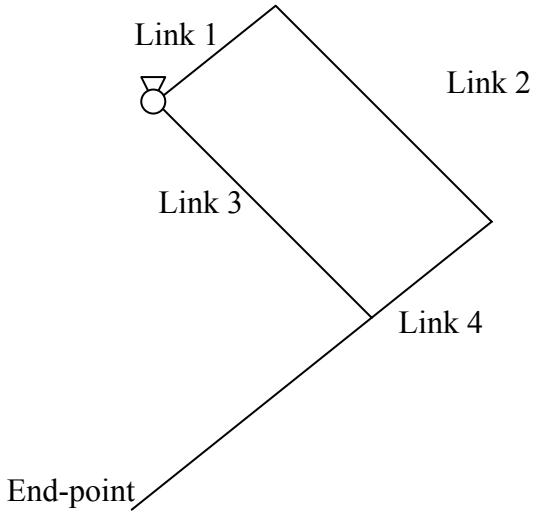


**Figure 46. Link arrangement of P-TER**

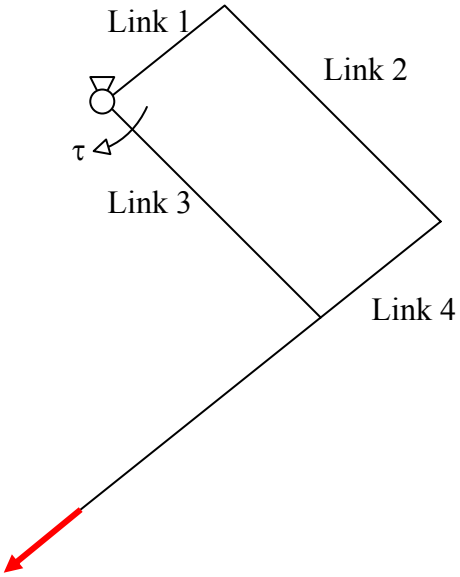


**Figure 47. Generated force component from the brake between the base and link 3**

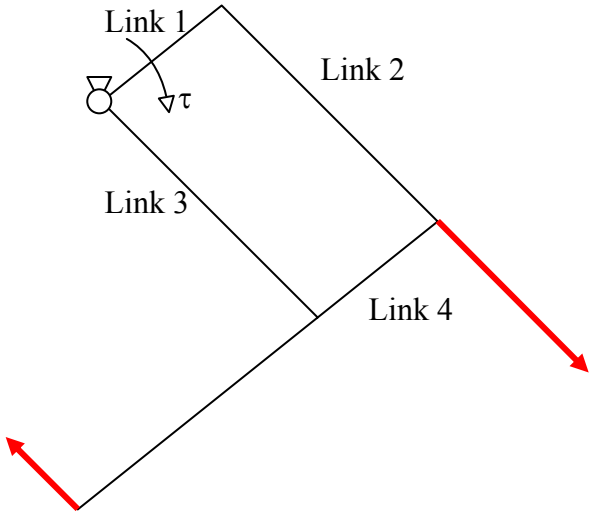


**Figure 48. Generated force component from the brake between the base and link 1**

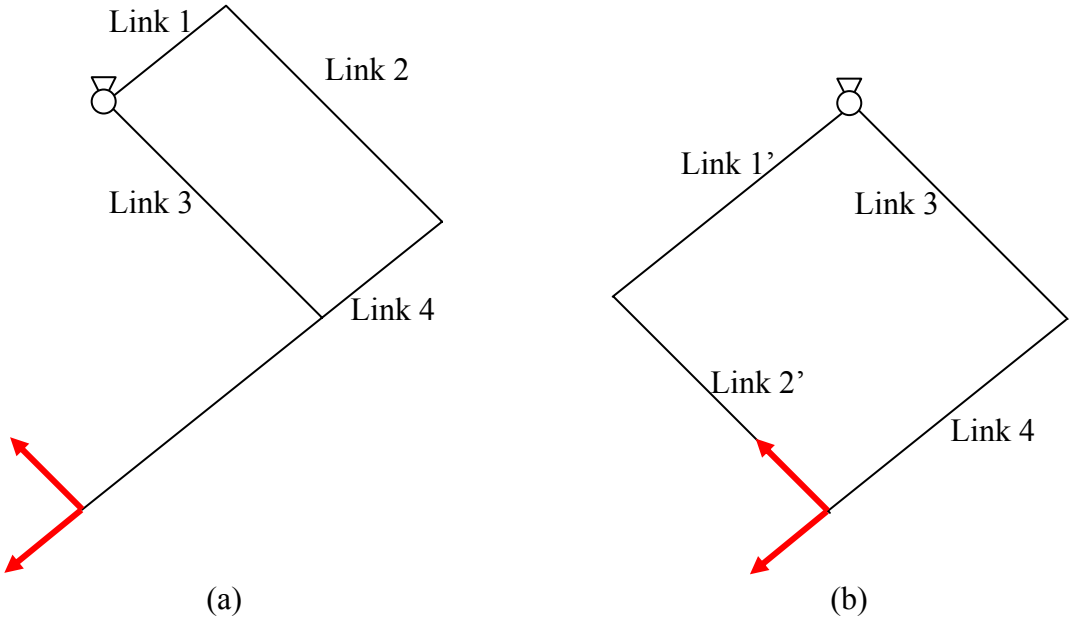


**Figure 49. Generated force for (a) P-TER from brakes and (b) its equivalent**

$\dot{\theta}_1$, $\dot{\theta}_3$ are the angular velocities of links 1 and 3 for P-TER as shown in Figure 50 (a). Then the angular velocity of link 4 is

$$\dot{\theta}_4 = \dot{\theta}_1 - \dot{\theta}_3 \tag{5.29}$$

The end-point velocity of P-TER is:

$$\vec{v} = \dot{\theta}_3 l_{34} \vec{v}_3 + \left(\dot{\theta}_1 - \dot{\theta}_3\right) l_4 \vec{v}_4 \tag{5.30}$$

And $\dot{\theta}_{1D}$, $\dot{\theta}_{3D}$ are the angular velocities of links 1' and 3 for the diamond shaped one as shown in Figure 50 (b). Then the angular velocity of link 4 is

$$\dot{\theta}_{4D} = \dot{\theta}_{1D} - \dot{\theta}_{3D} \tag{5.31}$$

The end-point velocity is:

$$\vec{v} = \dot{\theta}_{3D} l_{34D} \vec{v}_{3D} + \left(\dot{\theta}_{1D} - \dot{\theta}_{3D}\right) l_{4D} \vec{v}_{4D} \tag{5.32}$$

Because of the geometries of the manipulators, $l_{34} = l_{34D}$, $l_4 = l_{4D}$, $\vec{v}_3 = \vec{v}_{3D}$ and $\vec{v}_4 = \vec{v}_{4D}$. If the angular velocities of the links are equal, which is to say, if $\dot{\theta}_3 = \dot{\theta}_{3D}$ and $\dot{\theta}_1 = \dot{\theta}_{1D}$, the end-point velocities of the two structures are the same.

P-TER and the diamond shaped manipulator will have the same end-point velocities for same angular velocities at the links connecting with the base. The generated force at the end-point will be also the same for both manipulators when the same amount of torque is applied to these two links. From the force generation analysis in the previous section it is not hard to conclude that the two manipulators are equivalent in case of force generation if clutches are installed between the two links connecting with the base.

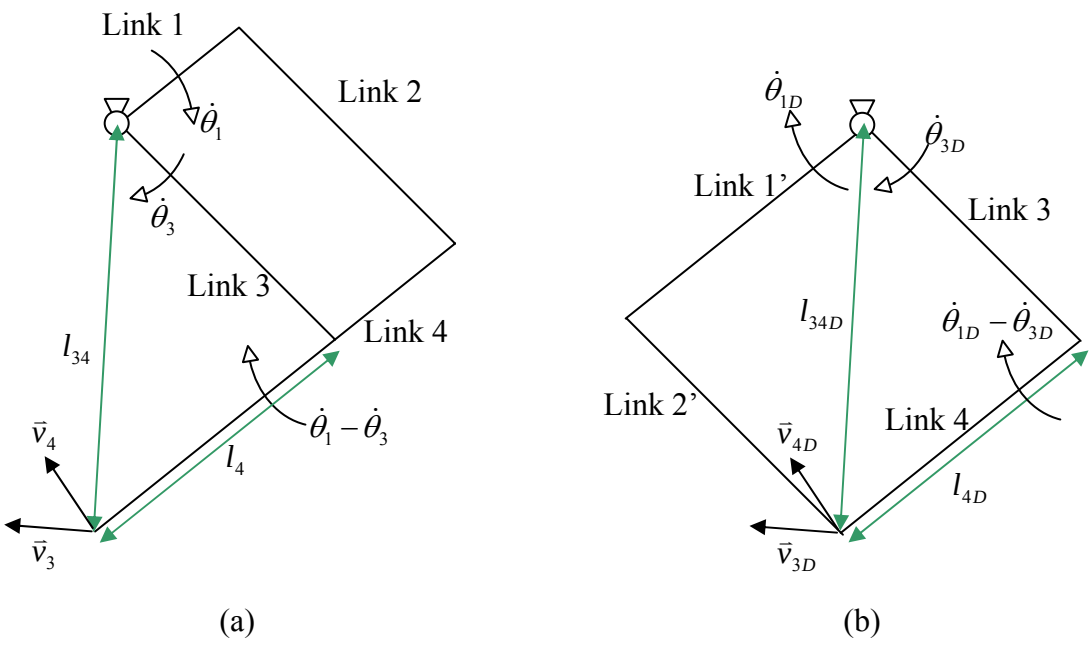


**Figure 50. Velocity comparison for (a) P-TER and (b) a diamond shaped manipulator**

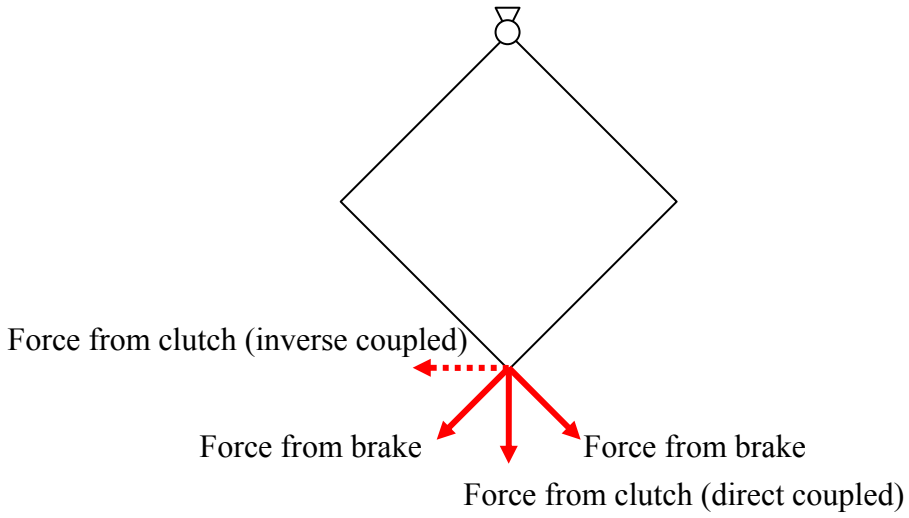


**Figure 51. Configuration when both clutches might be needed for motion redirection**

The force generation capability and therefore the steerability of P-TER is equivalent to a diamond shaped manipulator if the same brakes are installed between link 1' and the ground, link 3 and ground and if the same clutches supported by the ground are installed between links 1' and 3 with direct ( $a_{1'} = a_3 = 1$ ) and inverse ( $-a_{1'} = a_3 = 1$ ) coupling configurations.

The steerability of a diamond shaped manipulator with two brakes and one clutch was analyzed in a previous section. The fully steerable workspace of the manipulator with direct coupling configuration ( $a_{1'} = a_3 = 1$, Figure 33) is a circle centered at the base joint with a radius of $\sqrt{2}$ times the link length. The fully steerable workspace of the manipulator with inverse coupling configuration ( $-a_{1'} = a_3 = 1$, Figure 45) is a ring also centered at the base joint with an inner radius of $\sqrt{2}$ times the link length and an outside radius of two times the link length. The manipulator is fully steerable within any one of the two workspaces by selecting the correctly coupled clutch. At the overlapped boundary, the manipulator does not have universal full steerability with any one clutch because the value of $\alpha_{max}$ is $\pi/2$. But if both clutches are used, the manipulator has universal full steerability along this circle.

The diamond shaped manipulator with two brakes and two clutches has universal full steerability over its entire reachable workspace. Therefore P-TER also has universal full steerability over its entire reachable workspace.

The link arrangement of P-TER is unique. Since all actuators are placed at the base joint it has the same advantage of smaller internal dynamics as does Sakaguchi's device. While different from Sakaguchi's device or the equivalent diamond shaped manipulator,

P-TER has more clear space for the operator since the links are arranged further away. However this arrangement will also introduce more link dynamics into the device.

# 6. DYNAMICS OF THE SYSTEM ELEMENTS

The steerability analyses for planar manipulators in the previous chapters start with force generation analysis. The force generation analysis is based on the Virtual Work Principle to find the end-point force. As mentioned, one assumption is made for the Virtual Work Principle which is the static equilibrium of the structure. The analysis could be also used for a moving manipulator under an ideal situation when all the links, actuators etc. are massless. However the assumption is not valid for a real dissipative passive haptic interface. The actuation of dissipative passive actuators can only redirect existing motion, which requires a moving manipulator. Also, even though steps have been taken to reduce the mass of the link and other elements, the physical presence of the mass in all the elements still can not be neglected. On the other hand, sometimes keeping more mass in the link will improve the system stability. Therefore the study of the influence of system dynamics on the steerability is necessary and important.

## 6.1 Steerability and manipulability

Before the study of the influence of the system dynamics on the manipulator's steerability, some concepts need to be refreshed from the introduction specifically the manipulability concepts.

Manipulability concepts were developed to evaluate the manipulator's performance. The velocity manipulability ellipsoid is used to describe the manipulator's ability to change the end-effector position and orientation at a given configuration. The force manipulability ellipsoid is used to describe the manipulator's ability to generate force at the end-effector under the physical limitations of the actuators at a given configuration.

Steerability analysis starts with the force generation analysis. Therefore it's reasonable to study the relationship between the steerability and the force manipulability ellipsoid of a robot.

The force manipulability ellipsoid could be obtained by considering the sphere in the space of joint torques

$$\tau^T \tau = 1 \tag{6.1}$$

where $\tau$ is the vector that consists of all the actuator torques. The torques could also be normalized by the output limit of the actuators.

Substituting equation 4.1 into equation 6.1, the force manipulator ellipsoid can be written as

$$\vec{F}^T \left( JJ^T \right) \vec{F} = 1 \tag{6.2}$$

where $\vec{F}$ is the generated force at the end-effector of the manipulator expressed in task space.

If only one of the actuators, say brake #*i* has unit torque output $\tau_i$ and none of the other ones has output, the torque vector is

$$\tau_i = \left( 0 \quad \cdots \quad 0 \quad \overset{ith}{1} \quad 0 \quad \cdots \quad 0 \right)^T \tag{6.3}$$

It still satisfies equation 6.1 and it's one of the principal axes of the sphere. The generated force $\vec{F}_i$ from $\tau_i$ obtained by using equation 4.1 satisfies equation 6.2. It represents a vector from the center of the force manipulability ellipsoid to a point on the ellipsoid in the task space. Even though the unit torques $\tau_i$ are a set of orthonormal vectors in the torque space, the generated forces $\vec{F}_i$ are not necessarily perpendicular to each other.

As a dissipative passive manipulator, an actuator output could either be $+\tau_i$ or $-\tau_i$ depending on the rotation direction of the joint. As a result, only $1/2^n$ of the joint torque sphere described in equation 6.1 is achievable where $n$ is the number of actuated joints. So only a part of the force manipulability ellipsoid of the manipulator is achievable.

This can be easily visualized through a two-dimensional example. In the analysis of force generation in chapter 4, equations 4.3 and 4.4 are the direction vectors for the $\vec{F}_i$ s that could be obtained through equation 6.3 in a 2D case. Instead of the whole force manipulability ellipsoid, the manipulator could only achieve one part of it. For example, Figure 52 shows a 2R manipulator with its force manipulability ellipsoid at this configuration. If positive rotations exist for both joints, only the part of ellipsoid within the labeled force range which is bounded by the force component vector is achievable. In a two-dimensional case, the manipulability ellipsoid is divided into 4 pieces and a maximum number of one of them is achievable at any instant.

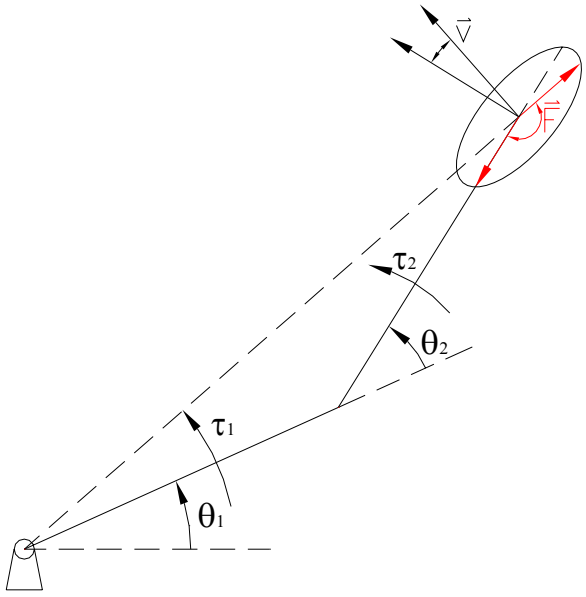


**Figure 52. Force manipulability ellipsoid and its achievable part**

The steerability of the manipulator is measured through this achievable piece of the force manipulator ellipsoid. The passive steerable angle defined before for the 2D manipulator is the angle between the boundaries of the achievable piece of the ellipsoid.

## 6.2 Dynamic Force Manipulability Ellipsoid

When solving a mechanics problem in dynamics, D'Alembert's principle can be used to reduce it to a problem in statics by introducing an inertial fictitious force. The inertial force has the magnitude equal to the product of the mass of the body and its acceleration. Its direction is opposite to the acceleration. The result is a condition of "kinetic equilibrium".

The steerability analysis starts in a static equilibrium condition. If the dynamics of the manipulator elements could be somehow treated similarly as the mechanics problems, the steerability concepts could then be applied to real manipulators. Based on this idea, a dynamic force manipulability ellipsoid could be developed as follows.

If a set of torques $\vec{\tau}$ are applied to the actuators on a moving dissipative passive non-redundant manipulator, a force $\vec{F}$ will be generated at the end-effector. Define $\vec{\tau}_{static}$ as the set of the torques that will generate the same force $\vec{F}$ at the end-effector of the same manipulator with the same configuration when the manipulator is massless. Then the difference between $\vec{\tau}$ and $\vec{\tau}_{static}$ is caused by the introduction of the manipulator's mass which is defined as **mass-induced torque** $\vec{\tau}_{mass}$. So,

$$\vec{\tau} = \vec{\tau}_{static} + \vec{\tau}_{mass} \tag{6.4}$$

Mass-induced torque $\vec{\tau}_{mass}$ is the torque that could maintain kinetic equilibrium of the manipulator. It includes the terms of dynamics of the elements, gravity terms etc.

Neglecting the various friction terms, the dynamic model of an open-chain manipulator with *n* rigid links is

$$\tau = M(q)\ddot{q} + C(q,\dot{q}) + G(q) \tag{6.5}$$

where $q$, $\dot{q}$ and $\ddot{q}$ are the joint position, velocity and acceleration vectors, $M(q)$ is the positive definite inertia matrix which is configuration-dependant, matrix $C(q,\dot{q})$ includes terms of inertial forces, and $G(q)$ includes gravity related terms. (Parallel manipulators are treated as several serial manipulators.)

The velocity in joint space and the velocity in task space are related by

$$\dot{x} = J(q)\dot{q} \tag{6.6}$$

The derivative of equation 6.6 with respect to time gives a relationship for accelerations.

$$\ddot{x} = J(q)\ddot{q} + \dot{J}(q,\dot{q})\dot{q} \tag{6.7}$$

Since the inertial matrix $M(q)$ is invertible, $\ddot{q}$ can be solved in equation 6.5 and substitute into equation 6.7 which gives

$$\ddot{x} = JM^{-1}(\tau - C - G) + \dot{J}\dot{q} \tag{6.8}$$

Substitute equation 6.4 into 6.8

$$\ddot{x} = J(q)M^{-1}(q)\tau_{static} + J(q)M^{-1}(q)(\tau_{mass} - C(q,\dot{q}) - G(q)) + \dot{J}(q,\dot{q})\dot{q} \tag{6.9}$$

Only the last two terms on the right hand side of the equation are caused by the system dynamics and gravity. And by definition, $\vec{\tau}_{static}$ should generate the same force as $\vec{\tau}$ at the end-effector. Therefore the same acceleration could be expected at the end-effector of the manipulator in the static equilibrium situation and the kinetic equilibrium situation. So,

$$\ddot{x} = J(q)M^{-1}(q)\tau_{static} \tag{6.10}$$

Mass-induced torque $\vec{\tau}_{mass}$ could be found using the equation below.

$$J(q)M^{-1}(q)(\tau_{mass} - C(q,\dot{q}) - G(q)) + \dot{J}(q,\dot{q})\dot{q} = 0 \tag{6.11}$$

The dynamic force manipulability ellipsoid could also be obtained by starting with the sphere in the space of joint torques

$$\vec{\tau}^T\vec{\tau} = (\vec{\tau}_{static} + \vec{\tau}_{mass})^T(\vec{\tau}_{static} + \vec{\tau}_{mass}) = 1 \tag{6.12}$$

From equation 4.1,

$$\vec{\tau}_{static} = J^T\vec{F}_{static} \tag{6.13}$$

And if the manipulator is non-redundant,

$$\vec{\tau}_{mass} = J^T\vec{F}_{mass} \tag{6.14}$$

Then the dynamic force manipulability ellipsoid could be written as

$$(\vec{F}_{static} + \vec{F}_{mass})^T JJ^T(\vec{F}_{static} + \vec{F}_{mass}) = 1 \tag{6.15}$$

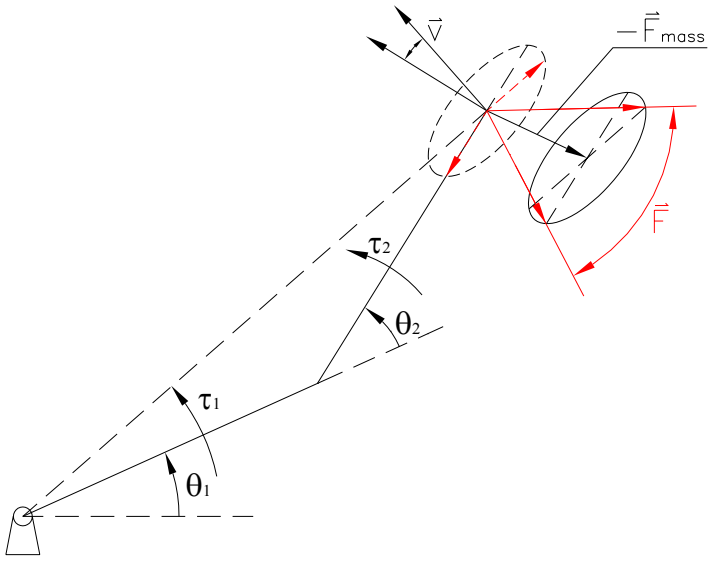


**Figure 53. Dynamic force manipulability ellipsoid**

For a non-redundant manipulator with a non-singular configuration,

$$\vec{F}_{static} = J^{-T}\vec{\tau}_{static} = J^{-T}MJ^{-1}\ddot{x} \tag{6.16}$$

$$\begin{aligned}\vec{F}_{mass} &= J^{-T}\vec{\tau}_{mass} = J^{-T}\left\{-MJ^{-1}\dot{J}(q,\dot{q})\dot{q} + C(q,\dot{q}) + G(q)\right\} \\ &= -J^{-T}MJ^{-1}\dot{J}(q,\dot{q})\dot{q} + J^{-T}C(q,\dot{q}) + J^{-T}G(q)\end{aligned} \tag{6.17}$$

The dynamic force manipulability ellipsoid shown in equation 6.15 has the same shape with the corresponding static force manipulability ellipsoid (equation 6.2) since the shapes in both cases are defined by the matrix $JJ^T$. However the center of the ellipsoid is shifted from the end-effector by $-\vec{F}_{mass}$. This is shown in Figure 53.

## 6.3 Influence of Dynamics on Steerability

The influence of system dynamics (and other mass-induced terms, such as gravity etc.) on the force manipulability ellipsoid is to shift the ellipsoid by a distance $-\vec{F}_{mass}$. As discussed before, the steerability of the manipulator is measured through this achievable piece of the force manipulator ellipsoid. The shift brought by the dynamics changed the shape of the achievable piece of the force manipulability ellipsoid and therefore the steerability.

If the shift of the force manipulability ellipsoid makes the angle between the boundaries of the achievable portion of the ellipsoid decrease, the steerability which is measured by the achievable force range is also decreased. This can be seen in Figure 54 where the achievable force range labeled by $\vec{F}$ is smaller than the force range without considering the system dynamics which is labeled by $\vec{F}_{static}$. On the other hand, the steerability could also be increased if the shift of the force manipulability ellipsoid makes the angle between the boundaries of the achievable portion of the ellipsoid increase. This

can be seen in Figure 55 where the achievable force range labeled by $\vec{F}$ is larger than the force range without considering the system dynamics which is labeled by $\vec{F}_{static}$. (The relationship between $-\vec{F}_{mass}$ and the end-point velocity can not be determined explicitly using equation 6.17. It is possible that $-\vec{F}_{mass}$ has different directions relative to the velocity.)

From equation 6.17, the shift of the force manipulability ellipsoid is determined by the mass, velocity and configuration of the manipulator. Even though it is possible to determine the shift for a special situation, it might not be realistic to find out the shift for all possible conditions. However, there are approaches to estimate the shifts for a special application. For example, the applications of dissipative passive haptic interfaces are guiding systems. Guiding systems in industrial environments, for example a training robot for welding operators to follow a complex path, are normally moving at a relatively low speed. And the mass of the robot elements would be optimized for a less significant dynamics but would still ensure motion without jerkiness. In these cases, the shift brought on by the system dynamics would be relatively small. An upper limit of the shift might be found and used for robot design. On the other hand, a haptic interface has human involvements. By practicing with the robot, the operator would have a rough idea about the dynamics (just like he has an idea about his own body dynamics). He/she would expect to compensate for the dynamics to a certain amount. This would definitely degrade the interface transparency. But passive manipulators do not have the capability to improve the system transparency as the active ones. And even for the active manipulators a completely transparent system is impossible to achieve and also undesirable.

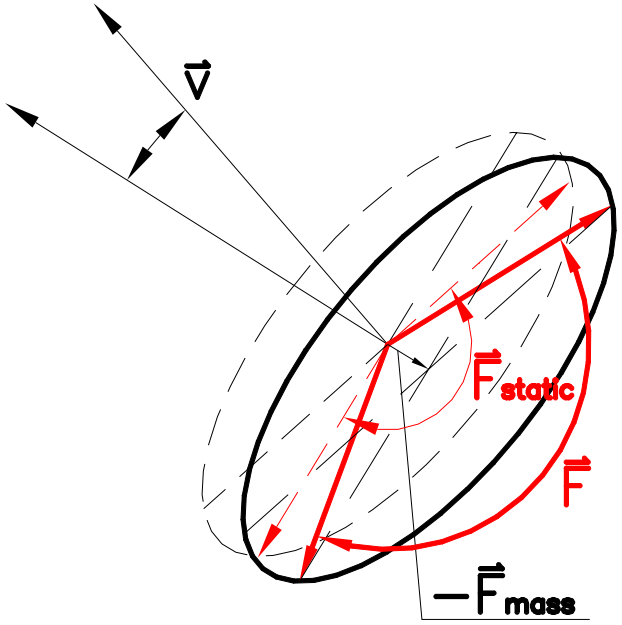


**Figure 54. Steerability decreases because of the dynamics**

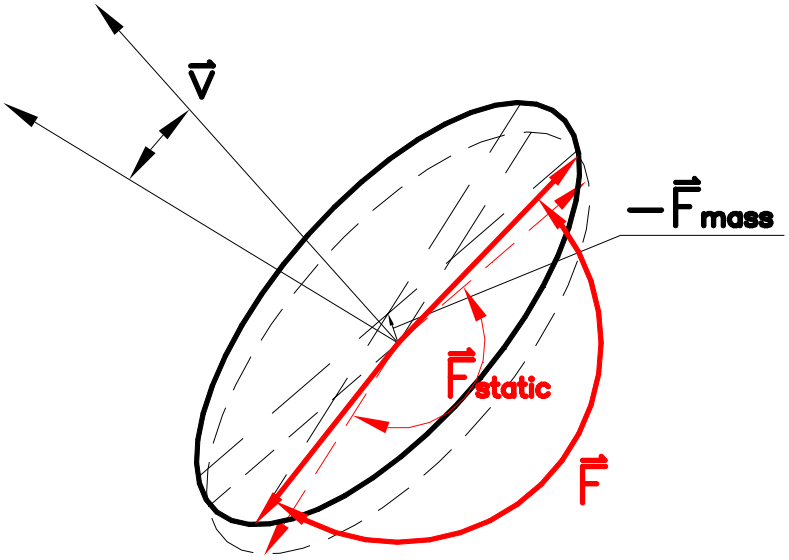


**Figure 55. Steerability increases because of the dynamics**

# 7. DESIGN OF PLANAR DISSIPATIVE PASSIVE HAPTIC INTERFACES

Dissipative passive haptic interfaces are naturally safe systems and therefore are potentially very important especially for applications with large power inputs. However the control limitations brought by the dissipative passive actuators impedes researchers from designing and developing devices. The steerability research in the previous chapters has already clearly defined the control limitation. A way of minimizing the limitation has also been found. It is possible then to design a dissipative passive haptic interface which could redirect motions similarly to active devices. This chapter provides some general thoughts and examples.

## 7.1 The Design Requirements for a Interface

Not every application has the same requirements; therefore the devices that are used are not the same. Based on the targeted application design requirements could be determined and could serve as the design guidelines.

One of the most important requirements for a dissipative passive haptic interface is the ability to redirect motions. Different applications might have a different emphasis on this requirement. A welder guiding system for tracking small scale welds precisely will have high requirement in the ability of motion redirection; while an assisting robot in an automobile assembly line for helping the worker load a seat into a vehicle might not need as much ability as the previous example.

Another important parameter is the power output of the system. Based on the application a proper power output should be defined. The power output should be large

enough for the task that the robot is performing. But larger does not always mean better especially in the haptic interface design. A haptic interface involves direct human machine interaction. Excessive machine power could cause some discomfort of the operator physically and psychologically. It is important for the following designing process in the actuator selection.

There could be some other detail requirements associated with the application. Space limitation, for example, exists for some design tasks. Since the device needs to be mounted or placed in a special location, more or less there will be restrictions on how much space the device might occupy. Sometimes one structure type is preferable for the design. The available actuators play an important role in the design too. In practice they set extra restrictions in the design process. Finally insufficient budget could seriously degrade the final system performance.

## 7.2 Interface Design

Based on the targeted application, one design parameter must be clear at first which is desired ability of motion redirection. Even though there hasn't been any practically used measure yet, the steerability analysis provides a good way to evaluate the ability.

For a planar manipulator, two-sided steerability is the minimum requirement for the manipulator to redirect a 2D motion. A passive steerability angle was required to be larger than $\pi/2$ to guarantee two-sided steerability. Two-sided steerability only guarantees the ability to generate force perpendicular to the velocity. The effectiveness of the motion redirection, however, depends on how effectively the manipulator could generate force perpendicular to the velocity. It varies when the velocity direction changes relative to the generated force range. For example, a manipulator will have more capability in

generating force perpendicular to the velocity $\vec{v}_1$ to the right in Figure 56 than to the velocity $\vec{v}_2$ even though the manipulator is fully steerable for both velocities. So the manipulator will be more efficient in redirecting a motion to the right for $\vec{v}_1$ than $\vec{v}_2$.

The concepts of the ability of motion redirection and the effectiveness of motion redirection are entirely different but somehow related. The steerability measures define the lower limit of the effectiveness of motion redirection. The manipulator could still be very ineffective even though two-sided steerability exists. But by increasing the passive steerability angle the lower limit of the effectiveness of motion redirection could be increased. This could be done by setting the operational workspace within one of the fully steerable workspaces. One obvious disadvantage here is the resulting smaller workspace.

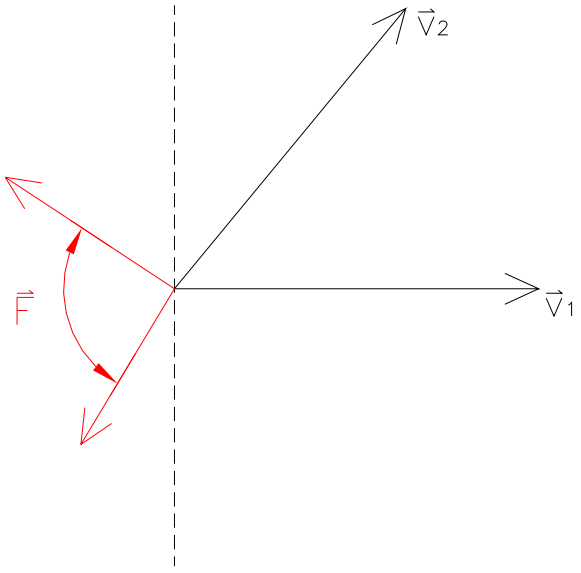


**Figure 56. Comparison in the effectiveness in motion redirection**

After determining the steerability requirement for the manipulator, the next step would be to look for the correct structure design and the proper actuators to go with the structure.

As discussed earlier, multiple-joint serial linkage has kinematic redundancy and is very complex in steerability analysis. Extra assumptions have to be made in order to analyze a serial manipulator. And because of the restrictions brought by the assumptions, the fully steerable workspace of a serial manipulator might be very small compared to its reachable workspace. The same concern happens in parallel manipulators if kinematic redundancy exists in a leg. So a parallel structure with non-redundant legs would be a simpler choice for the design of a dissipative passive haptic interface. Brakes are chosen as a standard actuator for the discussion of manipulator designs.

There are many parameters that could be tuned in a parallel manipulator design, such as link lengths, base spacing, symmetry and number of legs etc. The examples in the change of some of the parameters have been seen in the analyses of the previously developed devices. A more comprehensive study will be performed here.

One example case is shown in the analysis of MR P-TER for the change of link length and its influence on the system steerability. By shortening the links connecting to the ground from 30.5 cm to 26.4 cm, the size of the larger fully steerable workspace decreases (see Figure 26 and Figure 34) but the distribution of steerability in the fully steerable workspace is much smoother. There exists a larger continuous area located at the center of the fully steerable workspace where higher steerability exists for the robot.

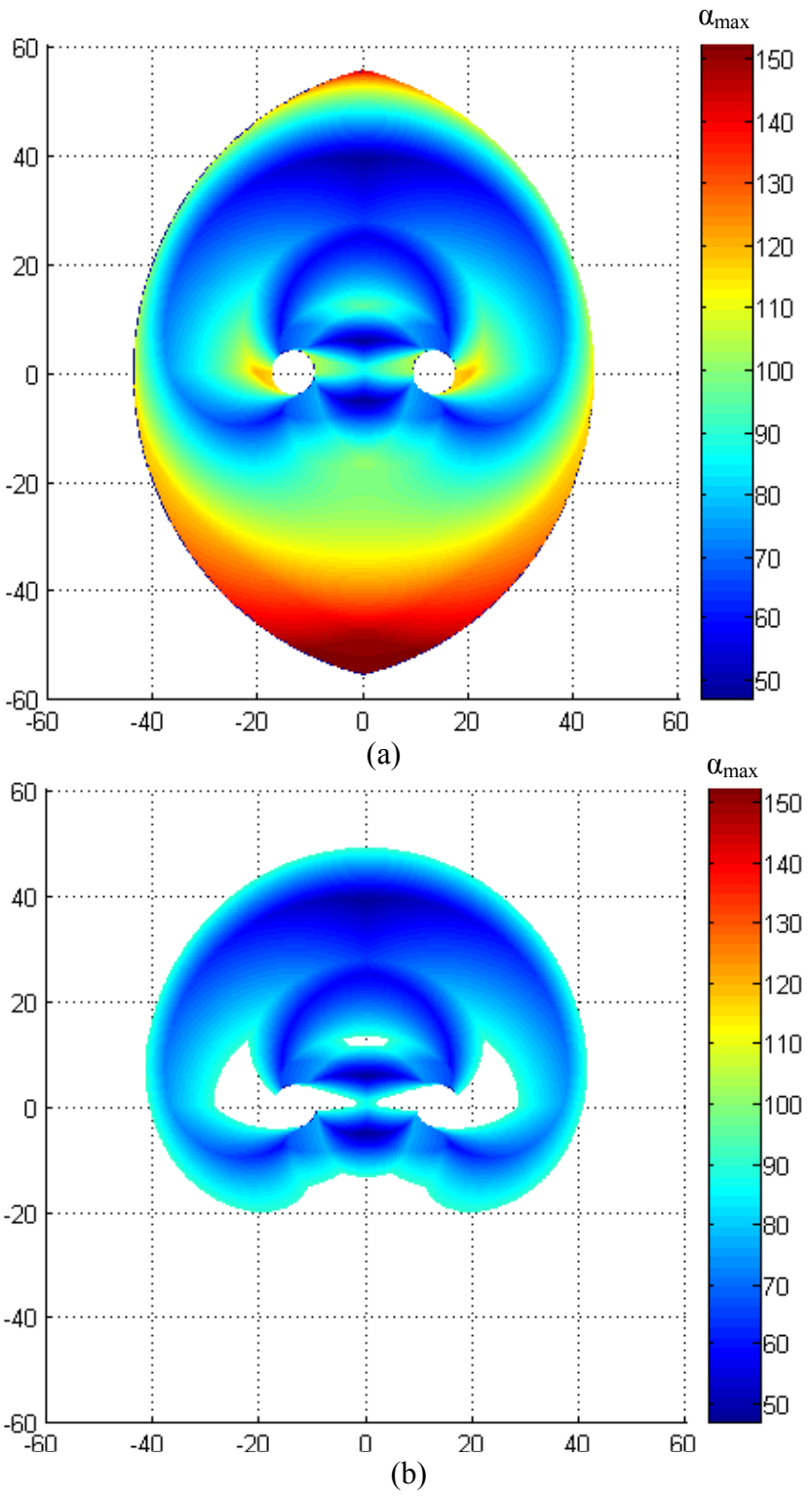


**Figure 57. (a) $\alpha_{max}$ and (b) fully steerable workspaces for MR P-TER with short links connecting the end-point and longer links connecting the ground**

Instead of length change for the links connected to the ground in the previous example, the links connected to the end-point of the manipulator could be changed. For example, if the links connected to the end-point are shortened to 26.4 cm and the links connected to ground are changed back to 30.5 cm, the distribution of the values of $\alpha_{max}$ becomes more complex in the reachable workspace of the manipulator (Figure 57 a). The two fully steerable workspaces in the previous configurations are connected with each other and form three voids in the overall fully steerable workspace (Figure 57 b). The distribution of the steerability becomes more uneven. It will be harder to define an operational workspace for this manipulator if a higher requirement on steerability is presented.

The manipulators in the examples above use a unique distance between the two base joints. A change of base joint spacing could significantly change the steerability of the manipulator over the reachable workspace too. This has been seen in the example shown in Figure 33 and Figure 34 where the base joint spacing changed from zero to a non-zero value and the steerability changed dramatically. Also by tuning the value of the base spacing, the shape and other details of the fully steerable workspace could be changed. MR P-TER is given a more desirable fully steerable workspace when different link length selections are chosen and therefore is used again as an example for comparison. If the base joint spacing of MR P-TER is narrowed from 26.7 cm to 10 cm, the distribution of the values of $\alpha_{max}$ could be seen in Figure 58 (a) for the locations in the reachable workspace of the manipulator. The two fully steerable workspaces can be seen in Figure 58 (b). They locate more in the center of the reachable workspace than MR P-TER. The steerability distribution is even smoother than MR P-TER within the fully steerable

workspace A and the size of fully steerable workspace B is almost negligible. But compared to MR P-TER the minimal value of $\alpha_{max}$ is not small. This indicates that MR P-TER has the best configuration in steerability. As another option, if the base joint spacing of MR P-TER is widened from 26.7 cm to 35 cm, the distribution of the values of $\alpha_{max}$ could be seen in Figure 59 (a) for the locations in the reachable workspace of the manipulator. The two fully steerable workspaces can be seen in Figure 58 (b). The fully steerable workspace A moves away from the center of the reachable workspace and touches the boundary of the reachable workspace. The size of fully steerable workspace B is larger than the one in MR P-TER. It could be predicted that when the joint spacing increases the fully steerable workspace A will keep moving away from the center of the reachable workspace; the size of fully steerable workspace B would keep increasing and eventually turn in to the larger fully steerable workspace which is similar to the example of a 4R parallel manipulator shown in Figure 25.

All of the manipulator structures discussed above are symmetric about the perpendicular bisector of the line segment bounded by the two base joints if the end-point is at the center of the reachable workspace. The four links of the manipulator are arranged into an "M" shape. If one branch of the "M" shaped manipulator is replaced by a two-link robot which is symmetric to the branch about the line from its base joint to the end-point, the links of the manipulator are then arranged in a "^▽" form. The structure is symmetric about the line through the center of the reachable workspace and normal to the 2D plane. In this arrangement the two moving joints and the end-point align together when the end-point is at the center of the reachable workspace. The two stationary joints and the end point are aligned together too. So the steerability of the manipulator is decreased near the

center of the reachable workspace. The distribution of the values of $\alpha_{max}$ could be seen in Figure 60 (a). The two fully steerable workspaces are away from and symmetric about the center of the reachable workspace (Figure 60 b).

The symmetry of the structure brings the symmetric steerability properties. It is natural choice to select symmetry in the manipulator design because it reduces the complexity of the system. However, a manipulator design might have non-symmetric steerability requirements for a special application. An easy solution is to still use a symmetric design which at least fulfills the requirements. But sometimes this might not be feasible because of some external restrictions. For example, a symmetrical manipulator design which satisfies the steerability requirements might be too large to fit in the available space. Also if the targeted application only strongly emphasizes steerability at one end of the operational space, a symmetrical manipulator design might be over-qualified for the application and therefore be a waste of resources.

A non-symmetric structure could bring in the non-symmetry in the steerability of the manipulator. For example, if the links at one leg of MR P-TER are shortened from 26.4 cm and 30.5 cm to 20 cm and 26.4 cm, the distribution of the values of $\alpha_{max}$ could be seen in Figure 61 (a) for the locations in the reachable workspace of the manipulator. The two fully steerable workspaces can be seen in Figure 61 (b). The left leg of the manipulator is the one with shortened links. The steerabilities of the locations at the left part of the reachable workspace are better than the ones at the right. The left part could then be designated for tasks with a higher requirement in motion redirection.

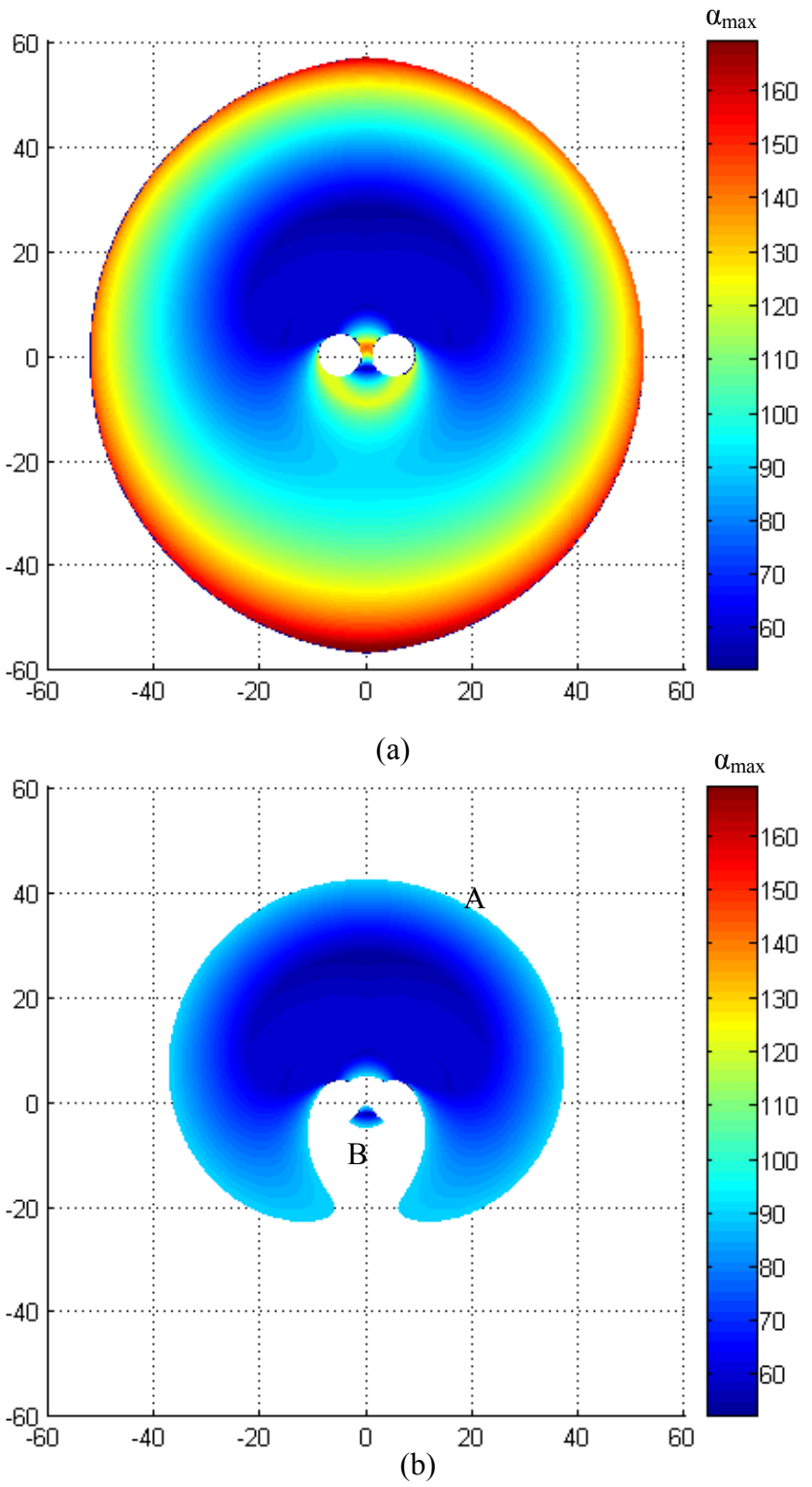


**Figure 58. (a) $\alpha_{max}$ and (b) fully steerable workspaces for MR P-TER with smaller base joint spacing of 10 cm**

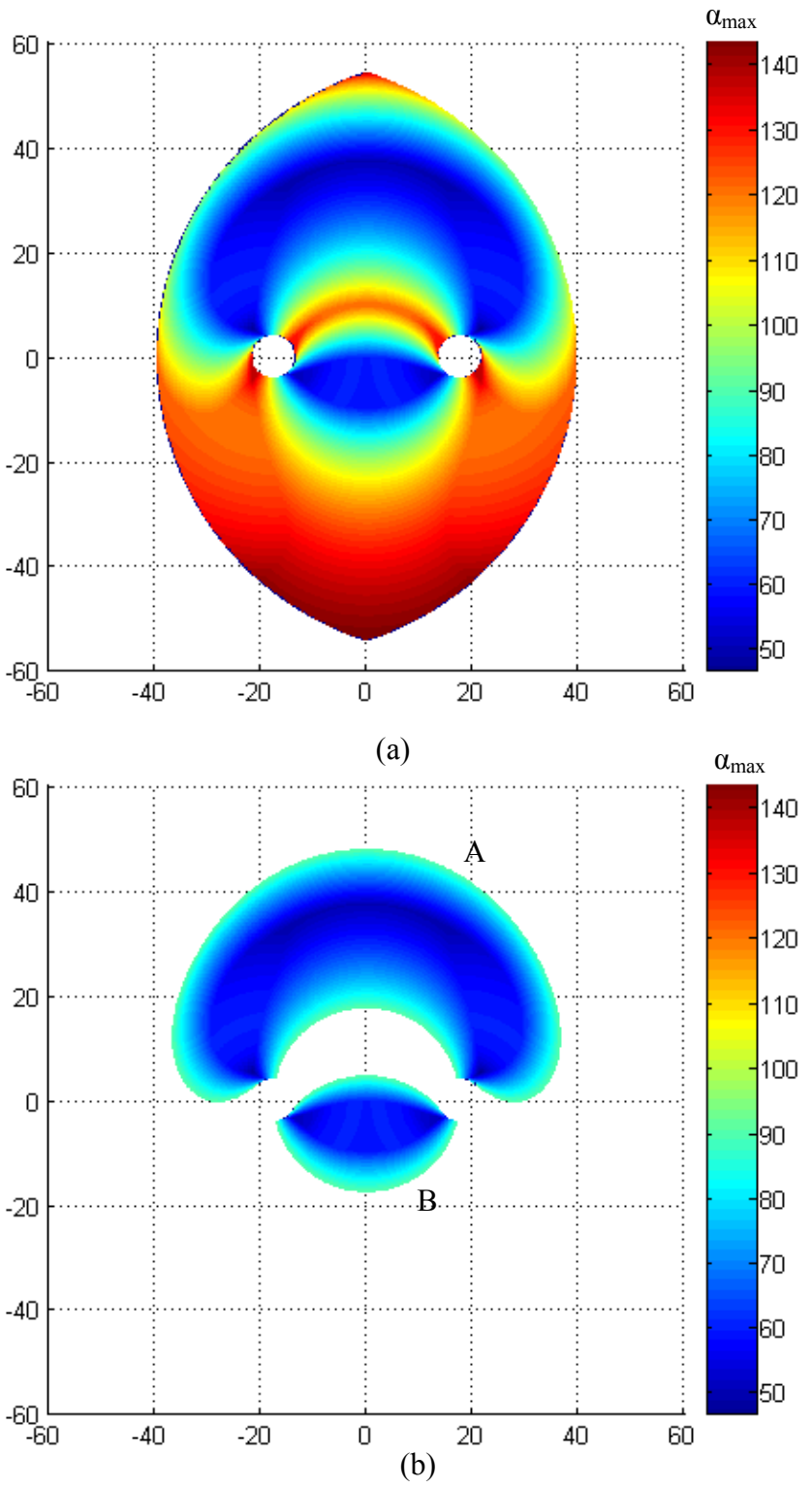


**Figure 59. (a) $\alpha_{max}$ and (b) fully steerable workspaces for MR P-TER with larger base joint spacing of 35 cm**

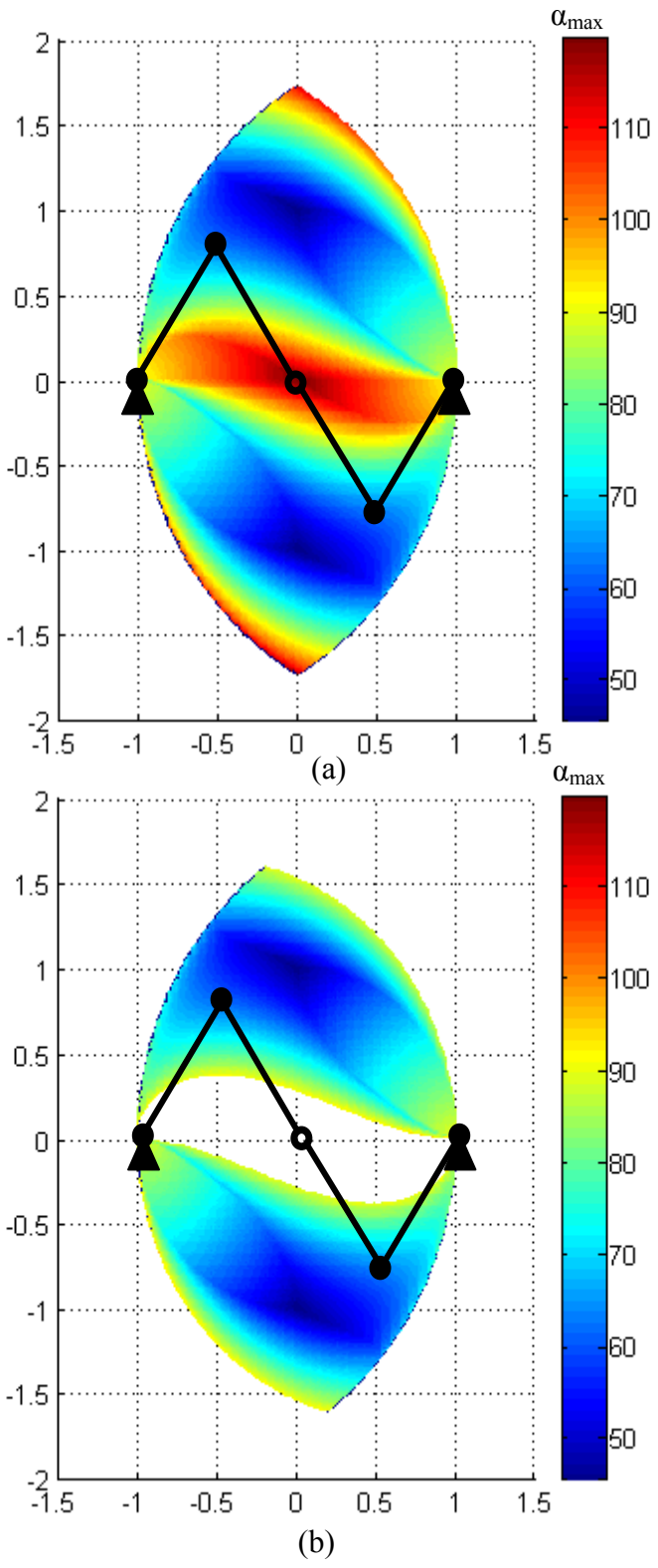


**Figure 60. (a) $\alpha_{max}$ and (b) fully steerable workspaces for a "^∨" shaped four-link parallel manipulator**

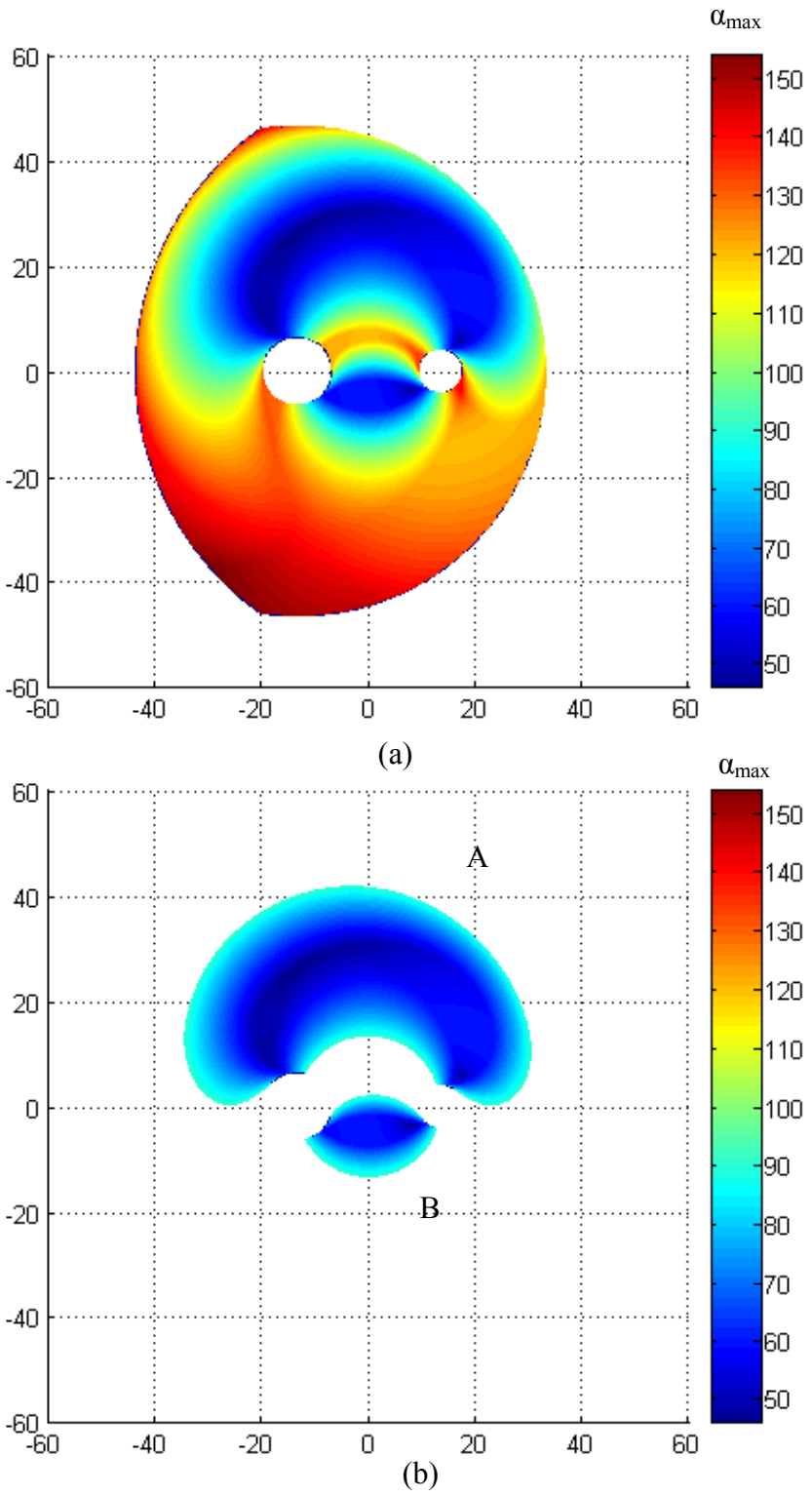


**Figure 61. (a) $\alpha_{max}$ and (b) fully steerable workspaces for MR P-TER with left leg links of 20 cm and 26.4 cm**

The four-link parallel manipulators studied above have improved steerability because they combine the steerability of two non-redundant legs. The minimum values of $\alpha_{max}$ are close to its theoretical minimum of 45 degrees. If more legs are used, the theoretical minimum value of $\alpha_{max}$ is even smaller. The steerability of a parallel manipulator could be improved further. For example, a parallel manipulator with three two-link legs could have a theoretical minimum value of $\alpha_{max}$ of 30 degrees. A simple structure is studied here where all the links are of equal length. The base joints of the legs are arranged as the three vertices of an equilateral triangle which has a side length as twice of the link length. The legs are arranged like the three blades of a fan when the end-point is at the center of the triangle. The values of $\alpha_{max}$ for the points within the reachable workspace are shown in Figure 62 (a). The minimum value of $\alpha_{max}$ for this special manipulator is below 40 degrees. For almost all the locations in the reachable workspace the manipulator has universal full steerability. The fully reachable workspace is shown in Figure 62 (b). Even though adding extra legs will improve the steerability, the cost and complexity of the manipulator will also increase. More interference will be expected too.

In the previous discussion of manipulator designs brakes are used as the default actuators. Clutches are another actuator choice for a manipulator design. The use of clutches could improve the steerability and decrease the dynamics. However the design of a manipulator with clutches will be more complex compared to a system with brakes and will not be included in here.

The design of a dissipative passive haptic interface involves the adjustment of many parameters. The interaction of the parameters will complicate the design process. Iterations might be necessary for a satisfactory design.

Through the previous studies, a planar interface could be designed using only dissipative passive actuators to redirect motion similarly to an active device.

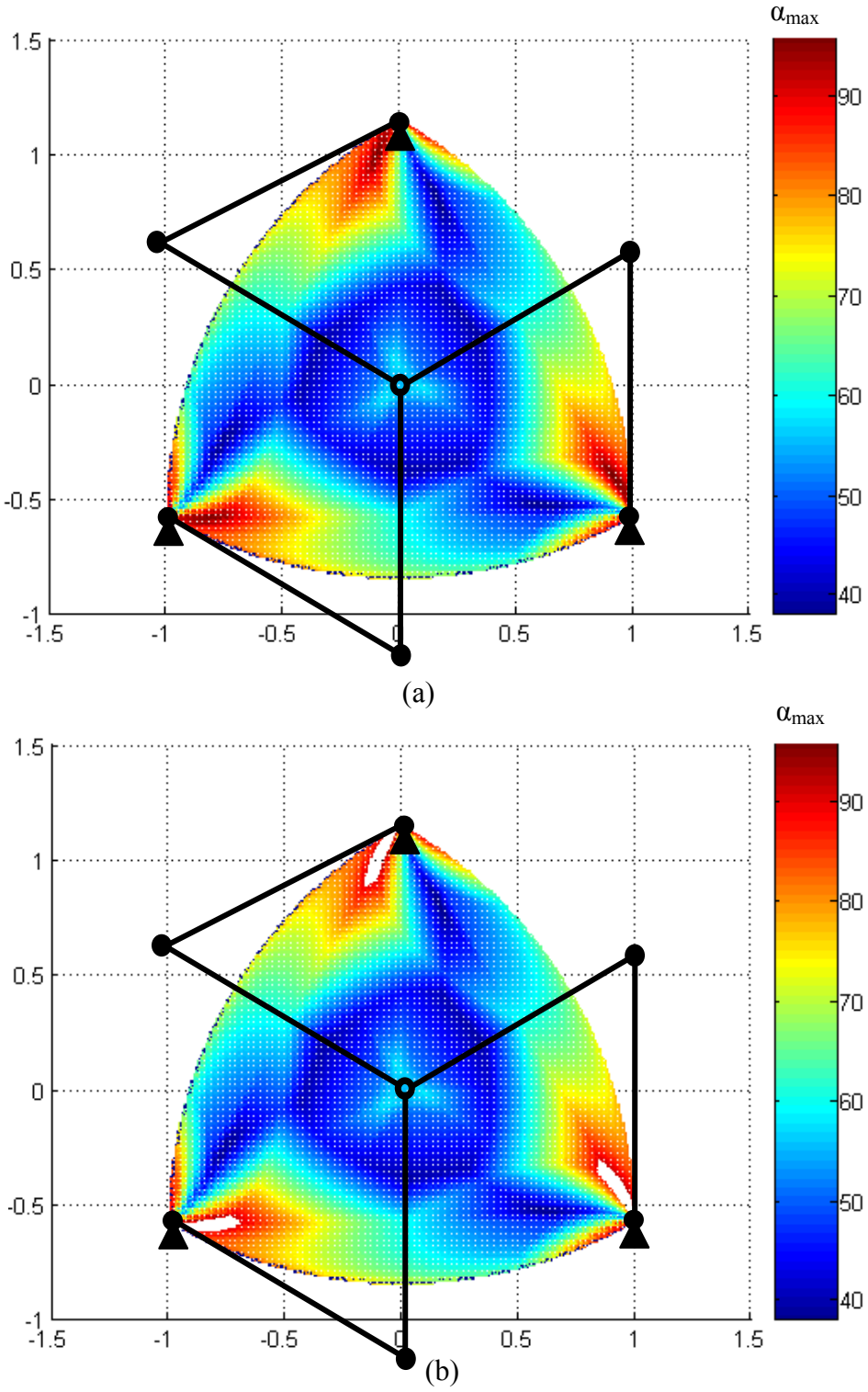


**Figure 62. (a) $\alpha_{max}$ and (b) fully steerable workspaces for a three-leg parallel manipulator**

# 8. STEERABILITY ANAYSIS FOR THREE-DIMENSIONAL MANIPULATORS

As stated in chapter 3, three-dimensional motion redirection is much more complex than 2D cases. It is even more difficult for dissipative passive manipulators because of the effects of gravity on the elements. There has been only one developed 3D dissipative passive haptic interface by Matsuoka et al. [32]. However there are potential applications for three-dimensional dissipative passive haptic systems, such as a 3D haptic interface in space where gravity is negligible or a backup strategy for a very large 3D system under the circumstances of failure of the active actuators. Similar applications can be also found in cable manipulators or grasping robots. So the research on the control ability and limitations for 3D dissipative passive haptic interfaces is valuable and will be studied in this chapter.

## 8.1 Control Ability and Limitation of a Three-Dimensional Dissipative Passive Haptic Interface

As discussed in chapter 3, the control ability of dissipative passive haptic interfaces is redirection of existing motion. Three-dimensional motion redirection problems are much more complex than two-dimensional cases. A current motion could be redirected to any possible direction away from the motion. The possibility is infinite compared to only two directions for 2D cases. The desired control ability for a three-dimensional motion redirection problem is therefore to have the ability to steer the velocity to any possible direction away. The control limitation is that sometimes the actuations fail to redirect motion away to some possible directions from the current velocity. We use the only 3D

device, Matsuoka's 3D manipulator as an example. Matsuoka's device basically consists of a universal joint and a prismatic joint. The schematic drawing is shown in Figure 63. When the velocity only involves the motion of the prismatic joint $\vec{v} = \vec{v}_p$, Matsuoka's device can not redirect the current velocity to any other direction. It can only slow down the velocity.

## 8.2 Force Generation Analyses for a Non-Redundant Manipulator

Similar to the analysis in the 2D motion redirection problems, the capability of dissipative passive actuators in generating forces in the end-point should be studied in order to study the control ability and limitation of a haptic interface.

If only the position of the end-effector is considered, a three-dimensional haptic interface has three degree of freedom (DOF). Therefore it needs a minimum of 3 1-DOF joints. The velocity of the end-effector can be related to the velocity of each joint's motion by using the Jacobian matrix.

For a serial manipulator

$$\dot{x} = \begin{bmatrix} \dot{x}_1 \\ \dot{x}_2 \\ \dot{x}_3 \end{bmatrix} = \begin{bmatrix} J_1 & J_2 & J_3 & \dots & J_n \end{bmatrix} \begin{bmatrix} \dot{q}_1 \\ \dot{q}_2 \\ \dot{q}_3 \\ \dots \\ \dot{q}_n \end{bmatrix} = J\dot{q} \tag{8.1}$$

where for revolute joint

$$J_i = \hat{p}_{n+1,i} \times \hat{e}_i \tag{8.2}$$

$\hat{p}_{n+1,i}$ is the position vector from end-effector to joint $i$, $\hat{e}_i$ is the axis of joint $i$;

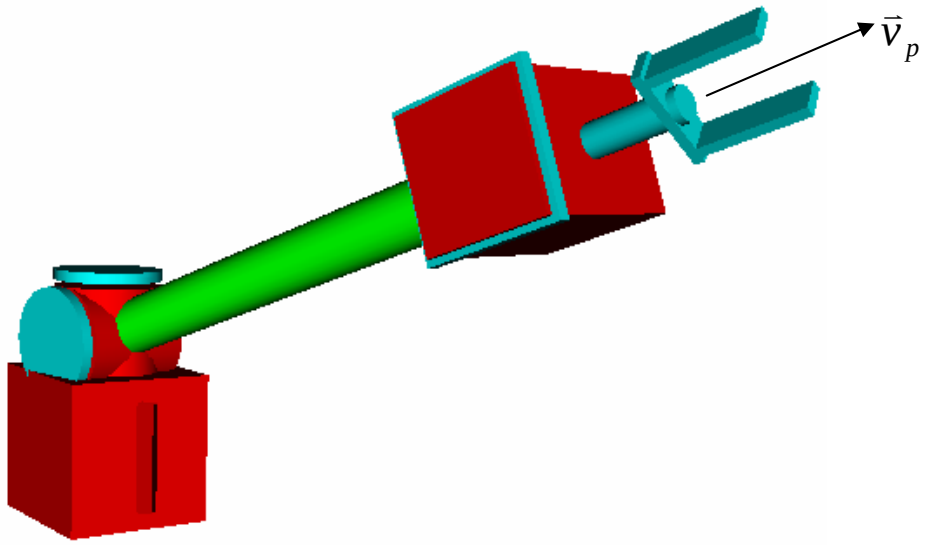


**Figure 63. The schematic drawing for Matsuoka's device**

and for prismatic joint

$$J_i = \hat{e}_i \tag{8.3}$$

$J_i$ represents the end-effector velocity component from unit motion of joint *i*.

If gravity and dynamics are not important, from the Virtual Work Principle

$$\tau = J^T F \tag{8.4}$$

where force *F* could be generated at the end-effector when the actuation $\tau$ is applied to the robot. The force is used to redirect end-point motion.

For simplicity, non-redundant robots are first studied where *n*=3. Equation 8.1 is simplified to

$$\dot{x} = \begin{bmatrix} \dot{x}_1 \\ \dot{x}_2 \\ \dot{x}_3 \end{bmatrix} = \begin{bmatrix} J_1 & J_2 & J_3 \end{bmatrix} \begin{bmatrix} \dot{q}_1 \\ \dot{q}_2 \\ \dot{q}_3 \end{bmatrix} = J\dot{q} \tag{8.5}$$

If the robot is not at a singularity position $\det(J) \neq 0$, the generated force at the end-point can be expressed as

$$F = \left(J^T\right)^{-1}\tau = J^{-T}\tau \tag{8.6}$$

where

$$J^{-T} = \frac{1}{\det(J)}\begin{bmatrix} J_2 \times J_3 & J_3 \times J_1 & J_1 \times J_2 \end{bmatrix} \tag{8.7}$$

It could be also written as

$$J^{-T}{}_i = \frac{1}{\det(J)}\varepsilon_{ijk} J_j \times J_k \tag{8.8}$$

$\varepsilon_{ijk}$ is the permutation symbol.

$J^{-T}{}_i$ represents the generated force component at the end-effector from unit actuation of the *i*th actuator.

If no motion exists at joint $i$ ($\dot{q}_i = 0$), the end-effector's velocity can be defined as the lock-joint velocity similar to the 2D cases. The lock-joint velocity is a span of 3D subspace by vectors $J_j$ and $J_k$ where $i \neq j$, $i \neq k$ and $j \neq k$. Therefore, the generated force component at the end-effector from the actuator at joint *i* is perpendicular to the velocity subspace when no motion exists at joint *i*.

As a dissipative passive actuator, the torque (or force for prismatic actuator) is always working to remove system kinetic energy. Therefore the generated force component is always 90 degrees away from the current velocity direction. So the generated force component at the end-effector from unit actuation of a dissipative passive actuator at joint *i* can be written as

$$f_i = -\text{sgn}\left(\dot{x} \cdot J^{-T}{}_i\right) J^{-T}{}_i \tag{8.9}$$

The inner product in equation 8.9 can be simplified as

$$\dot{x} \cdot J^{-T}{}_i = \left( \sum_{m=1}^{3} J_m \dot{q}_m \right) \cdot \left( \frac{1}{\det(J)} \varepsilon_{ijk} J_j \times J_k \right) = \frac{1}{\det(J)} \sum_{m=1}^{3} \left\{ \varepsilon_{ijk} J_m \cdot \left( J_j \times J_k \right) \dot{q}_m \right\}$$
$$= \frac{1}{\det(J)} \varepsilon_{ijk} J_i \cdot \left( J_j \times J_k \right) \dot{q}_i = \dot{q}_i \tag{8.10}$$

where from definition

$$\det(J) = \varepsilon_{ijk} J_i \cdot \left( J_j \times J_k \right) \tag{8.11}$$

Therefore

$$f_i = -\operatorname{sgn}(\dot{q}_i) J^{-T}{}_i \tag{8.12}$$

If there is motion at one 1DOF joint of a non-redundant 3D robot, the actuation of the brake on this joint will generate an equivalent force at the end-effector. The generated force is parallel to the corresponding column of the inverse transpose matrix of the robot Jacobian matrix. The direction of the generated force depends on the sign of the motion. A positive motion could result in a generated force which is on the opposite direction of the corresponding column of the inverse transpose matrix while a negative motion could result in a force component which is on the same direction of the column.

## 8.3 Steerability Analysis for Non-Redundant 3D Manipulators

In a three-dimensional case, steerability involves the ability to redirect manipulator's motion away from the current velocity to any possible directions. Steerability metrics should be defined in order to evaluate the steerability of a 3D manipulator. A quantitative metric similar to the passive steerability angle in 2D cases is difficult to define for a 3D manipulator. But a concept for the desired steerability could be defined as a qualitative metric.

### *8.3.1 Full Steerability Definition for a Non-Redundant 3D Manipulator*

For a 3D non-redundant serial robot with three 1DOF joints, the Jacobian matrix can relate the task space velocity with the joint space velocity as $\dot{x} = J\dot{q}$. A dissipative passive actuator is installed at each joint. If the robot is not at a singularity configuration, the generated force component at the end-effector from unit actuation of a dissipative passive actuator at joint *i* is $f_i = -\text{sgn}(\dot{q}_i)J^{-T}{}_i$, *i*= 1, 2, 3. If the solution to the equation

$$\dot{x} + fa = 0 \tag{8.13}$$

where $f = [f_1 \quad f_2 \quad f_3]$, is positive, which is a>0, then the robot is called **fully steerable** or has **full steerability** for the current velocity $\dot{x}$.

Similarly, **Universal full steerability** is defined when full steerabilities exist for all velocities of a robot configuration.

The three generated force component vectors share a common point, which is the start point of each vector. It is located at the end-point of the robot. The three generated force components vectors could be considered as the three edges of a pyramid. Their common point is the apex of the pyramid. The pyramid could be called the **force pyramid** of the robot. For a 3D non-redundant robot, the force pyramid is a triangle pyramid. Based on the definition, the solution of equation $\dot{x} + fa = 0$ is positive when the opposite vector of the velocity vector which starts also from the apex lies in the force pyramid (Figure 64). By having the force components in these positions, it is possible to generate a force with the component perpendicular to the velocity in any possible direction. Therefore the velocity is possible of being steered away to any direction in a three-dimensional space. Full steerability exists for the velocity.

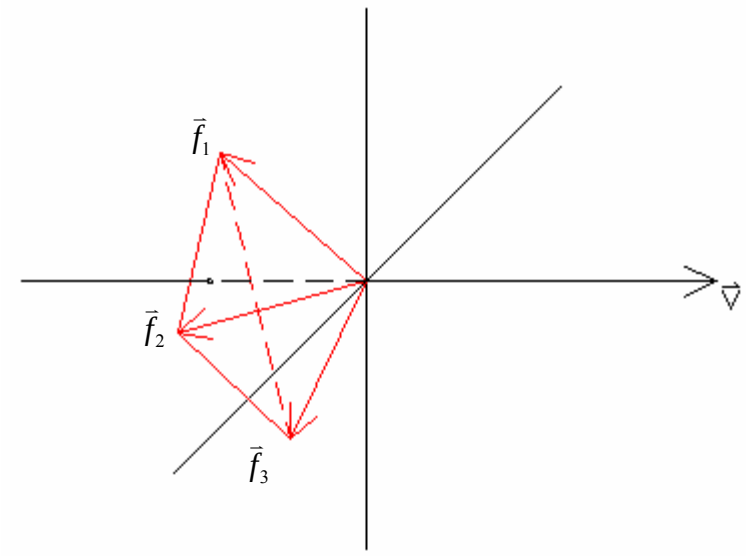


**Figure 64. Full steerability definition**

### *8.3.2 Sufficient Condition of Full Steerability for a Non-Redundant 3D Manipulator*

Similar to the 2D cases, a sufficient condition of full steerability can be also found for the non-redundant 3D manipulators.

For a 3D non-redundant serial robot with three 1DOF joints, a dissipative passive actuator is installed at each joint. If the robot is not at a singularity configuration, the generated force component at the end-effector from unit actuation of a dissipative passive actuator at joint *i* is $f_i = -\mathrm{sgn}(\dot{q}_i)J^{-T}{}_i$, *i*= 1, 2, 3, *J* is the Jacobian matrix.

If $f_i \cdot f_j < 0$ for all cases when $i \neq j$, then the robot has full steerability for the configuration and current velocity $\dot{x}$.

Proof:

Based on the definition of full steerability, the solution of equation 8.13 should be positive.

Multiply equation 8.13 by $f^T$

$$f^T\dot{x} + f^T f a = 0 \tag{8.14}$$

Since $\det(J) \neq 0$, the solution is

$$a = \left(f^T f\right)^{-1}\left(- f^T\dot{x}\right) \tag{8.15}$$

The last term in equation 8.15

$$- f^T\dot{x} = \left[- f_1\cdot\dot{x} \quad - f_2\cdot\dot{x} \quad - f_3\cdot\dot{x}\right]^T \tag{8.16}$$

From equation 8.9, $- f_i\cdot\dot{x} \geq 0$ and equal sign is chosen only when $f_i = 0$. So

$$- f_i\cdot\dot{x} > 0 \tag{8.17}$$

And, the first term in the right hand side of equation 8.15

$$\left(f^T f\right)^{-1} = \frac{1}{\{\det(J)\}^2}\left(f^T f\right)^{\text{adjoint}} = \frac{1}{\{\det(J)\}^2}\left\{\left(f^T f\right)^{Cofactor}\right\}^T \tag{8.18}$$

Because

$$\left[f^T f\right]_{ij} = \left[f_i\cdot f_j\right] = \begin{bmatrix} \|f_1\|^2 & f_1\cdot f_2 & f_1\cdot f_3 \\ f_1\cdot f_2 & \|f_2\|^2 & f_2\cdot f_3 \\ f_1\cdot f_3 & f_2\cdot f_3 & \|f_3\|^2 \end{bmatrix} \tag{8.19}$$

So

$$\left(f^T f\right)^{Cofactor} =$$

$$\begin{bmatrix} \|f_2\|^2\|f_3\|^2 - (f_2\cdot f_3)^2 & (f_1\cdot f_3)(f_2\cdot f_3) - (f_1\cdot f_2)\|f_3\|^2 & (f_1\cdot f_2)(f_2\cdot f_3) - (f_1\cdot f_3)\|f_2\|^2 \\ (f_1\cdot f_3)(f_2\cdot f_3) - (f_1\cdot f_2)\|f_3\|^2 & \|f_1\|^2\|f_3\|^2 - (f_1\cdot f_3)^2 & (f_1\cdot f_2)(f_1\cdot f_3) - (f_2\cdot f_3)\|f_1\|^2 \\ (f_1\cdot f_2)(f_2\cdot f_3) - (f_1\cdot f_3)\|f_2\|^2 & (f_1\cdot f_2)(f_1\cdot f_3) - (f_2\cdot f_3)\|f_1\|^2 & \|f_1\|^2\|f_2\|^2 - (f_1\cdot f_2)^2 \end{bmatrix} \tag{8.20}$$

For the diagonal elements of $\left(f^T f\right)^{Cofactor}$, $\|f_i\|^2\|f_j\|^2-\left(f_i\cdot f_j\right)^2\geq 0$ and the equal sign is chosen only if $f_i=cf_j$ where c is a scalar. Therefore the diagonal elements of $\left(f^T f\right)^{Cofactor}$ are positive. Off diagonal elements of $\left(f^T f\right)^{Cofactor}$ is $\left(f^T f\right)^{Cofactor}{}_{ij}=\left(f_i\cdot f_k\right)\left(f_j\cdot f_k\right)-\left(f_i\cdot f_j\right)\|f_k\|^2$, where $i\neq j$, $i\neq k$ and $j\neq k$. Because $f_i\cdot f_j<0$ when $i\neq j$ the off diagonal elements of $\left(f^T f\right)^{Cofactor}$ are all positive. Therefore,

$$\left(f^T f\right)^{-1}>0 \tag{8.21}$$

Substituting equations 8.17 and 8.21 into 8.15, the solution of equation 8.13 is $a>0$. Full steerability exists for the current velocity $\dot{x}$.

The sufficient condition of full steerability of a non-redundant 3D robot is proved.

A geometrical explanation could be used to better understand the sufficient condition. If $f_i\cdot f_j<0$, the force pyramid is a squatty pyramid (Figure 65). Because of passivity any part of the pyramid has to be at least $\pi/2$ away from the velocity. That says, if the velocity is a pole on ground pointing up, the pyramid apex is at the base of the pole and the pyramid can only exist under the ground. Because the pyramid is squatty, no matter how it moves under the ground around its apex, the opposite of the pole is always inside the force pyramid. Therefore the full steerability always exists.

Definition:

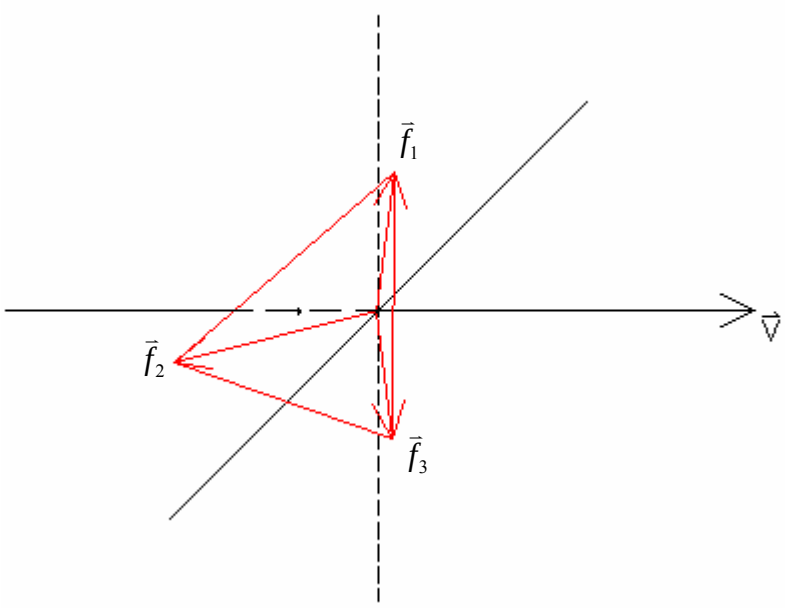


**Figure 65. Sufficient condition of full steerability of a non-redundant 3D manipulator**

For a convex pyramid with infinitely long edges, if there exist 3 orthogonal vectors inside the pyramid starting from the apex, the pyramid is defined to be larger than one-eighth of the 3D space.

The sufficient condition of full steerability for a non-redundant 3D manipulator can be written as:

If the force pyramid is larger than one-eighth of the 3D space full steerability exists.

### *8.3.3 Optimal Steering Configuration for a Non-Redundant 3D Manipulator*

For a non-redundant 3D robot with only dissipative passive actuators full steerability exists for some velocity directions at a certain configuration. But if at a velocity at least one of the inner products of $f_1 \cdot f_2$, $f_2 \cdot f_3$ and $f_3 \cdot f_1$ is non-negative, steerability for this velocity is not guaranteed. Or if at a certain velocity the inner products of the generated

force vectors are all negative, $f_1 \cdot f_2 < 0$ , $f_2 \cdot f_3 < 0$ and $f_3 \cdot f_1 < 0$ where $f_i = -\text{sgn}(\dot{q}_i) J^{-T}{}_i$ as defined, full steerability exists for this velocity. For the same configuration, if the motion at one of the joints changes direction, for example joint 1, then the generated force components are $f_1' = -f_1$, $f_2' = f_2$ $f_3' = f_3$. Because $f_1' \cdot f_2' > 0$, full steerability for this velocity is not guaranteed. So the universal full steerability doesn't exist for a non-redundant 3D dissipative passive manipulator.

Even though the universal full steerability doesn't exist for a non-redundant 3D robot, an optimal configuration could be found where the full steerability could exist for more end-point velocity directions than other configurations.

Similar to the 2D analysis, an optimal configuration can be found when the three generated force components are perpendicular to each others, $f_1 \perp f_2$ , $f_2 \perp f_3$ and $f_3 \perp f_1$. At this optimal configuration, as long as the velocity is not perpendicular to any generated force component vector (all joints are in motion), full steerability exists. Matsuoka's 3D manipulator uses the optimal configuration. The three axes of the joints are perpendicular to each other and therefore the three generated force components are perpendicular to each other. Another example of manipulator using the optimal configuration is a PPP (prismatic joints) robot with joints axes perpendicular to each other.

## 8.4 Steerability Improvement for a 3D Dissipative Passive Haptic Interface

As demonstrated, full steerability is guaranteed for a velocity whose force pyramid is larger than one-eighth of the 3D space. A non-redundant 3D robot has three generated

force components. They can only divide a 3D space into a maximum of $2^3$=8 possible force pyramids. It's not possible for all 8 possible force pyramids to be larger than one-eighth of the 3D space. Therefore full steerability can not be guaranteed for all velocities. The optimal configuration obtained above is where all the 8 possible force pyramids are of equal size.

The approach of subdividing used for the 2D manipulator could be applied here again to improve the steerability. Since some force pyramids are not big enough and some are, those that aren't big enough could make themselves larger by subdividing the nearby bigger ones and borrowing the divided parts. In this way universal full steerability can be achieved for the manipulator. The approach of subdividing involves new generated force components. The new force components are brought by the redundancy introduced by either parallel or serial structures.

### *8.4.1 Generated Force Components for a Redundant 3D Manipulator*

A 3D redundant serial robot has more than three active 1DOF joints. Because the Jacobian matrix is not a square matrix, generally there is no solution for equation 8.4. A solution exists only if the values of the actuations are a linear combination of the columns of the transpose Jacobian matrix of the manipulator. The physical explanation is that the Virtual Work Principle can not be used for a random actuation input. Only input that could bring about a static equilibrium of the manipulator will satisfy the Virtual Work Principle. Other input will bring the robot into motion.

Similar to the 2D analysis, locking extra joints transforms a redundant manipulator into a non-redundant one. If only 3 1DOF joints of a serial 3D redundant robot are

unlocked, the Jacobian matrix then consists of 3 columns of the original Jacobian. For example, joints *i*, *j* and *k* are unlocked and the Jacobian is

$$J_{Lijk} = \begin{bmatrix} J_i & J_j & J_k \end{bmatrix} \tag{8.22}$$

If the robot is not at a singularity configuration, the generated force component at the end-effector from unit actuation of a dissipative passive actuator at joint *i* is

$$f_i = -\mathrm{sgn}(\dot{q}_i)\left(J_{Lijk}\right)^{-T}{}_i = -\mathrm{sgn}(\dot{q}_i)\frac{1}{\det\left(J_{Lijk}\right)}\varepsilon_{ijk} J_j \times J_k \tag{8.23}$$

By choosing different locking schemes, different generated force components might result. They all have a general form as equation 8.23. The force components might be parallel to each other even though the magnitude might be different. If the magnitude is not considered,

$$f_L = -\mathrm{sgn}\left\{\dot{x}\cdot\left(J_j \times J_k\right)\right\} J_j \times J_k \tag{8.24}$$

can be defined as the generated force component direction vectors. There are maximal $n(n\text{-}1)/2$ components for an *n*-joint serial robot.

Unlike two-dimensional cases, not all random combinations of 3 vectors among the $n(n\text{-}1)/2$ components can be achievabled by locking all joints except for 3. From the definition of force components above, a force component is the cross product of two columns of the Jacobian which involve two joints. If a selection of 3 force vectors involves more than 3 joints, it is inconsistent with the statement that only 3 joints are unlocked. Therefore the $n(n\text{-}1)/2$ $f_L$s can not be grouped randomly. Only the 3 force vectors generated by selected 3 joints can be generated simultaneously. This difference brings significant trouble when we analyze steerability of a 3D redundant serial

manipulator. For simplicity, serial structures are not considered. And for parallel structures, each branch is a non-redundant robot.

For a parallel robot, the force generated at the end-point is the superposition of the force components from all branches. So the force generation capability could be considered as the summation of the capabilities of each branch. The generated force components for a parallel robot with *m* branches will be the union set of the force component set from each serial robot with $n_k$ joints and it has a maximum of $\sum_{k=1}^{m} n_k(n_k-1)/2$ elements. Since only non-redundant legs are considered the total number of force components is 3*m*.

### *8.4.2 Full Steerability Definition for a Redundant 3D Manipulator with Non-redundant Legs*

A 3D parallel robot with non-redundant legs is studied here. This means that each branch of the robot is a non-redundant 3D robot with three 1DOF joints. Dissipative passive actuators are installed. If a 3D dissipative passive manipulator is not at a singularity configuration, each leg could generate three force components and all the components are $\bar{f}_{L1}$, $\bar{f}_{L2}$, …

If there exists a solution to the equation $\dot{x} + fa = 0$, where

$$f = [f_{L1} \quad f_{L2} \quad f_{L3} \quad \dots \quad] \tag{8.25}$$

is positive, which is a>0, then the robot is called fully steerable or has full steerability for the considered configuration and current velocity $\dot{x}$.

The force pyramid concept was used to visualize the steerability concept of non-redundant robot. If the generated force components are again considered as the edges, a force pyramid could be also defined for a redundant robot where the apex is the starting point for the force component vectors. Because the number of edges is larger than three, the selection of lateral surfaces might not be unique. But a pyramid with a base which is a convex polygon can always be found where the force component vectors are either the edge or inside the pyramid. It is called the **convex force pyramid** for the robot.

Based on the definition, the full steerability of a redundant passive robot with non-redundant legs exists when the opposite vector of the velocity vector lies in the convex force pyramid. By having the force components in these positions the velocity can be steered away to any direction in a three-dimensional space.

As for to non-redundant robots, a sufficient condition could also be found for full steerability of a redundant parallel robot with non-redundant branches using the convex force pyramid concept: If the convex force pyramid formed by $\vec{f}_{L1}$, $\vec{f}_{L2}$, … is larger than one-eighth of the 3D space, then the robot has full steerability for the current velocity $\dot{x}$.

## 8.5 A Sufficient Condition for Universal Full Steerability of a Redundant 3D Manipulator with Non-redundant Legs

A sufficient condition for universal full steerability of a redundant 3D manipulator with non-redundant legs could be found. It is similar to the steerability theorem in 2D analysis.

A redundant 3D dissipative passive manipulator with non-redundant legs can generate force components from the actuators. The lines which the force vectors lie on intersect at the end-point of the manipulator. The three-dimensional space could be divided by these lines into finite numbers of triangle pyramids. The apexes of the pyramids are at the end-point and the legs are infinitely long. The triangle pyramids are not overlapping with each other. They can be called the **elementary triangle pyramids**. For a non-redundant robot, the 3D space is uniquely divided into 8 elementary triangle pyramids. But the way of dividing the 3D space is not unique generally for a redundant robot.

If a 3D redundant dissipative passive manipulator with non-redundant legs is not at a singularity configuration, a sufficient condition for universal full steerability is that there exists a way of dividing the elementary triangle pyramids such that they are all smaller than one-eighth of the 3D space.

Proof:

Sufficiency could be proved by considering the three cases:

Case I, if $-\dot{x}$ is inside one of the elementary force pyramids, the edges of the pyramid are the current generated force component vectors because they are at least $\pi/2$ away from $\dot{x}$. Therefore $-\dot{x}$ is inside the convex force pyramid. Based on the definition, full steerability exists.

Case II, if $-\dot{x}$ is on one lateral surface of one of the elementary force pyramids, there exists another elementary force pyramid which shares this same lateral surface and two edges. The two pyramids contain the vector $-\dot{x}$ and so does the convex force pyramid. Based on the definition, full steerability exists.

Case III, if $-\dot{x}$ is on one edge of one of the elementary force pyramids, there exist several other elementary force pyramids which share this same edge. These elementary force pyramids enclose $-\dot{x}$. So the convex force pyramid contains $-\dot{x}$. The full steerability exists.

Sufficiency is proved.

This is a very strong sufficient condition. It is very easy to find a situation where the universal full steerability exists without fulfilling the condition. For example, a redundant 3D dissipative passive manipulator with non-redundant legs can generate force components $\vec{f}_{L1}$, $\vec{f}_{L2}$, … $\vec{f}_{Ln}$, $n$ is a large integer. At a configuration the lines where the force components lie in forms a double cone with the apex at the end-point (Figure 66). The open angle of the cone is larger than $\pi/2$. This manipulator does not satisfy the sufficient condition at the configuration. But the universal full steerability exists.

(For a velocity near the center of the cone $\vec{v}_1$, it is easy to find three force components $\vec{f}_{L1}$, $\vec{f}_{L2}$ and $\vec{f}_{L3}$ to form a pyramid which contains $-\vec{v}_1$. If the velocity is near the cone surface, $\vec{v}_2$, the plane over the apex which is perpendicular to $\vec{v}$ intersects the cone with two lines. The force components on the cone surface are achievable if they are on one side of the plane which the velocity is not found in. It is not hard to find three force components, for example $\vec{f}_{La}$, $\vec{f}_{Lb}$ and $\vec{f}_{Lc}$ where the pyramid formed by them contains $-\vec{v}$. The case for the velocity outside the cone could be proved similarly.)

Due to the complexity of 3D steerability analysis, a sufficient and necessary condition of universal full steerability of a manipulator is not found in the time frame of this research.

## 8.6 Planar Steerability Analysis as a Special Case of 3D Analysis

The steerability analysis of a 3D manipulator uses planar analysis as a guide line. The planar analysis should be a special case of the 3D analysis.

The planar steerability analysis of a non-redundant manipulator could be obtained by using the 3D analysis by adding a third prismatic joint whose axis is perpendicular to the plane. The steerability measure in the form of pyramids in 3D analysis changes to the measure of angles. The universal full steerability could exist only if redundancy is used. The analysis of universal full steerability is less complex in planar case because there is one less degree of freedom.

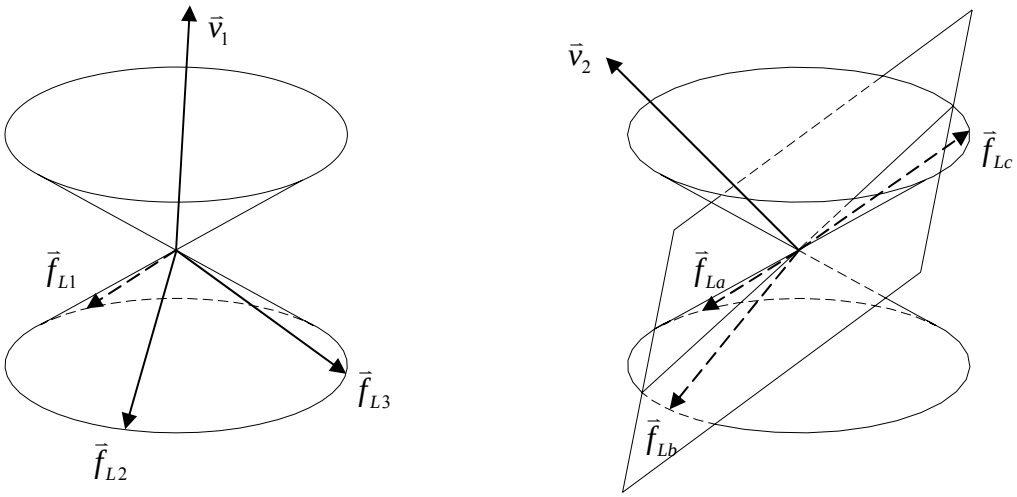


**Figure 66. Example of universal full steerability but the sufficient condition not satisfied, (a) velocity near cone center and (b) velocity near cone surface**

# 9. CONCLUSIONS AND FUTURE WORK

## 9.1 Summary and Conclusions

There are three primary objectives of this research. The first is to clearly identify the control ability and limitations of a dissipative passive haptic interface. The second is to evaluate the control ability and limitations and then to improve the control ability of a dissipative passive haptic interface. The final objective is to design a planar dissipative passive haptic interface with improved control ability similar to an active haptic interface.

The study began with the identification of the ability and limitations of dissipative passive actuators to generate control effects in a passive haptic interface in chapter 3. The ability was identified as steerability, the ability to redirect motions of a manipulator. In order to properly redirect motions a planar manipulator must have the ability to redirect the motion to the left or the right. A manipulator in three-dimensional space must have the ability to redirect motion to any direction away from the velocity. The control limitation was then identified as the incapability of the manipulator to redirect the motion to a certain direction.

Planar dissipative passive haptic interfaces are simpler to study not only because they have only two degrees of freedom but because of the convenience of not considering gravity. The steerability analysis of planar manipulator starts in chapter 4. The force generation of an individual actuator was chosen as a tool to evaluate the steerability. The passive steerability angle was defined as quantitative measure of the steerability. The two-sided steerability concept was defined as the desired steerability for motion redirection of planar manipulators. It's not surprising to see that a non-redundant planar

dissipative passive manipulator does not have full steerability for all the possible velocities at any configuration. But there could be a configuration which guarantees full steerability for more velocity possibilities. The configuration is called an optimal steering configuration and was actually used in a previously developed device, Sakaguchi's device.

The limited steerability of a non-redundant planar dissipative passive manipulator could be improved by redundancy. The redundancies brought by serial and parallel structure were studied. Their improvements on steerability were proved equal under certain assumptions. A serial structure has a larger workspace but the analysis and design could be very complex compared to a parallel structure with non-redundant legs. A steerability theorem was then developed in order to determine the universal full steerability of a planar dissipative passive manipulator with multiple joints. The steerability theorem was applied to the previously developed devices. Fully steerable workspaces could be found in some of the devices.

In the previously developed dissipative passive devices, only brakes and clutches were used as actuators. Chapter 5 focuses on the influence of clutches on the steerability of a manipulator. A clutch behaves like a brake at a virtual location. By changing the coupling methods and gear ratios, the location of the virtual brake changes. Therefore the use of clutches on a manipulator will bring in a lot of conveniences but also possible complexity.

Even though assumed negligible in our studies, the dynamics of a haptic interface could influence the steerability of a manipulator. Chapter 6 developed a dynamic force manipulability ellipsoid and used it to illustrate the influence.

After knowing the control ability and the way of improving ability, an interface could be designed for a special application. Chapter 7 talks about the design of a planar dissipative passive haptic interface. The design process starts with the translation of requirements from the application. The structure and actuator type could then be selected. The structure detail will significantly change the manipulator's performance in case of the steerability. Iterations may be taken to refine a design to a satisfactory level. A planar dissipative passive haptic interface could then be achieved to redirect any motion to either side similarly to an active device.

Knowing the potential difficulties, this research still stepped into the field of three-dimensional dissipative passive manipulators in chapter 8. The studies for planar manipulators provide a good example and guideline for the study of 3D steerability. The force generation analysis, full steerability definition and optimal steering configuration etc. were also given in a general 3D way. A non-redundant 3D manipulator does not have full steerability for all possible velocities. A general redundant 3D manipulator could improve the steerability but will be very complex to analyze. Instead, redundant 3D manipulators with non-redundant legs were studied for their steerabilities. A sufficient condition for universal full steerability was obtained for a redundant 3D dissipative passive manipulator with non-redundant legs at all velocities.

## 9.2 Contributions of this Work

The contributions from this research are:

- The identification of motion redirection as the controlling effect of the dissipative passive actuators in a dissipative passive haptic interface

- The identification of the limitation of dissipative passive actuators in generating controlling effect in a dissipative passive haptic interface
- The determination of generated force of an individual dissipative passive actuator, a brake or a clutch at the end-point of a dissipative passive haptic interface which may be used to describe the limitation of the dissipative passive actuators in generating controlling effect in the dissipative passive haptic interface
- Qualitative and quantitative metrics which may be used to evaluate the steerability, the ability to redirect motion of a dissipative passive haptic interface
- A theorem of steerability that provides a sufficient and necessary condition for full steerability for all velocities of a multiple-joint planar dissipative passive haptic interface
- A sufficient condition for full steerability for all velocities of a three-dimensional dissipative passive haptic interface
- The determination of the fully steerable workspaces of a planar dissipative passive haptic interface
- The influence of system dynamics on the ability to redirect motion of dissipative passive haptic interfaces

As discussed in chapter 2, there was no direct research on the control ability and limitations of dissipative passive haptic interfaces. The research in this work is the first.

## 9.3 Future Work

In addition to the positive contributions, this work provides opportunities for continuing research.

As a theoretical research, this work leaves plenty of space in applied practical work. Applying the steerability study result into a real manipulator design and control not only proves the value of the research but also provides practical information which will enrich the study. For example, when defining desired steerability, two-sided steerability was used for a planar manipulator. As mentioned, this concept is only a minimum requirement. The higher the requirement the better the ability to redirect motions. But a practical metric of steerability for motion redirection with smooth and comfortable feel to the operators could not be defined without human involvement. A lot of work could be done to define a set of standards on steerability requirements for different applications. What's more, the influence of system dynamics on displaying haptic effects is another topic that needs human operator' involvements. It is very valuable to find to what extent a human operator would be significantly influenced by the system dynamics from receiving the desired guiding information.

The design discussion mainly focused on brakes as the chosen actuators. Clutches, used in P-TER, have shown their advantages over brakes. The design of a manipulator with clutches would require some careful and intelligent work. If the gear ratio could be adjusted a resulting manipulator design might be a pleasant surprise.

The analysis of three-dimensional manipulators is much more complicated than planar cases. Even though more than expected was achieved there is still a lot to do. The most practical step is to find a better sufficient condition or even a sufficient and necessary condition for universal full steerability. The sufficient condition stated is too strong and it will be very hard to find a usable sized fully steerable workspace. And if

possible a more general discussion of 3D manipulators might even give us more clues in developing devices.

# Appendix

Proof of Equation 5.24:

$$\frac{\sin\alpha}{l_1 s_2} + \frac{\sin\beta}{l_4 s_3} = 0$$

The parameters in the equation are defined and shown in Figure 37 and Figure 39.

The equation could be written as

$$\frac{\sin\alpha}{-l_1 s_2} = \frac{\sin\beta}{l_4 s_3}$$

From Figure 67, $\frac{\sin\alpha}{-l_1 s_2} = \frac{1}{l_{1e}}$ and $\frac{\sin\beta}{l_4 s_3} = \frac{1}{l_{4e}}$.

Since $l_{1e} = l_{4e}$, equation 5.24 is valid.

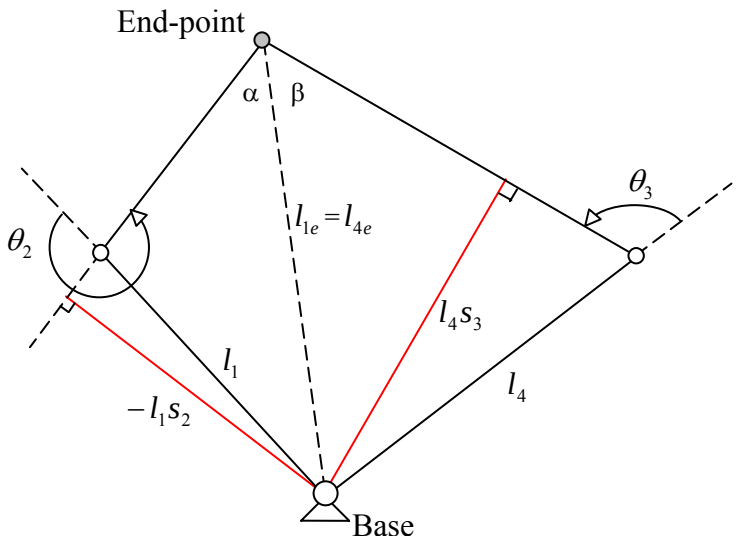


**Figure 67. Proof of equation 5.24**

# References


[1] S. Munir, L. Tognetti, and W. J. Book, "Experimental evaluation of a new braking system for use in passive haptic displays," presented at Proceedings of the 1999 American Control Conference, 2-4 June 1999, San Diego, CA, USA, 1999.

[2] J. Melli-Huber, B. Weinberg, A. Fisch, J. Nikitczuk, C. Mavroidis, and C. Wampler, "Electro-rheological fluidic actuators for haptic vehicular instrument controls," presented at Proceedings 11th Symposium on Haptic Interfaces for Virtual Environment and Teleoperator Systems, 22-23 March 2003, Los Angeles, CA, USA, 2003.

[3] M. R. Reed, "Development of an improved dissipative passive haptic display," Master's thesis, Georgia Institute of Technology, 2004, pp. 133.

[4] M. R. Reed and W. J. Book, "Modeling and control of an improved dissipative passive haptic display," New Orleans, LA, United States, 2004.

[5] J. E. Colgate, W. Wannasuphoprasit, and M. A. Peshkin, "Cobots: robots for collaboration with human operators," presented at Proceedings of the ASME Dynamic Systems and Control Division, 17-22 Nov. 1996, Atlanta, GA, USA, 1996.

[6] M. A. Peshkin, J. E. Colgate, W. Wannasuphoprasit, C. A. Moore, R. B. Gillespie, and P. Akella, "Cobot architecture," *IEEE Transactions on Robotics and Automation*, vol. 17, pp. 377-90, 2001.

[7] C. A. Moore, M. A. Peshkin, and J. E. Colgate, "Cobot implementation of 3D virtual surfaces," presented at Proceedings 2002 IEEE International Conference on Robotics and Automation, 11-15 May 2002, Washington, DC, USA, 2002.

[8] C. A. Moore, Jr., M. A. Peshkin, and J. E. Colgate, "Cobot implementation of virtual paths and 3D virtual surfaces," *IEEE Transactions on Robotics and Automation*, vol. 19, pp. 347-51, 2003.

[9] H. Flemmer and J. Wikander, "Transparency and stability analysis of a surgical teleoperator system," presented at Proceedings 11th Symposium on Haptic Interfaces for Virtual Environment and Teleoperator Systems, 22-23 March 2003, Los Angeles, CA, USA, 2003.

[10] B. Hannaford and J.-H. Ryu, "Time-domain passivity control of haptic interfaces," *Robotics and Automation, IEEE Transactions on*, vol. 18, pp. 1-10, 2002.

[11] Y. Yokokohji, T. Imaida, and T. Yoshikawa, "Bilateral control with energy balance monitoring under time-varying communication delay," presented at ICRA 2000: IEEE International Conference on Robotics and Automation, Apr 24-Apr 28 2000, San Francisco, CA, USA, 2000.

[12] K. Kanaoka and T. Yoshikawa, "Passivity monitor and software limiter which guarantee asymptotic stability of robot control systems," presented at 2003 IEEE International Conference on Robotics and Automation, Sep 14-19 2003, Taipei, Taiwan, 2003.

[13] H. Lipkin and J. Duffy, "Sir Robert Stawell Ball and methodologies of modern screw theory," *Proceedings of the Institution of Mechanical Engineers, Part C: Journal of Mechanical Engineering Science*, vol. 216, pp. 1, 2002.

[14] J.-P. Merlet, *Parallel robots*, vol. 74: Kluwer Academic Publishers, 2000.

[15] J. H. Lee, H. W. Kim, B.-J. Yi, and I. H. Suh, "Singularity-free algorithms and design scheme for a new 6-DOF parallel haptic device," presented at Proceedings 2002 IEEE International Conference on Robotics and Automation, 11-15 May 2002, Washington, DC, USA, 2002.

[16] P. A. Voglewede, "Measuring closeness to singularities of parallel manipulators with application to the design of redundant actuation," Ph.D. thesis, Georgia Institute of Technology, 2004.

[17] L. Sciavicco and B. Siciliano, *Modeling and control of robot manipulators*. New York: McGraw-Hill Companies, Inc., 2000.

[18] M. T. Rosenstein and R. A. Grupen, "Velocity-dependent dynamic manipulability," presented at Proceedings 2002 IEEE International Conference on Robotics and Automation, 11-15 May 2002, Washington, DC, USA, 2002.

[19] M. W. Spong, "The swing up control problem for the Acrobot," *Control Systems Magazine, IEEE*, vol. 15, pp. 49-55, 1995.

[20] K. M. Lynch, N. Shiroma, H. Arai, and K. Tanie, "Motion planning for a 3-DOF robot with a passive joint," presented at Robotics and Automation, 1998. Proceedings. 1998 IEEE International Conference on, 1998.

[21] A. De Luca and G. Oriolo, "Trajectory planning and control for planar robots with passive last joint," *International Journal of Robotics Research*, vol. 21, pp. 575-590, 2002.

[22] K. M. Lynch and M. T. Mason, "Dynamic manipulation with a one joint robot," presented at Robotics and Automation, 1997. Proceedings., 1997 IEEE International Conference on, 1997.

[23] S. Hirose, *Biologically inspired robots: snake-like locomotors and manipulators*: Oxford University Press, 1993.

[24] L. Birglen and C. M. Gosselin, "Kinetostatic analysis of underactuated fingers," *IEEE Transactions on Robotics and Automation*, vol. 20, pp. 211-221, 2004.

[25] K. Ito, F. Matsuno, and R. Takahashi, "Underactuated crawling robot," presented at Proceedings. 2000 IEEE/RSJ International Conference on Intelligent Robots and Systems (IROS 2000), 31 Oct.-5 Nov. 2000, Takamatsu, Japan, 2000.

[26] S. J. Hall, *Basic Biomechanics*, First Edition ed: James M. Smith, 1995.

[27] V. C. Scanlon and T. Sanders, *Essentials of Anatomy and Physiology*, Fourth Edition ed: F. A. Davis Company, 2003.

[28] W. Book, R. Charles, H. Davis, and M. Gomes, "Concept and implementation of a passive trajectory enhancing robot," presented at Proceedings of the 1996 ASME International Mechanical Engineering Congress and Exposition, Nov 17-22 1996, Atlanta, GA, USA, 1996.

[29] M. Waldorff Gomes and W. J. Book, "Control approaches for a dissipative passive trajectory enhancing robot," presented at Proceedings of IEEE/ASME International Conference on Advanced Intelligent Mechatronics, 16-20 June 1997, Tokyo, Japan, 1997.

[30] D. K. Swanson and W. J. Book, "Path-following control for dissipative passive haptic displays," presented at Proceedings 11th Symposium on Haptic Interfaces for Virtual

Environment and Teleoperator Systems, 22-23 March 2003, Los Angeles, CA, USA, 2003.

[31] D. K. Swanson and W. J. Book, "Obstacle avoidance methods for a passive haptic display," presented at 2001 IEEE/ASME International Conference on Advanced Intelligent Mechatronics. Proceedings. AIM '01, 8-12 July 2001, Como, Italy, 2001.

[32] Y. Matsuoka and W. Townsend, "Design of life-size haptic environments," *Proceedings of the ISER Seventh International Symposium on Experimental Robots*, 2000.

[33] M. Sakaguchi, J. Furusho, and N. Takesue, "Passive force display using ER brakes and its control experiments," presented at Virtual Reality, 2001. Proceedings. IEEE, 2001.

[34] C. Cho, M. Kim, and J.-B. Song, "Performance analysis of a 2-link haptic device with electric brakes," presented at Proceedings 11th Symposium on Haptic Interfaces for Virtual Environment and Teleoperator Systems, 22-23 March 2003, Los Angeles, CA, USA, 2003.

[35] M. Sakaguchi and J. Furusho, "Development of 2 DOF force display system using ER actuators," presented at Advanced Intelligent Mechatronics, 1999. Proceedings. 1999 IEEE/ASME International Conference on, 1999.